UNIVERSIDADE FEDERAL DE SANTA CATARINA
PROGRAMA DE PÓS-GRADUAÇÃO EM ENGENHARIA MECÂNICA

Cassiano Tecchio

DESENVOLVIMENTO DE SISTEMAS DE REFRIGERAÇÃO PASSIVOS PARA AERONAVES

Florianópolis
2017

Cassiano Tecchio

DESENVOLVIMENTO DE SISTEMAS DE REFRIGERAÇÃO PASSIVOS PARA AERONAVES

Dissertação submetida ao Programa de Pós-Graduação em Engenharia Mecânica da Universidade Federal de Santa Catarina para a obtenção do Grau de Mestre em Engenharia Mecânica.
Orientadora:
Profa. Márcia B. H. Mantelli, Ph.D
Coorientador:
Prof. Kleber V. Paiva, Dr. Eng.

Florianópolis
2017

Ficha de identificação da obra elaborada pelo autor,
através do Programa de Geração Automática da Biblioteca Universitária da UFSC.

Tecchio, Cassiano
Desenvolvimento de sistemas de refrigeração passivos para aeronaves / Cassiano Tecchio ; orientadora, Márcia Barbosa Henriques Mantelli ; coorientador, Kleber Vieira de Paiva. - Florianópolis, SC, 2017.
171 p.

Dissertação (mestrado) - Universidade Federal de Santa Catarina, Centro Tecnológico. Programa de Pós-Graduação em Engenharia Mecânica.

Inclui referências

1. Engenharia Mecânica. 2. Aeronaves. 3. Refrigeração passiva. 4. Tubos de calor. 5. Aviônicos. I. Mantelli, Márcia Barbosa Henriques. II. Vieira de Paiva, Kleber . III. Universidade Federal de Santa Catarina. Programa de Pós-Graduação em Engenharia Mecânica. IV. Título.

Cassiano Tecchio

DESENVOLVIMENTO DE SISTEMAS DE REFRIGERAÇÃO PASSIVOS PARA AERONAVES

Esta dissertação foi julgada adequada para a obtenção do título de **Mestre em Engenharia Mecânica**, especialidade Engenharia e Ciências Térmicas e aprovada em sua forma final pelo Programa de Pós-Graduação em Engenharia Mecânica.

Florianópolis, 15 de Fevereiro de 2017

Prof. Jonny Carlos da Silva, Dr. Eng.
Coordenador do Programa de Pós-Graduação
em Engenharia Mecânica

Banca examinadora:

Profa. Márcia B. H. Mantelli, Ph.D. - Orientadora - UFSC

Prof. Kleber V. Paiva, Dr. Eng. - Coorientador - UFSC

Prof. Júlio C. Passos, Dr. - UFSC

Prof. Fernando H. Milanese, Dr. Eng. - UFSC

Ricardo Gandolfi, Dr. Eng. - EMBRAER

Profa. Cintia Marangoni, Dr. Eng. - UFSC

Aos meus pais, Alcibides e Nelci,
pelo apoio e incentivo constantes.

À todos que contribuíram
com a realização deste trabalho.

AGRADECIMENTOS

Primeiramente, e em especial, agradeço aos meus pais, Nelci T. Z. Tecchio e Alcibides L. Tecchio, pelo apoio e incentivo nesta jornada e, sobretudo, pela educação que me concederam durante todos esses anos. Serei eternamente grato por me mostrarem o valor da vida.

À Profa. Márcia B. H. Mantelli, minha orientadora, pela confiança depositava no meu trabalho e pela oportunidade de participar de um excelente grupo de trabalho, permitindo-me um grande crescimento profissional.

Aos meus coorientadores, Profs. Kleber V. Paiva e Jorge L. G. Oliveira, pela dedicação, incentivo e ajuda indispensáveis para o sucesso deste trabalho.

À todos que trabalharam no Projeto Tucal, em especial aos colegas e amigos Luiz Domingos, Yago Braun, Clayton Muller, Leandro Setubal, Kênia W. Milanez do LABTUCAL e ao Ricardo Gandolfi da EMBRAER.

Aos engenheiros, técnicos e pilotos do time de teste em voo da EMBRAER de Gavião Peixoto e São José dos Campos - SP pelo auxílio na preparação da aeronave e do experimento para realização dos testes. Ao Leonardo K. Slongo do LABTUCAL pelo auxílio na parte elétrica e eletrônica da bancada experimental.

Devo agradecer aos meus colegas da pós-graduação em engenharia mecânica da UFSC, os quais proporcionaram maravilhosos momentos de estudo, descontração e evolução como ser humano. Agradeço em especial aos colegas Luis A. B. Arboleda, Juan P. F. Mera, Luis H. R. Cisterna, Nelson Y. L. Pabon, João C. Pozzobon, Marcus V. V. Mortean, Franciene I. P. de Sá, Andrés P. S. Cajamarca, Felipe de Castro, Juliano Oestreich, Indyanara B. Marcelino, Felipe G. Battisti, Gregory Rosinski, Guilherme P. Jaenisch e Herlon Linemburg. Aos meus amigos da UFSC de Joinville, em especial os meus colegas Bruno Backes e Hermann L. Lebkuchen.

À UFSC e ao POSMEC pela oportunidade de cursar uma pós-graduação de excelência.

À EMBRAER e a CAPES pelo apoio à pesquisa.

"A mente que se abre a uma nova ideia
jamais voltará ao seu tamanho original"
Albert Einstein

"Nunca se pode concordar em rastejar
quando se sente ímpeto de voar"
Helen Keller

"Uma vida sem desafios não vale a pena ser vivida"
Sócrates

RESUMO

Um novo sistema de trocador de calor (HES) foi avaliado experimentalmente em solo e em voo objetivando o resfriamento passivo de sistemas aviônicos. O protótipo de trocador de calor consiste em dois condensadores, conectados a um mesmo evaporador através de dois *loop* termossifões em paralelo. O fluxo de ar externo à fuselagem da aeronave e o sistema de ar condicionado servem como sumidouros de calor. Um tubo de calor e quatro termossifões foram empregados como elementos intermediários de transferência de calor (IHTEs) entre fontes de calor e o evaporador do trocador de calor. Os parâmetros de projeto dos IHTEs tais como razão de enchimento, ângulo de inclinação, razão de aspecto e geometria dos condensadores (contato entre condensador do IHTE e evaporador do HES) foram avaliados. Água foi utilizada como fluido de trabalho. Os protótipos HES e IHTEs foram qualificados para voo após avaliações térmicas em laboratório e testes de cumprimento de requisitos. Os testes foram executados em números de Mach de até 0,78 e em altitudes de até 12 km, correspondendo à temperatura estática do ar de -56 ºC. Em condições de voo em cruzeiro, o HES é capaz de dissipar 900 W mantendo temperaturas de vapor abaixo dos valores típicos para operação de aviônicos; *e.g.* 70 à 100 ºC. Demonstra-se a capacidade de funcionamento dos termossifões mesmo em condições de congelamento do fluido de trabalho. O fenômeno de *geyser boiling* eventualmente promove intensas vibrações no evaporador do trocador de calor. Mudanças térmicas nos sumidouros de calor afetam fracamente os IHTEs. Tubo de calor e termossifões com 0,7 m de comprimento podem dissipar 120 W e 500 W, respectivamente. Convecção forçada pode ser uma alternativa onde condução de calor entre aviônicos e evaporadores dos IHTEs não é possível. Condensadores cônicos e cilíndricos dos IHTEs demonstram ser possíveis geometrias para o acoplamento térmico entre condensadores de IHTE e evaporador do HES.

Palavras-chave: Aeronaves. Aviônicos. Tubos de calor. Refrigeração passiva. *Geyser boiling*. Condições térmicas variadas.

DESENVOLVIMENTO DE SISTEMAS DE REFRIGERAÇÃO PASSIVOS PARA AERONAVES

Introdução: Com o advento da tecnologia *fly-by-wire*, o número de componentes eletrônicos em aeronaves tem aumentado significativamente. As vantagens associadas às aeronaves *fly-by-wire* são diversas, tais como proteção do envelope de voo, fácil manutenção e redução do consumo de combustível. No entanto, a integridade e funcionalidade desses componentes deve ser garantida por meio de controle térmico e, portanto, a dissipação do calor gerado por efeito *Joule* tem sido um problema prático de engenharia a ser explorado. Usualmente, a dissipação térmica de componentes eletrônicos é realizada por meio de convecção forçada utilizando ventiladores. Embora efetiva, essa solução é energeticamente ineficiente, uma vez que requer consumo de energia. Geração de ruído e manutenção periódica são outras desvantagens adicionais. Portanto, novas tecnologias para dissipação de calor, tais como tubos de calor e termossifões, vêm sendo consideradas para aplicações aeronáuticas. Dispositivos de transferência de calor baseados na tecnologia de tubos de calor operam em um ciclo bifásico fechado fazendo uso de calor latente de vaporização para transferir calor mediante pequenas diferenças de temperatura. O princípio de funcionamento dessa tecnologia é como segue: calor inserido na região do evaporador faz com que o fluido de trabalho seja vaporizado e escoe em direção ao condensador, onde condensação ocorre e calor latente de vaporização é rejeitado. Em termossifões, o líquido condensado retorna ao evaporador devido à gravidade, enquanto que em tubos de calor essa tarefa é realizada por meio de um bombeamento capilar. A principal motivação do presente trabalho é o fato de que, em voo de cruzeiro, a fuselagem da aeronave pode ser interpretada como uma aleta exposta a um fluxo de ar externo à cabine com temperaturas estáticas de aproximadamente -56,5 ^{o}C (à 11 km de altitude) e velocidades de 850 km/h, configurando-se um excelente sumidouro de calor. Por outro lado, em solo, calor pode se removido através do sistema de ar-condicionado da própria aeronave. Dessa forma, dispositivos de controle térmico passivos para aviônicos, assistidos pela tecnologia de tubos de calor, o qual faz uso de sumidouros de calor pouco explorados do envelope de voo de aeronaves, são propostos neste trabalho.

Objetivo: O objetivo principal desse trabalho é o desenvolvimento de sistemas de refrigeração passivos baseados na tecnologia de tubos de calor para controle térmico de fontes de calor em aeronaves.

Metodologia: Um protótipo de trocador de calor (HES) foi desenvolvido, consistindo em dois condensadores, conectados a um mesmo evaporador através de dois *loop*-termossifões em paralelo. O fluxo de ar externo à fuselagem da aeronave e o sistema de ar-condicionado servem como sumidouros de calor. Testes em laboratório e a bordo de uma aeronave foram realizados a fim de avaliar o desempenho térmico do protótipo. Em condições reais de voo, os testes foram executados em números de Mach de até 0,78 e em altitudes de até 12 km, correspondendo à temperatura estática do ar de -56 ºC. Posteriormente, termossifões e um tubo de calor foram avaliados em laboratório e em voo como elementos intermediários de transferência de calor (IHTEs) entre fontes de calor independentes e o evaporador do HES . Geometrias cônicas e cilíndricas foram empregadas para o acoplamento mecânico. Os efeitos de manobras como *roller-coaster* e G-*load* no comportamento térmico dos elementos intermediários foram avaliados.

Resultados: Em condições de voo em cruzeiro, o HES dissipa 900 W mantendo temperaturas de vapor abaixo dos valores típicos de operação de aviônicos, *e.g.* 70 à 100 ºC, com dissipação de calor predominante ($\approx 90\%$) no sumidouro de calor da fuselagem. Por outro lado, em solo, a dissipação térmica ocorre preferencialmente através do sistema de ar-condicionado, quando existe fluxo de ar no interior do duto do ar-condicionado. O funcionamento eficiente da tecnologia de tubos de calor é verificada mesmo em condições de congelamento do fluido de trabalho (água) no interior do condensador da fuselagem. Superaquecimento ou falha estrutural não foram evidenciadas. Observou-se que o fenômeno de *geyser boiling* pode eventualmente promover intensas vibrações do evaporador do HES. Mudanças térmicas nos sumidouros de calor afetam fracamente os IHTEs. Tubo de calor e termossifões com 0,7 m de comprimento podem dissipar 120 W e 500 W, respectivamente. Convecção forçada pode ser uma alternativa onde condução de calor entre aviônicos e evaporadores dos IHTEs não é possível. Condensadores cônicos e cilíndricos dos IHTEs demonstram ser possíveis geometrias para o acoplamento térmico entre condensadores de IHTE e evaporador do HES. Os efeitos das manobras da aeronave são irrelevantes para a tecnologia de tubos de calor, exceto em elevados ângulos de *pitch* para o evaporador dos HES, onde superaquecimento ocorre.

DEVELOPMENT OF PASSIVE AIRCRAFT COOLING SYSTEMS

ABSTRACT

A novel design for a heat exchanger system (HES) was experimentally evaluated on ground and in-flight conditions aiming the passive cooling of avionics systems. The heat exchanger prototype consists of two condensers, linked to one shared evaporator by two parallel loop-thermosyphons. The air stream on the external side of the fuselage and the air conditioning system served as heat sinks. A heat pipe and four thermosyphons were employed as intermediary heat transfer elements (IHTEs) between heat sources and the HES evaporator. The IHTE design parameters such as filling ratio, inclination angle, aspect ratio and coupling geometries (contact between condenser of IHTE and evaporator of HES) were evaluated. Water was applied as the working fluid. The HES and IHTEs prototypes were qualified for flight after thermal assessments in laboratory and constrained acceptance tests. The tests were conducted at flight Mach numbers up to 0.78 and at altitudes of up to 12 km, corresponding to air static temperatures of -56 ºC. Under cruise flight conditions, the HES is able to dissipate 900 W maintaining vapor temperatures below typical working values for avionics; *e.g.* 70 to 100 ºC. Efficient performance of thermosyphon was also shown in freezing conditions of the working fluid. Geyser boiling phenomenon eventually yields intense vibrations at the HES evaporator. Thermal changes in the heat sinks hardly affect IHTEs. Heat pipe and thermosyphons with 0.7 m length can dissipate 120 W and 500 W, respectively. Forced convection can be an alternative where heat conduction between avionics and IHTE evaporators is not possible. Conical and cylindrical IHTEs condensers were demonstrated as possible fitting geometries for thermal couplings.

Keywords: Aircraft. Avionics. Heat pipe. Passive cooling. Geyser boiling. Variable thermal conditions.

LIST OF FIGURES

LIST OF TABLES

NOMENCLATURE

Acronyms

AC	Air conditioning
CTS	Thermosyphon with conical plug
EMBRAER	Empresa Brasileira de Aeronáutica
FTS	Thermosyphon with fins welded to the evaporator
Fus	Fuselage
HES	Heat exchanger system
HP	Heat pipe
IHTEs	Intermediary heat transfer elements
LABTUCAL	Laboratório de Tubos de Calor
TS	Thermosyphon with cylindrical plug
UFSC	Universidade Federal de Santa Catarina
VOF	Volume of Fluid

Greek alphabet

Δt	Time interval	[s]
ΔT	Temperature difference	[°C]
ΔT_{ml}	Logarithmic mean temperature difference	[°C]
ϵ	Porosity	[–]
γ	Ratio of the specific heats	[–]
μ	Dynamic viscosity	[Pa · s]
ϕ	Inclination angle from horizontal axis	[°]
ρ	Density	[kg/m^3]
σ	Surface tension	[N/m]

Roman alphabet

$\aleph$	Number of merit	[kg/(K$^{3/4}$s$^{5/2}$)]
$\bar{v}$	Average velocity	[m/s]
$\dot{m}$	Mass flow rate	[kg/s]
$\overline{T}$	Average temperature	[°C]
A	Area	[m^2]

$a(t)$	Acceleration	$[\mathrm{m/s^2}]$
AR	Aspect ratio (l_{adiab}/d_{adiab})	[–]
c_p	Specific heat at constant pressure	$[\mathrm{J/(kg\,K)}]$
d	Diameter	[m]
d_w	Wire diameter	[m]
FR	Filling ratio ($\mathrm{V_{fluid}/V_{evap}}$)	[–]
$G(t)$	Pressure rate	[Pa/s]
h	Convective heat transfer coefficient	$[\mathrm{W/m^2K}]$
h_{lv}	Latent heat of vaporization	[J/kg]
H_{sl}	Altitude above seal level	[m]
k	Thermal conductivity	$[\mathrm{W/(m\,K)}]$
L	Lift	[N]
l	Characteristic length	[m]
N	Mesh number	$[\mathrm{inch^{-1}}]$
p_{sat}	Pressure of the saturated vapor	[Pa]
Q	Energy	[J]
q	Heat transfer rate	[W]
q''	Heat transfer flux	$[\mathrm{W/m^2}]$
q_{AC}	Heat transfer rate at the AC heat sink	[W]
q_{Fus}	Heat transfer rate at the Fus heat sink	[W]
q_{in}	Input power	[W]
q_{lat}	Vaporization latent heat	[W]
q_{TRAN}	Heat transfer due to transient effects	[W]
R	Thermal resistance	[°C/W]
$R_{h,AC}$	Convective thermal resistance at the AC heat sink	[°C/W]
$R_{h,Fus}$	Convective thermal resistance at the Fus heat sink	[°C/W]
R_h	Convective thermal resistance	[°C/W]
R_k	Conductive thermal resistance	[°C/W]
S	Crimping factor	[–]
T	Temperature	[°C]
t	Time	[s]
T^*	Temperature of the air stream	[°C]

T_∞	Static air temperature	[°C]
T_{adiab}	Adiabatic temperature	[°C]
T_{AW}	Adiabatic wall temperature	[°C]
T_{Fus}	Temperature on the outer fuselage	[°C]
T_{in}	Inlet temperature	[°C]
T_{out}	Outlet temperature	[°C]
T_o	Operating temperature	[°C]
T_{tb}	Temperature of the thermal bath	[°C]
T_v	Vapor temperature	[°C]
T_w	Wall temperature	[°C]
u	Aircraft velocity	[m/s]
V	Volume	[m^3]
V^*	Effective volume	[m^3]
W	Aircraft weight	[N]
x, y, z	Cartesian coordinates	[–]

Subscripts

ad	Adiabatic
ap	Apparent
$cond$	Condenser
$evap$	Evaporator
hp	Heat pipe
in	Input
l	Liquid
max	Maximum
s	Solid
tb	Thermal bath
th	Thermosyphon

Dimensionless numbers

M	Mach number
N_z	Vertical load factor
r	Recovery factor
Bi	Biot number

Pr	Prandtl number
Re	Reynolds number

CONTENTS

1 INTRODUCTION

1.1 CONTEXT

The amount of electronic components in aircrafts has been increased since the introduction of digital fly-by-wire flight control systems by the National Aeronautics and Space Administration (NASA) in 1972. Fly-by-wire systems include several on-board electronic equipment designed to replace conventional pneumatic, hydraulic and mechanical powered systems. This allows for the use of redundant flight control architectures, making aircrafts safer, lighter and more stable aerodynamically. Fly-by-wire systems also reduce the fuel consumption required to fly, increasing the aircraft autonomy. However, the electric power needed to assist electrically powered systems and electronics has risen thereby requiring the dissipation of high heat loads. Size and weight are also significant penalties for aircraft components and, as they get smaller and powerful, the power dissipation density also increases [1–3].

Most avionics installed on aircraft cockpit are certified to work in ambient temperatures up to 70 ºC, whereas their internal temperatures can reach up to 100 ºC [4]. Effective cooling systems must ensure that avionics temperatures do not surpass these limits. Excess temperatures, out of the tolerable level, may compromise the electronics functionality and, therefore, the aircraft control. Natural and forced convection have been used as avionics cooling mechanisms. In natural convection, there are inherently high thermal resistances between heat sources and heat sinks. Forced convection of air by means of fans increase the heat transfer coefficients, reducing the inefficiency of air cooling systems. This last mechanism has been widely used by the aeronautic industry as cooling system for several electronic equipment in aircrafts. However, this approach has some drawbacks, such as size, periodic maintenance, noise generation and, mainly, power consumption. Therefore, in order to install on-board electronics with high heat dissipation requirements, it is necessary to implement more efficient techniques to remove heat from such devices [5–8].

Novel cooling systems based on heat pipe technologies have been studied for aeronautic purposes. In this context, the present study presents some technological and scientific advances in passive aircraft cooling systems, recently achieved within the frame of a joint effort between the Heat Pipe Laboratory (Labtucal/EMC/UFSC) and EMBRAER Aerospace Company.

1.2 MOTIVATION

The main motivation of the present work comes from the need to develop reliable thermal management systems, capable of providing passive heat dissipation for avionics. In cruise conditions, the aircraft fuselage skin can be seen as a large fin exposed to the air stream environment at temperatures of -56.5 ºC (at 11 km above sea level) [9] and with velocities of approximately 850 km/h. Therefore, the aircraft fuselage outer surface is an excellent heat sink. On the other hand, on-ground, heat can be removed by forced convection through the already available aircraft air conditioning system. Passive thermal control devices to be used in avionics, assisted by heat pipe technologies, which makes use of the poorly-explored aircraft flight envelope heat sinks, are proposed in this work.

1.3 HEAT PIPE TECHNOLOGY

According to Grover [10] and Gaugler [11], a heat pipe can be described as follows: "With certain limitations on the manner of use, a heat pipe may be regarded as a synergistic engineering structure which is equivalent to material having a thermal conductivity greatly exceeding that of any known metal". Because of this, heat pipes and similar technologies are also known as heat superconductors. Basically, a thermosyphon (wickless heat pipe) consists of a sealed and evacuated container in which a suitable amount of working fluid is inserted. The device is commonly divided into three main regions: evaporator, adiabatic and condenser. Schematics of the working principles of typical thermosyphons and heat pipes are shown in Fig. 1. The produced vapor at the evaporator, due to a slight pressure increase, flows towards the condenser where condensation takes place and latent heat of vaporization is released. In thermosyphons, the liquid flows back to the evaporator due to the gravitational effect whereas in heat pipes this task is performed by a capillary pumping through a wick structure (see Figs. 1a and 1b). Therefore, heat pipes can be used in gravity-free environments. On the other hand, thermosyphons work properly only with the aid of gravity and are convenient for industrial applications.

One should note that thermosyphons and heat pipes can work even when the temperature differences between evaporator and condenser are small. In general, they present very high effective conductances and so, in many applications, can be used to promote uniform temperature distributions. Thermosyphons can also be used as thermal diodes: they transfer heat in only one direction (from the bottom to the upper regions), while heat pipes can transfer heat in both directions [12].

Heat pipe technologies can present several geometries and arrangements. One of them, the loop-thermosyphon, is employed in the present work. The working principle of a loop-thermosyphon is similar to that described for a typical thermosyphon. An illustration of a loop-thermosyphon is shown in Fig. 2. In this configuration, the evaporator and condenser are separated by two sets of tubes within which only vapor or liquid is conducted. Besides the high geometry flexibility that this technology is able to handle, loop-thermosyphons are be able to transfer larger amounts of heat when compared to straight thermosyphons, as no counter current flow between vapor and condensate liquid is observed.

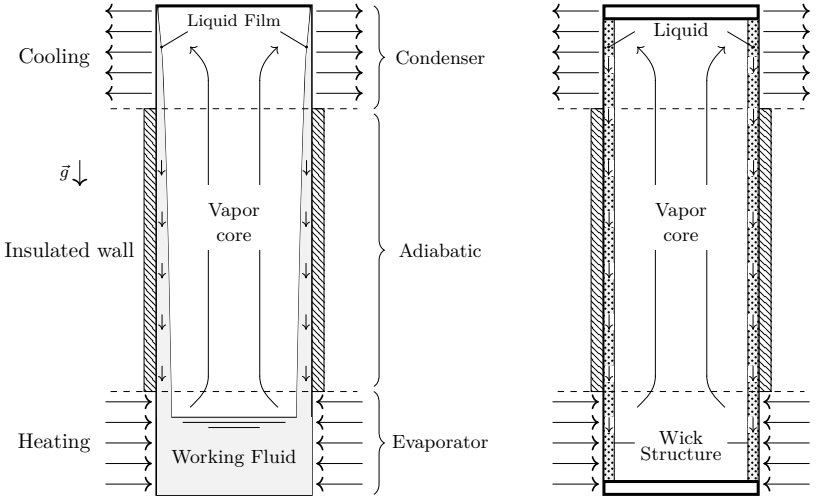

(a) Thermosyphon. (b) Heat pipe.

Figure 1 – Schematics of the working principle of typical thermosyphons and heat pipes.

1.4 OBJECTIVES

1.4.1 Global objective

This work aims to develop passive cooling systems based on heat pipe technologies to manage heat sources of a commercial aircraft on ground and in-flight operation.

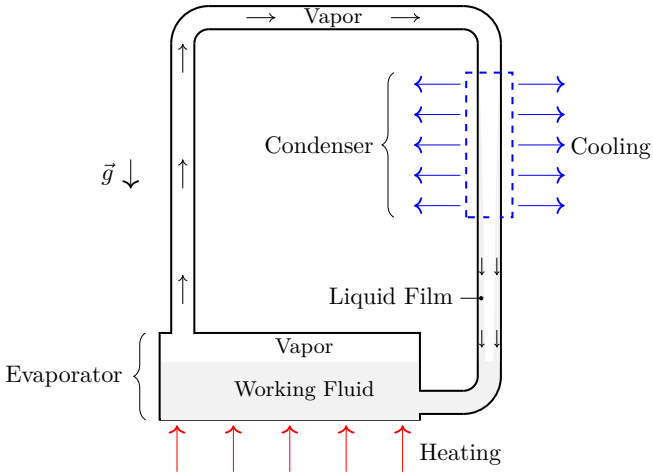

Figure 2 – Schematics of a loop-thermosyphon.

1.4.2 Specific objectives

To accomplish the main purpose described above, the following specific objectives are proposed:

- To review the pertinent literature on heat pipe technology, mainly applied to aerospace and aeronautical purposes;
- To assess the heat removal capacity of the prototype under typical thermal conditions of aircrafts operation, including real flight tests.
- To evaluate the behavior of water as working fluid exposed to subzero temperatures.
- To assess the effects of the geyser boiling phenomenon in loop-thermosyphons.
- To investigate ideal design parameters for thermosyphons connected in series.
- To assess the use of thermosyphons and heat pipe as intermediary heat transfer elements between a heat source and a heat sink;

1.5 STRUCTURE OF THE THESIS

The present thesis is divided into seven chapters. Apart from this introduction, the content of the five following chapters are based

on five manuscripts published or submitted to international journals as listed in Table 1. Note that Chapters 2, 3 and 6 consist of three articles already published in journals with outstanding scientific quality. The experimental apparatus and procedures are described in each chapter as well as pertinent literature reviews and concluding remarks.

The chapters contents are described as follows:

- Chapter 2: **Passive aircraft cooling systems for variable thermal conditions**. In this Chapter, a novel design for a heat exchanger system (HES) [13], for which a patent has been filed in, is described in details. Experimental tests were conducted in the laboratory to assess the HES thermal behavior under variable conditions, which resemble the operation of an aircraft on-ground and in-flight. In particular, it is shown the prototype thermal performance starting up from freezing conditions.

- Chapter 3: **In-flight testing of loop-thermosyphons for aircraft cooling**. This Chapter is dedicated to the HES thermal evaluation under real flight conditions, which could not be achieved at laboratory. On-ground and in-flight experiments were conducted in an Embraer test aircraft after constrained acceptance tests. HES condensers were submitted to actual heat transfer coefficients as observed in conventional commercial flights.

- Chapter 4: **Geyser boiling phenomenon in two-phase closed loop-thermosyphons**. Chapter 4 is devoted to the basic understanding of structural vibrations induced by geyser boiling phenomenon in two-phase closed loop-thermosyphons. Simultaneous thermal and vibrational assessments were performed in order to prevent the device premature failure by vacuum leakage due to intense vibrations.

- Chapter 5: **Thermal performance of thermosyphons in series connected by thermal plugs**. Chapter 5 focus on the thermal performance assessment of two thermosyphons connected in series. One thermosyphon served as intermediary heat transfer device between a heat source and the HES evaporator. A crucial point of this research was to find-out the best geometrical configuration that results in enhanced heat transfer and thermal performance of the device, as observed by reducing the operating temperature of the intermediary thermosyphon.

- Chapter 6: **Passive cooling concept for onboard heat sources in aircrafts**. In this Chapter, experimental results of in-flight

tests are shown for a passive cooling system including the HES prototype, presented in the previous chapters, and intermediary heat transfer elements (IHTE's). Based on the results from Chapter 4 and the aircraft space constraints, thermosyphons and a heat pipe were designed as intermediary heat transfer elements. Heat was transferred from heat sources passively thorough intermediary elements to the HES evaporator. Experiments comprise tests in cruise conditions and during conventional maneuvers, which could not be performed in laboratory.

- Chapter 7: **Conclusion**. The main concluding remarks are listed. Some suggestions for future works are also provided.

Table 1 – Scientific contributions of this thesis.

Thesis Chapter	**Article**
2	Oliveira, J.L.G.; Tecchio, C.; Paiva, K.V.; Mantelli, M.B.H.; Gandolfi, R.; Ribeiro, L.G.S. Passive aircraft cooling systems for variable thermal conditions, Appl. Therm. Eng. v. 79, p. 88-97, 2015
3	Oliveira, J.L.G.; Tecchio, C.; Paiva, K.V.; Mantelli, M.B.H.; Gandolfi, R.; Ribeiro, L.G.S. In-flight testing of loop thermosyphons for aircraft cooling, Appl. Therm. Eng. v. 98, p. 144-156, 2016
4	Tecchio, C.; Oliveira, J.L.G.; Paiva, K.V.; Mantelli, M.B.H.; Gandolfi, R.; Ribeiro, L.G.S. Geyser boiling phenomenon in two-phase closed loop-thermosyphons, Submitted to Int. J. Heat Mass Tran. In November, 10, 2016
5	Tecchio, C.; Oliveira, J.L.G.; Paiva, K.V.; Mantelli, M.B.H.; Gandolfi, R.; Ribeiro, L.G.S. Thermal performance assessment of thermosyphons in series, Submitted to Exp. Therm. Fluid Sci. In December, 20, 2016
6	Tecchio, C.; Paiva, K.V.; Oliveira, J.L.G.; Mantelli, M.B.H.; Gandolfi, R.; Ribeiro, L.G.S. Passive cooling concept for onboard heat sources in aircrafts, Exp. Therm. Fluid Sci. v. 82, p. 402-413, 2017

2 PASSIVE AIRCRAFT COOLING SYSTEMS FOR VARIABLE THERMAL CONDITIONS

The content of this chapter is based on the following article:

- OLIVEIRA, J. L. G.; TECCHIO, C.; PAIVA, K. V.; MANTELLI, M. B. H.; GANDOLFI, R.; RIBEIRO, L. G. S. Passive aircraft cooling systems for variable thermal conditions. Applied Thermal Engineering, v. 79, p. 88–97, 2015. DOI:10.1016/j.applthermaleng.2015.01.021

2.1 INTRODUCTION

In this chapter, a heat exchanger system (HES) consisting of two loop-thermosyphons with two parallel condensers and a common evaporator (one heat source and two heat sinks) is proposed for aircraft applications and is experimentally tested. The working principle of the two-phase heat exchanger is as follows. The loop-thermosyphons are positioned between one heat source (electrical resistance representing avionics equipment) and two heat sinks, namely aircraft cabin-external air and the air flux inside the aircraft air conditioning ducts. Fig. 3 illustrates this configuration. The cooling system receives heat from a heat source, which is transferred to the fuselage and/or air conditioning heat sinks by two condensers. The use of these two heat sinks is justified as follows. In flight conditions, forced convection acts at the fuselage outer surface. The cabin-external air temperature ranges from -62 to -20 ^{o}C according to the environment conditions at an altitude of approximately 9.1 km above sea level; see Table 2. The free-stream velocity is approximately 850 km/h for conventional commercial flights. In these conditions the external surface of the aircraft fuselage work as a heat sink with large area, available for heat exchange, exposed to a high average heat transfer coefficient (332 W/(m^{2}K); see Zhang *et al.* [14]). On ground, when the airplane is parked, the external surface is subjected to a high thermal resistance resulting from the natural convection. In this case, the air flux of the aircraft air conditioning duct can serve as a the heat sink, removing heat from the condenser positioned within the air conditioning duct by forced convection. Therefore, the proposed system provides a passive cooling of avionics equipment is possible either on the ground or in-flight.

Although other arrangements are possible [13], the evaporator is linked to each condenser by two parallel loop-thermosyphon arrangements. Water was used as the working fluid since other fluid refrigerants would

represent a hazard, in case of leakage. A crucial point in this research was to evaluate the behavior of water as a working fluid exposed to subzero temperatures (within the condenser of the HES exposed to the aircraft fuselage skin). The cooling system must handle the characteristic diversity of thermal conditions presented by aircraft operations.

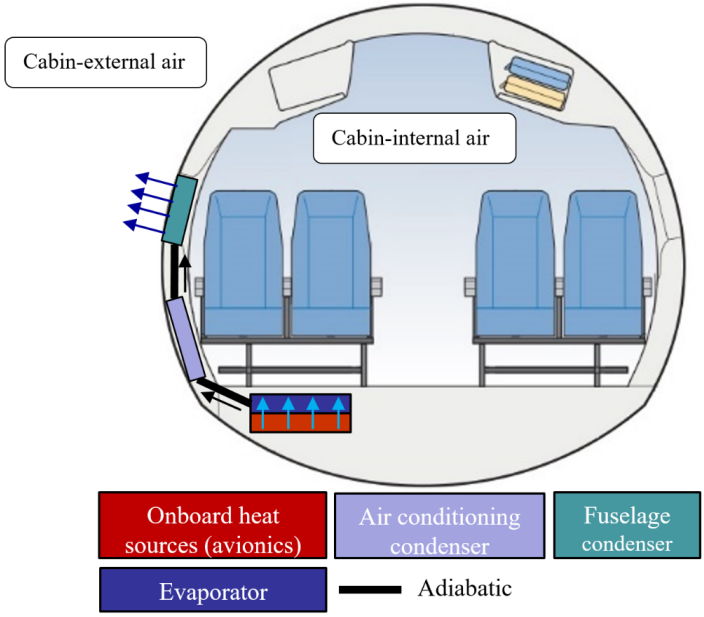

Figure 3 – Schematics of the heat path from onboard heat sources to the air conditioning and the fuselage condensers.

Table 2 – Typical temperatures for cold, standard and hot days.

Temperature	Cold day	Standard day	Hot day
Fuselage in cruise*, [ºC]	-62	-45	-20
Fuselage on-ground, [ºC]	-29	29	59
Air conditioning, [ºC]	57.2	18	1.7
Cabin-internal air, [ºC]	-15	29	55

Source – ASHRAE [15], RTCA DO-160G [4].

* Temperatures for an altitude of 9.1 km above sea level.

2.2 AEROSPACE COOLING SYSTEM REQUIREMENTS

According to the International Standard Atmosphere (ISA), under cruise flight conditions the unpressurized external air of a typical aircraft can achieve temperatures of approximately -60 ºC at the tropopause (11 km above seal level) [9]. Zhang *et al.* [14] reported an average external convective heat transfer coefficients on the whole fuselage length of approximately 332 W/(m^{2}K) in-flight. On the ground, however, natural convection takes place and temperatures vary according to the season and location. In this case, heat transfer coefficients for natural convection are dependent on the inclination angle, surface dimensions, fluid, temperature and atmosphere pressure [16,17]. Typical values for air natural convection vary roughly from 1 to 5 W/(m^{2}K).

The cabin-internal air is here represented by the air flux inside the air conditioning ducts. Cabin-internal temperatures of approximately 20 ºC are usual due to human comfort requirements. Air speeds can be as high as 20 m/s to satisfy internal cooling needs, and can be zero if the cabin refrigeration is switched off. In this case, natural convection will occur if a loop-thermosyphon condenser is positioned inside the duct.

A multitude of thermal conditions can take place for a cooling system with condensers exposed to the aircraft cabin-external air and to the aircraft cabin-internal air. Natural convection, forced convection and a combination of both at the condensers may occur at different temperatures, and the proposed cooling system should be able to cope with these variations.

2.2.1 Working fluid properties

The heat transfer capacity of thermosyphons and heat pipes is dependent on the working fluid applied. A measure of the influence of the working-fluid properties on the temperature drop for a given rate of heat transfer is provided by a figure of merit, $\aleph$. The figure of merit for thermosyphons, $\aleph_{th}$, is defined as [12]:

$$\aleph_{th} = \left(\frac{k_l^3 \sigma_l h_{lv}}{\mu_l} \right)^{1/4} ; \tag{2.1}$$

where σ_l, k_l, μ_l and h_{lv} stand for surface tension, thermal conductivity, dynamic viscosity and latent heat of vaporization, respectively. The subscript l denotes the value for the saturated liquid.

To obtain the best performance for the heat transfer, $\aleph_{th}$ should be maximized. Values of $\aleph_{th}$ for a series of fluid refrigerants commonly applied in thermosyphons are given in Fig. 4.

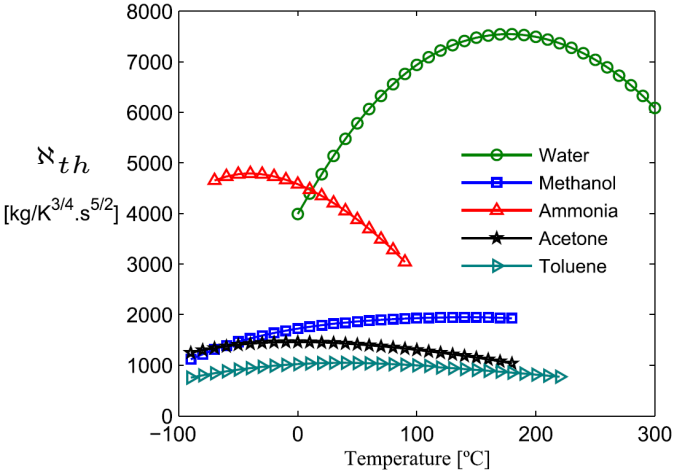

Figure 4 – Figure of merit for thermosyphons.

It should be noted that the wide temperature range covers all possible values for the air stream outside the aircraft in-flight or on the ground. It can be observed in Fig. 4 that water provides the highest mean value for temperatures above 0 ºC, whereas ammonia give the highest values for subzero temperatures.

While the ℵ value is a useful guide, it is not the only criterion for the selection of the working fluid. Other factors such as vapor pressure and the compatibility of materials, including fluid stability, are also important considerations [12, 18].

Non-toxic and fireproof working fluids inside cooling systems are desirable for aircraft applications. The design of an evacuation system could be necessary depending on the aircraft certification requirements and the fluid used. Therefore, the use of fluids such as ammonia, methanol, acetone, ethanol, toluene, R134a and R22 are discouraged. Water offers the greatest potential for application as a fluid (highest figure of merit, non-toxic, fireproof and low cost). However, subzero temperatures can freeze the fluid within the closed thermosyphon. Nevertheless, despite the freezing issue, water was selected as the working fluid in this study.

2.3 EXPERIMENTAL SETUP

In order to evaluate the present concept, a prototype was constructed and the cooling system requirements were reproduced. The experiments were performed at the Labtucal/Lepten laboratory of the

Mechanical Engineering Department at the Federal University of Santa Catarina, Brazil.

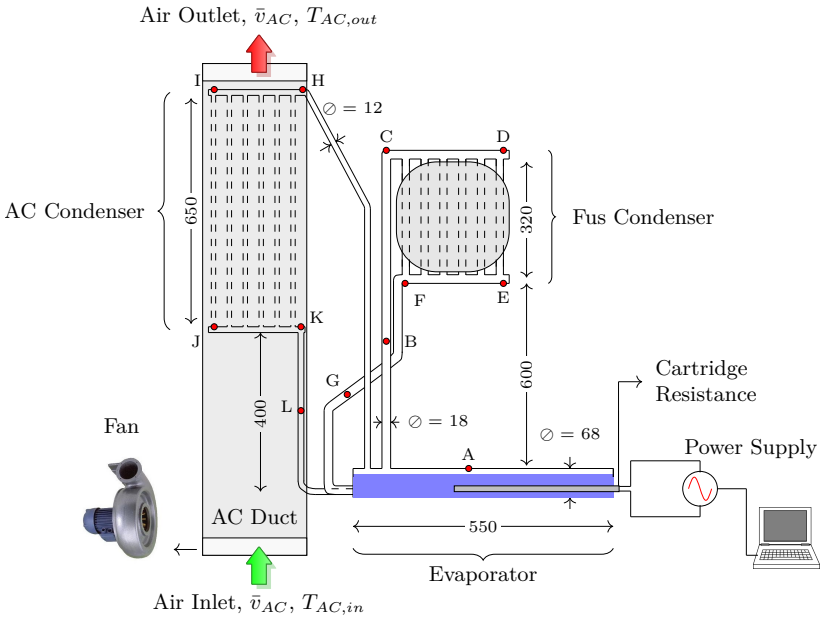

Figure 5 – Prototype illustration. Expressions Fus and AC stand for fuselage and air conditioning, respectively. Letters B to L designate temperature recording points. Main dimensions are shown in millimeters.

Fig. 5 shows a sketch of the prototype with the thermocouple positions (B to L). Two condensers (fuselage and air conditioning) are connected to the same evaporator by vapor and liquid lines. Expressions Fus and AC stand for fuselage and air conditioning, respectively. Each condenser consists of six parallel channels connecting inlet and outlet manifolds. After condensation takes place, liquid lines lead the liquid flow back to the evaporator base. The pipes, which comprise the condensers, were constructed according to the fuselage curvatures and space restrictions of a commercial aircraft. The air conditioning condenser pipeline was inserted inside an air conditioning system duct provided by Embraer S.A. Water and copper were used to ensure the fluid-material compatibility [18, 19]. A water volume of 0.85 L was placed into the evaporator after cleaning and vacuum operations. The total external area of the prototype is approximately 0.4 m^2. The external areas of the evaporator

and condensers are approximately 0.1 m^2 each, while the vapor and liquid lines are 0.07 and 0.03 m^2, respectively. Pipe outer diameters of 12 and 18 mm were applied to connect AC and Fus condensers to the evaporator, respectively.

The use of fins could enhance heat transfer by adding supplementary condenser area, and then improving the space arrangement within the aircraft which is intended to work as heat sink. However, the main reasons which prevented the use of fins at each condenser in this study are explained as follows. The prototype was designed to be installed at an Embraer 170 test aircraft for on-ground and in-flight tests. For safety reasons, the fuselage condenser cannot be directly exposed to the unpressurized air external to the aircraft. To satisfy the safety requisites, two aluminum blocks compress the copper pipes which comprise the fuselage condenser. The external surface of the outer aluminum block is milled with the same geometry of the aircraft passenger window, which allows integration with the aircraft fuselage structure. Thermal grease was applied to the copper pipes and the internal geometry of each aluminum block to decrease thermal contact resistance. Therefore, the presence of fins in the fuselage condenser would add extra complications to the aluminum milling process.

The prevention of fins in the AC condenser is justified as follows. The AC condenser was inserted within an AC system duct of an Embraer 170 test-aircraft. Two issues prevented the use of fins: the limited internal space of the AC duct which can prevent the complete prototype assembly, and the AC system design of the test-aircraft. Several AC ducts are linked to a common manifold. The use of fins can highly increase the pressure drop in the adapted AC duct. The installation of valves along the air circuit within the AC system is not handy or even allowed to our research group. If pressure drop is severely increased, the air stream will be redirected to other parallel AC ducts in the aircraft. As a consequence, the heat transfer can decrease in the AC condenser. The possibility of using fins at each condenser will be evaluated in a second generation of the prototype.

The temperature distribution was monitored by means of K-type thermocouples (TC), distributed according to Fig. 5. A National Instrument (SCXI-1000) data acquisition system was used to collect the data. A computer was employed to store the data and to control the experimental parameters. The letters from B to L designate temperature recording points whereas A represents the evaporator mean temperature determined from several measurement points along the evaporator. Ambient air temperatures were also obtained. Air velocity measurements at the air conditioning cross section, $\bar{v}_{AC}$, were acquired by hot wire

anemometry using a Kimo air velocity transmitter CTV 110 according to the Log-Tchebycheff rule [20]. The air flow rate was regulated by a centrifugal fan. Air speeds of up to 6.1 m/s were reached. The air inlet temperature was controlled by the internal laboratory refrigeration system, which could be reversed to work as a heating pump. Air velocity cross-section measurements revealed that the internal flow inside the duct had approximated mean velocities (1.5, 3.8 or 6.1 m/s). The effects of the flow entrance, duct curvature and short entrance length did not allow fully developed flow. The variable air flow rate promoted the indirect control of the heat transfer coefficients for the AC condenser.

A Lauda Proline thermal bath was used to control the heat transfer conditions at the fuselage condenser. This equipment can provide flow rates, $\dot{m}_{tb}$, and temperatures, T_{tb}, ranging from 0 to 25 L/min and -30 to 50 ºC, respectively. Heat is removed from the thermosyphon in the condenser fuselage by a heat exchanger, composed of two hollow aluminum blocks (see Fig. 6), which promotes contact of the circulating cooling fluid from a thermal bath with the copper pipelines. These aluminum blocks compress the copper pipes, which comprise the fuselage condenser setup. To achieve subzero temperatures, ethylic alcohol was employed as working fluid in the Lauda equipment. The alcohol solution exits the heat exchanger after crossing a distance within the aluminum block of approximately 4 m. Omega thermal grease was applied to the copper pipes and the semi-cylinder holes of each aluminum block to prevent thermal contact resistance. Power is provided to the evaporator section by an embedded cartridge heater with an external area, A, of approximately 0.02 m^2. The input power is adjusted by voltage control through a TDK Lambda power supply (GEN 300-5). The thermocouple temperature measurement uncertainty was ±1.1 ºC and the heat input uncertainty was observed to be approximately 3%. The velocity uncertainties at AC cross section were roughly ±3.0%.

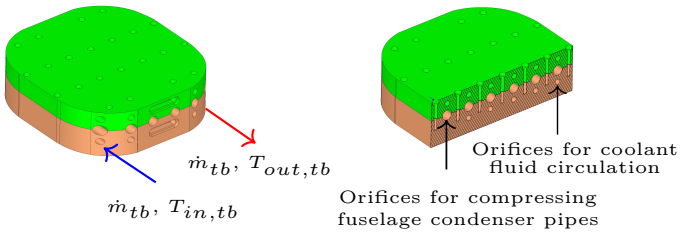

Figure 6 – Illustration of the heat exchanger assembly at the fuselage condenser. Coolant fluid circulates internally to the orifices.

2.4 EXPERIMENTAL PROCEDURE

Experiments were performed as follows. The prototype was tested under 15 different conditions as summarized in Table 3, with four main variations according to the condenser heat transfer mode: a) combined natural convection (case A1), b) forced convection at the fuselage and natural convection at the air conditioning system (cases A2-A10), c) forced convection at the air conditioning system and natural convection at the fuselage (cases A11-A13), and d) combined forced convection (cases A14 and A15).

Input power ranged from 100 to 900 W and power increments of 50 or 100 W were applied for the same test case. Each power step was kept constant for 30 min and then increased. This period was enough to achieve a quasi-steady regime only when the fuselage condenser was turned on. A wide range of temperatures (-30 to 50 ºC) was applied to the fuselage condenser with three flow rates: 0.0, 3.6 and 14.3 L/min. The air stream temperature of the air conditioning duct entrance was kept at 20 ºC. The inlet air stream mean velocities were adjusted to 0.0, 1.5, 3.8 and 6.1 m/s. It should be noted that cases A2-A10 and

Table 3 – Laboratory experiment conditions for the cooling system prototype. Input power ranged from 100 to 900 W with increments of 100 or 50 W in each case.

Case	AC inlet setting	Fus inlet settings		Aircraft representative
	$\bar{v}_{AC}$, [m/s]	$\dot{m}_{tb}$, [L/min]	T_{tb}, [ºC]	operation
A1	0.0	0.0	20	On-ground
A2	0.0	3.6	50	In-flight
A3	0.0	3.6	40	In-flight
A4	0.0	3.6	30	In-flight
A5	0.0	14.3	20	In-flight
A6	0.0	14.3	10	In-flight
A7	0.0	14.3	0	In-flight
A8	0.0	3.6	-10	In-flight
A9	0.0	14.3	-20	In-flight
A10	0.0	3.6	-30	In-flight
A11	1.5	0.0	20	On-ground
A12	3.8	0.0	20	On-ground
A13	6.1	0.0	20	On-ground
A14	3.0	3.6	-30	In-flight
A15	6.1	3.6	-25	In-flight

A14 and A15 approach in-flight conditions, while cases A1 and A11-A13 resemble on the ground conditions. In real situations, which mean during flights, the air conditioning system is always switched on, however, cases A6-A10 mainly represent low temperature at the fuselage reached in cruise conditions while cases A2-A5 represent temperatures during climb or descent attitudes.

2.5 RESULTS

2.5.1 AC and Fus condensers in natural convection: Case A1

Fig. 7 shows the evolution of the mean temperature for the evaporator (A), fuselage vapor line (B), air conditioning vapor line (H), fuselage liquid line (G) and air conditioning liquid line (L) for case A1. Heat is removed from AC and Fus condensers by natural convection. The input power to the evaporator, which is shown on the RHS of the Y-axis, ranges from 250 to 400 W with increments of 50 W. Evaporator and vapor line mean temperatures vary almost linearly. Temperatures of up to 73 ºC are reached with 400 W. The liquid line mean temperatures are lower (between 50 and 60 ºC) at the same power. The differences between the liquid and vapor mean temperatures (ca. 15 ºC) indicate that each condenser is operating in loop.

Heat transfer coefficients of approximately 3.5 W/(m^{2}K) have

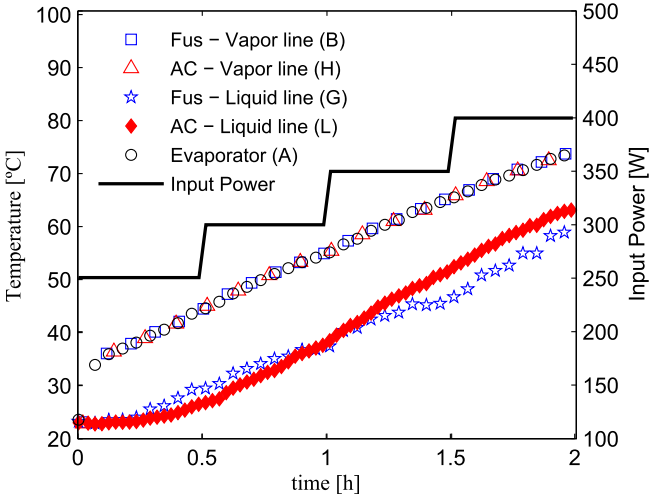

Figure 7 – Effect of the input power on the thermal behavior of the cooling system with both condensers turned off (case A1).

been reported for natural convection at vertical plates by Raithby and Hollands [16]. The mean heat transfer coefficients for the bottom and top of horizontal plates were 1.5 and 5 W/(m^{2}K), respectively [17]. For rough heat transfer modeling, it is here convenient to assume mean coefficients of 3.5 W/(m^{2}K) for the overall external prototype area.

Assuming an environment air temperature of 20 ºC and considering the external area of each condenser (approximately 0.1 m^2 for the air conditioning condenser and 0.2 m^2 for the external area of the aluminum blocks) it is possible to estimate the expected heat transfer rate. At an input power of 400 W the vapor reaches the inlet condensers at approximately 70 ºC. Assuming a constant flow temperature along the condensers (70 ºC), heat is removed at rates of 35.0 and 17.5 W by the fuselage and air conditioning system, respectively. Clearly, the external thermal resistance is high enough to promote high temperatures in the cooling system with reduced input power. A transient condition is observed. The water vapor mass increases in the cooling system and the latent heat, q_{lat}, mostly explains the gap between the heat transfer rates and the electrical power input. Equation (2.2) illustrates this heat balance:

$$q_{in} = q_{AC} + q_{Fus} + q_{lat}; \tag{2.2}$$

where q_{in}, q_{AC}, q_{Fus} and q_{lat} stand for input power from the electrical resistance, heat removed from the air conditioning system, heat removed from the fuselage and vaporization latent heat, respectively.

2.5.2 Fus in forced and AC in natural convection: Cases A2-A10

Cases A2-A4 are not expected for cruise flight conditions at high altitudes regardless of the season. High fuselage temperatures (30 to 50 ºC) are only expected during approach or climb in low altitudes. However, to investigate the cooling system in depth, these thermal conditions are also reported. Since the results for cases A2, A3 and A4 are similar, the presentation of only one case within this set is sufficient to illustrate the main results.

In Fig. 8, the results for case A3 are presented. The mean temperature evolution for the evaporator, vapor and liquid lines are shown in the LHS of the Y-axis whereas the corresponding input power to the evaporator is shown on the RHS. For time $[h] < 0.45$, the mean temperatures in the evaporator increase at a high rate (1.0 ºC per 8 W) up to 46 ºC at 200 W. For an input power of over 200 W, the mean temperature of the vapor in the cooling system increases at a rate of ca. 1 ºC per 67 W. At this stage, heat is properly removed by the fuselage condenser,

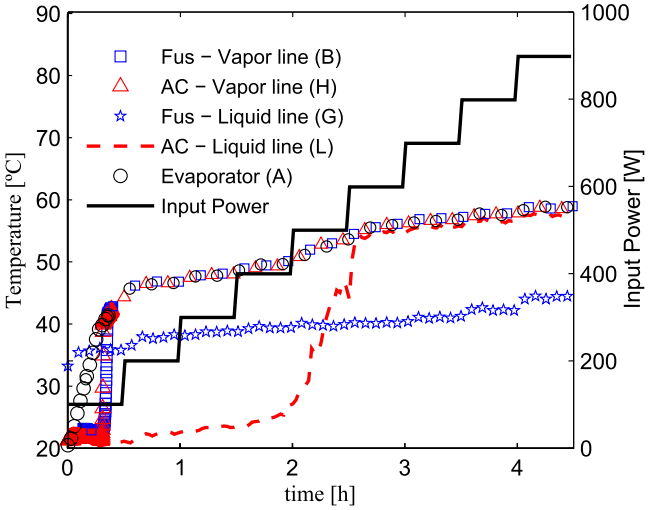

Figure 8 – Effect of the input power on the thermal behavior of the prototype with fuselage condenser on and air conditioning system in natural convection (case A3).

which operates as a loop-thermosyphon (note the temperature difference between the fuselage vapor inlet-B and liquid outlet-G). The operation system temperature (mean temperature of the vapor) is kept at 56 ºC at 900 W. For cases A2 and A4, vapor temperatures of approximately 63 and 53 ºC, respectively, are reached at 900 W. Observe that the fuselage liquid line shows temperatures close to the thermal bath settings (40 ºC). This shows that the fuselage condenser can perform reasonably at higher input power. It can be noted vapor presence in the AC liquid line for a power of over 500 W (see dashed line in Fig. 8). After this point, only sensible heat is removed in the AC system, and the AC loop does not work properly as a two-phase flow mechanism.

Fig. 9 compares the input power to the heat removal from the cooling system for case A3. The rate of heat transfer by natural convection was estimated considering the total area of the cooling system (evaporator, aluminum external area, air conditioning condenser, and vapor and liquid lines) and the corresponding mean temperatures for each above-mentioned area. The heat transfer coefficient for natural convection was taken as 3.5 W/(m^{2}K) as previously explained. Heat removal by natural convection is only a small fraction of the total input power (see diamonds in Fig. 9). The rate of heat transfer to the thermal bath is obtained by measuring the flow rate, and the entrance and exit temperatures for the fluid refrigerant

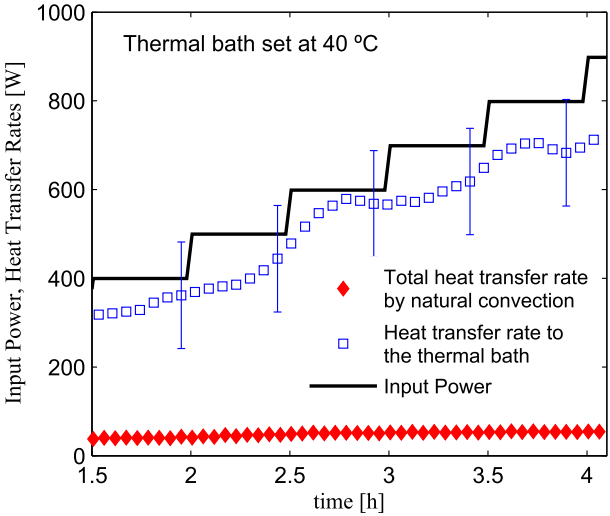

Figure 9 – Heat transfer rates to the thermal bath for case A3.

(see squares in Fig. 9). This figure shows that the fuselage condenser works appropriately as a heat sink. The sum of both heat parcels corresponds to the input power within the measurement error. Error-bars for the heat transfer to the thermal bath are estimated with the aid of the standard error within 95% confidence intervals; see Holman [21] and Coleman and Steele [22].

Cases A5-A7 aim to reproduce in-flight conditions at low altitudes on hot days, without forced convection on the air conditioning condenser. Fuselage temperatures ranged from 0 to 20 ºC. At 900 W, vapor temperatures of approximately 48, 45 and 43 ºC were obtained for cases, A5, A6 and A7, respectively.

Since the results for cases A5, A6 and A7 are similar, only one case within this set needs to be reported to illustrate the main results. The results for case A7 are shown in Fig. 10. The mean temperature in the evaporator and vapor lines reached 32 ºC at 100 W and slowly increased to 43 ºC at 900 W (1 ºC per 73 W). Heat is properly removed at the fuselage condenser, which operates as a loop-thermosyphon (note the temperature difference between the fuselage vapor inlet and liquid outlet). No relevant phenomenon was noted for the water within the fuselage condenser with the thermal bath set to 0 ºC.

Fig. 11 compares the input power and the heat removal from the cooling system for case A7. The rates of heat transfer by natural convection

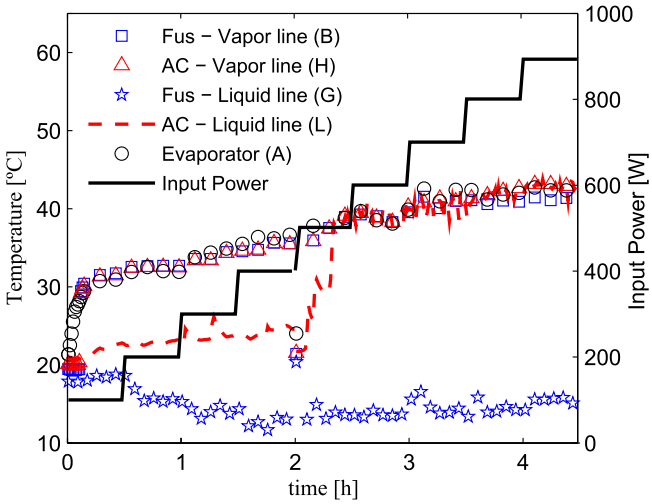

Figure 10 – Effect of the input power on the thermal behavior of the prototype with fuselage condenser on and air conditioning system in natural convection (case A7).

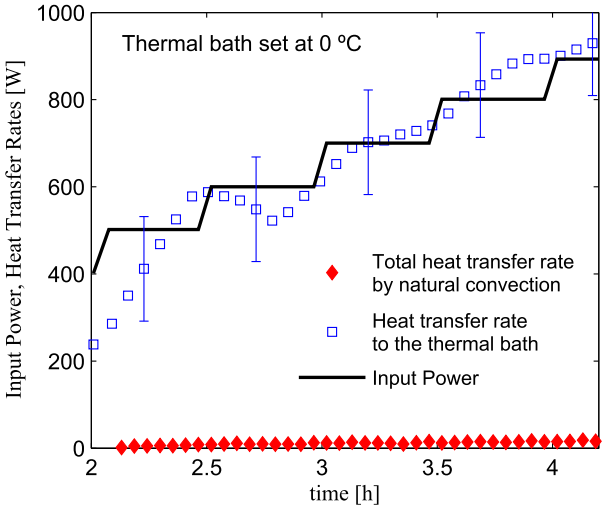

Figure 11 – Heat transfer rates by convection to the thermal bath for case A7.

and to the thermal bath were estimated in the manner described above. The heat removed by natural convection represents only a small fraction of the total input power (see diamonds in Fig. 11). Heat is mainly transferred

to the thermal bath; the fuselage condenser works appropriately as a heat sink. Note that the air conditioning condenser does not work properly as a two-phase flow mechanism for powers over 500 W. Vapor is observed to be present in the AC liquid line (see dashed line in Fig. 10).

Cases A8-A10 reproduce in-flight conditions at the fuselage condenser where the temperatures ranged from -30 to -10 ºC. Case A9 was chosen to illustrate the main results. At 800 W, vapor temperatures between 40 and 42 ºC were obtained for these experimental cases. Temperatures for the liquid lines as a function of the input power are shown in Fig. 12 for case A9. Fig. 13 shows temperatures of the evaporator and vapor lines also for case A9.

It can be noted that the temperature at the central point of the AC liquid line (L in Fig. 5) approaches that of the evaporator and vapor lines for an input power of over 500 W, indicating that the maximum heat removal capacity of the AC condenser was reached for an input power of 500 W. Heat removal occurs mostly at the fuselage heat sink in a fashion similar to that observed in Figs. 9 and 11.

Water inside the fuselage condenser is frozen during the startup and for an input power of less than 400 W. This can be noted in the temperature recordings at the fuselage liquid circuit in Fig. 12. Temperatures at the exit and at the closed-end of the fuselage outlet manifold (points

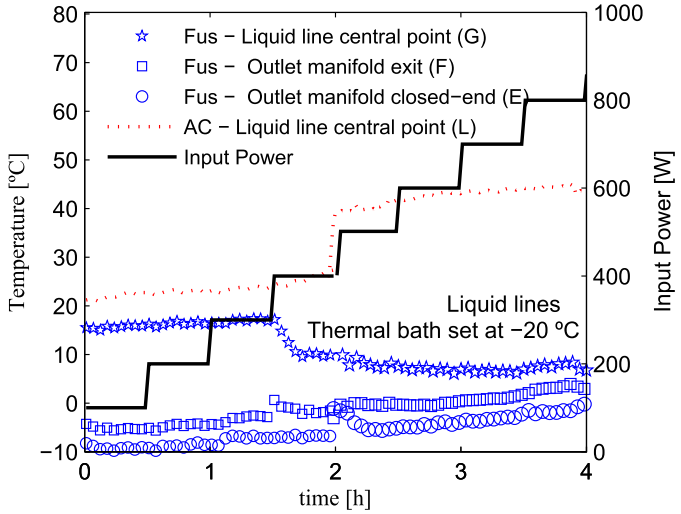

Figure 12 – Effect of the input power on the liquid returning lines temperatures for case A9.

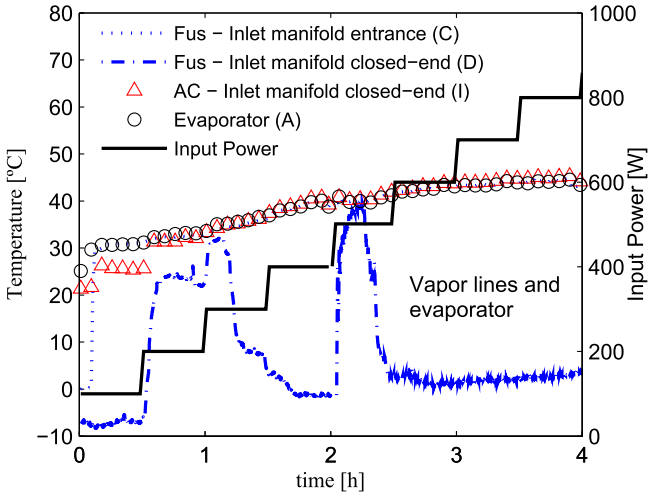

Figure 13 – Effect of the input power on the inlet manifolds and evaporator temperatures for case A9.

F and E, respectively, in Fig. 5) are below 0 ºC during the start-up. At the center of the fuselage liquid line (point G in Fig. 5), the temperature is reduced from 15 to 5 ºC during the experiment. This temperature reduction is abrupt and only occurs at 400 W, when the temperature is 0 ºC at the outlet manifold exit (Point F). The water melting allows the heat sink at the fuselage to work as a loop-thermosyphon and promotes a temperature reduction at point G at 400 W.

Temperatures at the evaporator and at the entrance of the fuselage inlet manifold (points A and C in Fig. 5) remain similar, whereas the temperature at the end of the fuselage inlet manifold (point D) varies intermittently between the evaporator temperature and 0 ºC; see Fig. 13. Note that point E is kept below 0 ºC, whereas point F is above 0 ºC for an input power greater than 300 W; see Fig. 12. Only the first channels of the fuselage heat sink seem to actually work as a loop.

2.5.3 Fus in natural and AC in forced convection: Cases A11-A13

Cases A11-A13 represent possible thermal conditions on the ground considering environment temperatures of approximately 20 ºC. The air conditioning condenser performance is evaluated for air velocities up to 6.1 m/s. Only one case within this experimental set is presented to show the main thermal characteristics.

Fig. 14 shows the evolution of temperatures for case A13. The

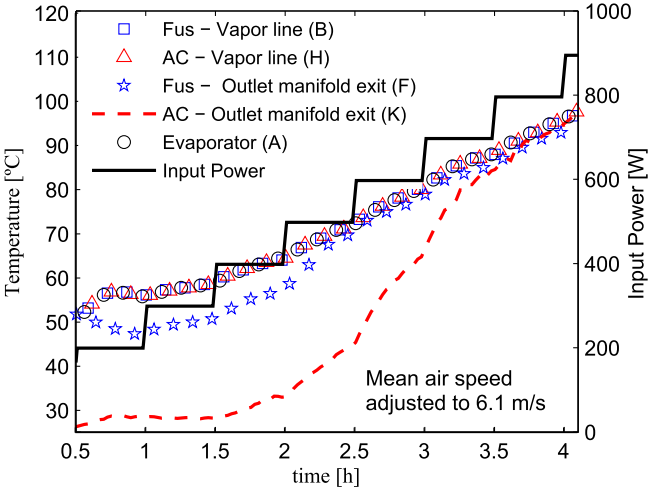

Figure 14 – Effect of the input power on the thermal behavior of the cooling system with the fuselage and AC condenser in natural and forced convections, respectively, for case A13.

corresponding input power to the evaporator is shown on the RHS of the Y-axis. The mean temperatures at the evaporator and the vapor lines are nearly coincident and increase almost linearly at over 300 W. The mean temperature of the evaporator reaches 100 ºC when 900 W is provided by the electrical resistance. A temperature of 100 ºC is achieved with 700 W for case A11 and with 800 W for case A12.

At the fuselage, the outlet manifold exit temperature almost coincides with the vapor line temperature for a power of over 500 W. At the air conditioning system, this occurs for a power of over 700 W. The vapor mass in the cooling system will increase with increasing input power. The rate of heat transfer to the air conditioning system is obtained by measuring the flow rate, and the entrance and exit temperatures of the air stream. When the vapor line reaches 100 ºC (at approximately 900 W input power), nearly 350 W are removed at the air conditioning condenser. At 100 ºC, the overall rate of heat transfer by natural convection is estimated to be 100 W. A transient condition is observed. Water vapor mass increases in the cooling system and latent heat, q_{lat}, mostly explains the gap between the heat transfer rates and input electrical power.

2.5.4 Fus and AC condensers in forced convection: Cases A14 and A15

Cases A14 and A15 simulate the thermal behavior for in-flight conditions, assuming that the fuselage condenser is exposed to temperatures of -30 and -25 ºC. The air conditioning condenser performance is evaluated with mean air velocities of up to 6.1 m/s. The air stream temperature at the duct inlet is 20 ºC. Only one case suffices to show the main characteristics of this test condition.

Fig. 15 shows the temperature distributions for the liquid lines and Fig. 16 for the evaporator and vapor lines for case A14. At 900 W, vapor temperatures of approximately 42 ºC were obtained for cases A14 and A15.

As observed in case A9, the temperature in the AC liquid line central point (letter L in Fig. 5) approaches the evaporator and vapor lines for an input power of over 500 W, indicating that the the maximum heat removal capacity of the AC condenser was reached at this power level. Water is frozen inside the fuselage condenser during the start-up and for an input power of less than 400 W. The temperature at the end of the fuselage condenser inlet manifold (point D in Fig. 5) varies intermittently (see Fig. 16). Only the first channels of the fuselage heat sink appear to actually work in a loop. This indicates that the total heat removal capacity of the fuselage heat sink is above 900 W. The general

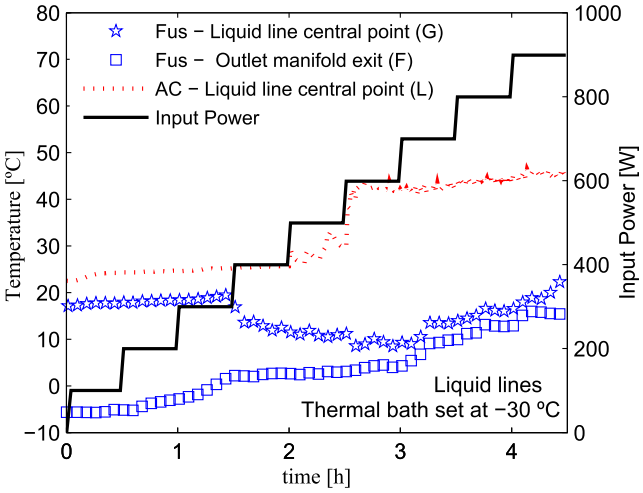

Figure 15 – Effect of the input power on the liquid returning lines of the cooling system with both condenser in forced convection (case A14).

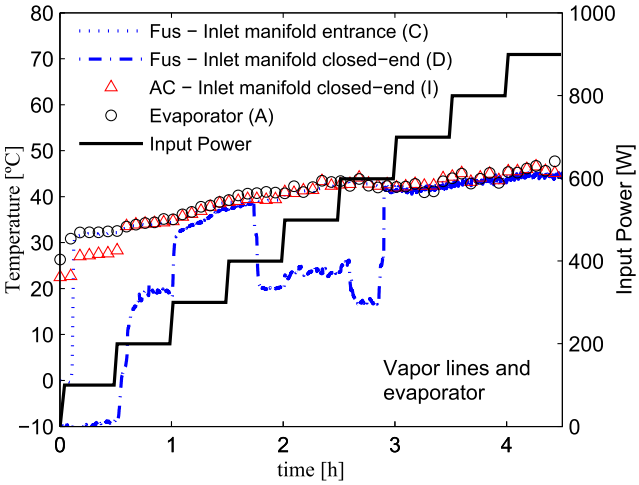

Figure 16 – Effect of the input power on the vapor lines and evaporator temperatures of the cooling system with both condensers in forced convection (case A14).

cooling system behavior for case A14 is similar to that shown in case A9 (see Figs. 15 and 16). For the sake of brevity, the reader is referred to section 2.5.2 for more information.

When the fluid refrigerant temperature is adjusted to -30 ºC (case A14, for instance) the thermal bath is able to remove limited power due to the low bath temperature. The heat removal capacity increases with increasing temperature in the thermal bath. As a consequence, the fluid temperature in the bath will increase if the heat removal exceeds a certain level of input power. In Fig. 15 for an input power of over 600 W, the thermal bath cannot be kept at -30 ºC. This explains also why temperatures in the fuselage liquid line rise to over 700 W (after 3 h).

The heat removal from the cooling system is compared to the input electrical power for case A14 in Fig. 17. The heat transfer rate by natural convection can be neglected in the analysis (see diamonds in Fig. 17). The heat transfer rate to the air stream increases for a power of over 500 W, but this is minor compared to the heat removal capacity at the fuselage. Less than 100 W of heat is removed from the AC with an electrical power supply of 900 W. The heat removal capacity of the fuselage heat sink is dominant. The sum of all heat parcels correspond to the input power within the measurement error.

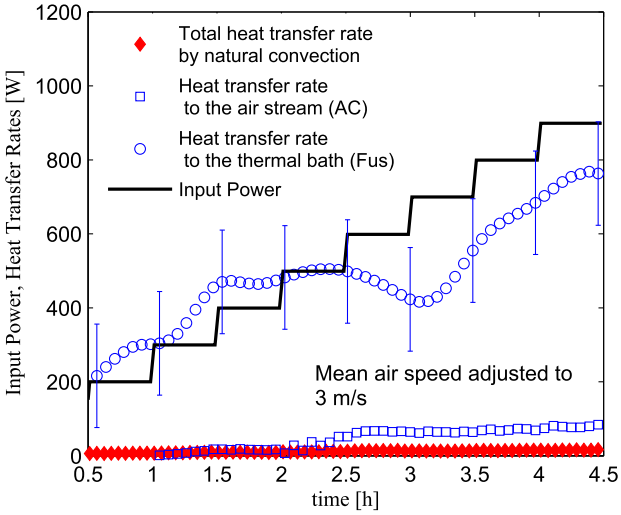

Figure 17 – Heat transfer rates to the thermal bath at the fuselage and to the air stream at the air conditioning duct for case A14.

2.6 DISCUSSION

The worst working scenario for the proposed heat exchanger is when the condensers are required to dissipate heat by natural convection. Temperatures of up to 75 ºC were reached with 400 W of input power. Considering the prototype external area (ca. 0.5 m^2 including the aluminum blocks) is exposed to ambient air at 20 ºC and the heat transfer coefficients are approximately 3.5 W/(m^2K), the total heat removal capacity is below 100 W. Most of the input power was absorbed as latent heat and the vapor mass increased within the cooling system.

When forced convection acts in the fuselage and the air conditioning system is off (cases A2-A10), evaporator temperatures rise at a rate of 0.125 ºC/W for input powers of between 100 and 200 W. For an input power of over 200 W, the evaporator temperatures rise at a rate of 0.014 ºC/W. This level of power is an indication of start-up for the prototype under in-flight conditions. The evaporator temperatures ranged from 63 to 40 ºC at 900 W with variations in the thermal bath temperature from 50 to -30 ºC.

The heat transfer coefficients, which were imposed on the fuselage condenser, can be estimated considering in-flight conditions. The air temperature is taken as the bath setting temperature. The fuselage condenser temperature was measured. The external condenser area is ca. 0.1 m^2.

The rate of heat transfer of the thermal bath was measured considering the ethylic alcohol mass flow rate and the entrance and exit temperature difference, and heat transfer coefficients of approximately 200 W/(m^{2}K) were observed. Zhang *et al.* [14] reported mean external convective heat transfer coefficients under in-flight conditions of 332.47 W/(m^{2}K). Therefore, from the present data, one can state that the fuselage condenser can work appropriately as a heat sink. Refrigeration by the fuselage can reduce the air conditioning requirements and therefore decrease the environmental control system cooling demands.

Cooling system malfunction is not observed when the water inside the fuselage condenser is frozen. The system was able to properly remove heat even when the fuselage was not operating as a loop-thermosyphon, keeping the evaporator temperature below 45 ºC (see Fig. 16, for example). Note that temperatures at the evaporator do not rise sharply. Electronic bays within an air airplane would only fail if they surpass temperatures approximately 70 to 100 ºC.

Observe that freezing at the fuselage condenser only occurs if the input power to the evaporator is low; e.g. approximately 300 W. At the fuselage condenser and with this power or below condensation, freezing and melting may occur simultaneously in the parallel channels. Heat is also removed in the AC condenser and temperatures at the evaporator are kept below 45 ºC. When the input power to the evaporator is continuously increased (equal or greater than 400 W), the system works once again as a stable loop-thermosyphon at the fuselage. It was shown that only the fuselage condenser could easily handle input power as high as 1 kW.

During flight, the air static temperature outside the aircraft can be as low as -60 ºC. Freezing, however, should not be a problem at these conditions. If the prototype geometry was kept the same, the only expected difference would be the increase in the input power which promotes water melting at the fuselage in order to achieve a stable loop-thermosyphon. Notice that a heat balance in the prototype is affected by the areas of each condenser, the heat transfer coefficients externally to these areas, the temperatures of the streams inside the AC duct and outside the aircraft, and the mean prototype temperature. These variables will determine the minimal input power to the evaporator which will avoid freezing at the fuselage.

If heat sources need to be refrigerated on the ground, the air conditioning condenser acts with lower heat transfer coefficients than the fuselage. The evaporator temperature can reach 100 ºC with input power ranging from 700 to 900 W depending on the air speed within the duct (see Section 2.5.3). Heat transfer coefficients for the AC condenser vary from 30 to 50 W/(m^{2}K). Typical heat transfer coefficients for forced

convection in air vary from 10 to 100 W/(m^{2}K) [23, 24]. In this situation, the external area of the AC condenser needs to be optimized with fins. Air duct speeds of over 6.1 m/s will be necessary to reduce the mean temperature of the cooling system.

When the AC system is turned on under cruise flight conditions, the vapor temperatures in the cooling system reach 42 ºC at 900 W. Cooling system malfunction is not observed when water within the fuselage condenser is frozen (during the start-up and for an input power of less than 400 W). Clearly, heat removal by the fuselage condenser is preferred. Although the air conditioning was turned on, approximately 10% of the total input power was removed by the AC condenser with an input power of 900 W. Thus, it can be concluded that the heat removal capacity of the fuselage heat sink is dominant.

2.7 SUMMARY AND CONCLUDING REMARKS

A cooling system prototype was tested in laboratory in a system which resembles those of electronic equipment cooling applications. The heat exchanger prototype consists of loop-thermosyphons with two condensers and a common evaporator. A multitude of thermal conditions was evaluated by simulating condensers exposed to the aircraft cabin-external air and to the aircraft cabin-internal air. Combined natural convection, combined forced convection and a combination of forced and natural convection at each condenser were replicated. The fuselage condenser performance was tested at temperatures ranging from -30 to 50 ºC, while the heat transfer coefficient ranged from natural convection to values as high as 200 W/(m^{2}K). The air supply to the air conditioning condenser was kept at 20 ºC and the heat transfer coefficients ranged from natural convection to 50 W/(m^{2}K). An input power of up to 900 W was provided to the evaporator base by an embedded electrical resistance. The main conclusions of this chapter are:

- While the input power is mostly consumed by the latent heat of water vaporization in combined natural convection, the cooling system evaporator temperature should be less than 80 ºC for an input power of 0.5 kW;
- When forced convection acts in the fuselage and the air conditioning system is off, evaporator temperatures rise at a rate of 0.014 ºC/W during the start-up. Under in-flight conditions, evaporator temperatures can be as low as 45 ºC for 0.9 kW of input power;
- Cooling system malfunction is not observed when water inside the fuselage condenser is frozen. The system was able to properly

remove heat even when the fuselage was not operating as a loop-thermosyphon, keeping the evaporator temperature below 50 ºC;

- When heat sources need to be refrigerated on the ground, the air conditioning condenser external area should be optimized with fins. Air duct speeds of over 6.1 m/s are required to keep the cooling system mean temperature below 100 ºC for an input power of approximately 1 kW;
- When the air conditioning system is turned on under in-flight conditions, vapor temperatures in the cooling system reach 41 ºC at 900 W. The heat removal capacity of the fuselage heat sink is largely dominant (approximately 90%).

3 IN-FLIGHT TESTING OF LOOP THERMOSYPHONS FOR AIRCRAFT COOLING

The content of this chapter is based on the following article:

- OLIVEIRA, J. L. G.; TECCHIO, C.; PAIVA, K. V.; MANTELLI, M. B. H.; GANDOLFI, R.; RIBEIRO, L. G. S. In-flight testing of loop-thermosyphons for aircraft cooling. Applied Thermal Engineering, v. 98, p. 144-156, 2016.
  DOI:10.1016/j.applthermaleng.2015.12.008

3.1 INTRODUCTION

In the previous chapter, the thermal behavior of a novel passive heat exchanger proposed by Oliveira *et al.* [13] was investigated under limited laboratory conditions. The HES fuselage condenser was tested with temperatures ranging from 50 to -30 ºC. The simulated heat transfer coefficients were imposed by the thermal bath that pumped cooled refrigerant. Air with speeds of up to 6.1 m/s and at temperatures of approximately 20 ºC simulated the airplane air conditioning duct. However, laboratory testing cannot be completed as the effect of the flight maneuvers on the prototype behavior could not be tested.

In the present chapter, the fuselage condenser is submitted to real flight conditions, and so is subjected to actual aerospace heat transfer coefficients and temperatures (approximately -56 ºC) whereas the air conditioner condenser is tested with air speeds of approximately 10 m/s and temperatures ranging from 10 to 50 ºC. The HES presented in chapter 2 was installed in an Embraer test aircraft after some adaptation. The prototype was evaluated on the ground and during flight. Conventional commercial flight protocols were employed during the tests, which occurred at flight Mach numbers of 0.78 and at altitudes up to 12 km (40000 ft). The main idea was to evaluate the effects of common flight parameters during maneuvers, namely roll and pitch angles, angular velocities (pitch, yaw and roll rates) and aircraft acceleration, on the thermal performance of the prototype. A literature review is provided highlighting the major scientific contributions of the experimental work presented in this chapter.

3.2 PASSIVE HEAT TRANSFER TECHNOLOGIES AND AEROSPACE APPLICATIONS

Passive two-phase heat transfer technologies such as heat pipes, thermosyphons, loop-thermosyphons, capillary pumped loops, loop heat pipes and vapor chambers have been intensively investigated recently by Sharifi *et al.* [25]. Owing to their intrinsic efficiency in heat transport, applications of passive heat transfer devices have been considered in fields ranging from solar air conditioning and refrigeration systems to power-engineering applications with abrasive and corrosive atmospheres at temperatures as high as 1000 °C; see Moradgholi *et al.* [26] and Meisel *et al.* [27], for example. Energy recovery systems based on heat pipe technology were also subject of research; see Hu *et al.* [28], Yau and Ng [29], Tiari *et al.* [30], Zhang and Lee [31] and Siddiqui [32]. The technologies previously mentioned are essentially discriminated by the approach of the liquid return to the evaporator (by gravity, by capillary pumping or by a combination of both) and by the displacements of vapor and liquid streams which can be completely separated in a loop design or with counter-current vapor-liquid flows presenting higher design compactness but with higher friction losses.

Zuo and Gunnerson [33] modeled a steady-state performance of a closed thermosyphon and compared the results obtained with experimental data. The parametric effects of operating temperatures, geometry, working fluid inventory and condenser thermal capacity were studied as well. More recently, Jiang *et al.* [34] and Shabgard *et al.* [35] developed a numerical model to simulate the transient operation of a closed-thermosyphon with various working fluid filling ratios. The heat transfer coefficients and the overall thermal resistance were investigated by adding solid fractions to the working fluid. They observed that the overall thermal resistance decreased with increasing solid holdup. The latter simulated the transient operation of a thermosyphon with various working fluid filling ratios. For preventing breakdown of the condensate film, they concluded that the working fluid should occupy over 10% of the evaporator volume to assure a roughly optimal and stable steady-state operation.

An analytical model for a loop-thermosyphon for cooling air inside a telecommunication cabinet was proposed by Chehade *et al.* [36]. These authors considered the model a combination of thermal and hydraulic management of two-phase flow in the device. An experimental study was also conducted and the mean deviation between predictions of the theoretical model and measurements were less than 6%. Bojić and Lukić [37] studied experimentally a single thermosyphon with two

condensers. The authors concluded that the thermosyphon behavior was controlled by the heat added to the evaporator and by the condenser with higher heat transfer capacity.

For aerospace applications, loop-heat pipes have been mainly researched in the past decade. Lu and Wei [38] investigated the stability and heat transfer efficiency of a conventional loop-heat pipe with a flat rectangular evaporator. Their research was focused on establishing the conditions for proper system start-up. Experimental attempts of keeping the high performance of loop-heat pipes at distances of 10 m were studied by Mitomi and Nagano [39], while Nishikawara and Nagano [40] investigated the effects of properties of working fluids such as ethanol, acetone and R134a on the performance of a miniature loop-heat pipe. Sarno *et al.* [41] developed an alternative completely passive cooling system based on a two-phase technology including heat pipes and loop-thermosyphons adequately integrated inside the seat structure and using the benefit of the seat frame as a heat sink. This device allowed heat transfer rates of 10–100 W from in-flight entertainment systems to the heat sink.

3.3 EXPERIMENTAL APPARATUS AND PROCEDURE

The heat exchanger prototype evaluated in this study was presented and described in Chapter 2, Section 2.3; (see Fig. 5). For the sake of brevity, the setup description and working principle will not be repeated here.

In order to evaluate the prototype thermal performance in real flight conditions, the setup was installed in an Embraer aircraft at the Embraer flight test division located in Gavião Peixoto, São Paulo, Brazil. A photo of the prototype inside the aircraft is shown in Fig. 18.

Dimensions of the device were chosen respecting the aircraft restrictions and available space. In Fig. 18, the evaporator (1) was positioned in parallel with the aircraft roll axis. For reference, the aircraft tail is located at the left side of the evaporator. Fus condenser (2) was attached to the aircraft fuselage (4) through the window since a structural coupling could compromise the flight safety. The AC condenser is positioned inside the aircraft air-duct (3). Photographs of the fuselage condenser assembly are shown for the cabin interior in Fig. 19 and the outside of the aircraft in Fig. 20. Note that the aluminum blocks were milled to decrease the weight.

The temperature history was acquired by means of K-type thermocouples, distributed according to Fig. 21, and recorded on a computer. Flight test instrumentation (FTI) was used to monitor and record the

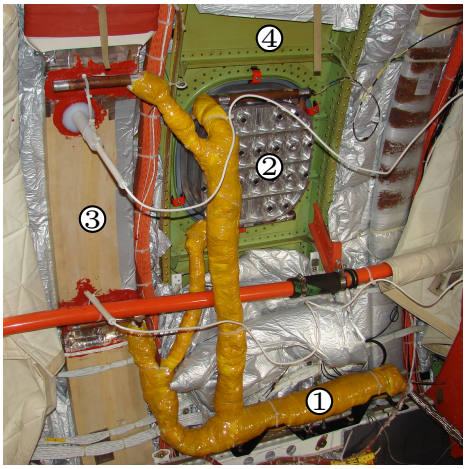

Figure 18 – Photograph of the prototype installed within the aircraft. Numbers denote heat exchanger evaporator (1), Fus-condenser (2), AC duct (3) and aircraft fuselage (4).

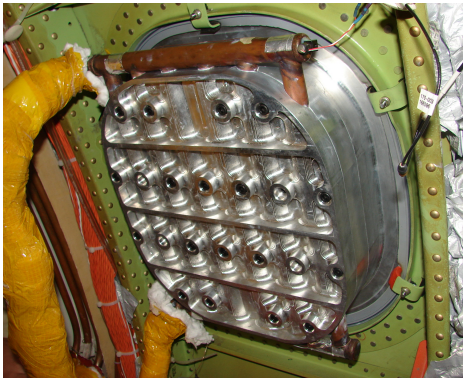

Figure 19 – Internal view of the fuselage condenser assembly.

experimental variables: temperature, cabin pressure, input power, aircraft acceleration and aircraft altitude. A computer was employed to store this data and to control the experimental parameters. The letters A–W in Fig. 21 designate the temperature recording points.

The aircraft cabin temperature, static external air temperature, and total external air temperature were also obtained. Insulation of the liquid and vapor lines as well as the evaporator section was provided using ceramic fibers; see Fig. 18. Power was provided to the evaporator

by an embedded electrical resistance. The input power was adjusted by voltage control through a TDK Lambda power supply (GEN 300-5). The heat input uncertainty was observed to be 3%. Air velocity measurements were taken at the air conditioning duct entrance (point V) and exit (point W) by hot wire anemometry (HWA) using a Kimo air velocity and temperature transmitter (CTV 110). The thermocouple measurement uncertainty was ±1.1 ºC, while the velocity and temperature measurement uncertainties of the transmitter were ±3% and ±0.5%, respectively.

Figure 20 – External view of the fuselage condenser assembly.

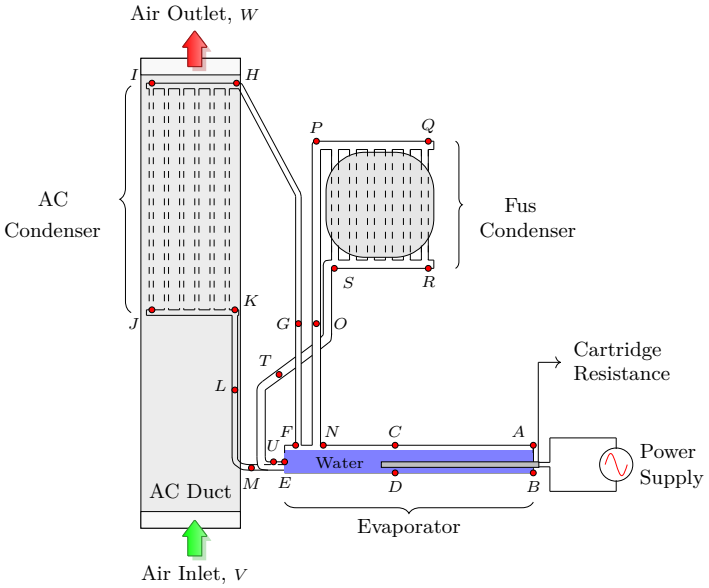

Figure 21 – Measurements sites in the setup. Letters A-W designate temperature recording points. Velocity was also recorded at points V and W.

3.3.1 Acceptance tests

In order to fulfill all the requirements imposed by the Radio Technical Commission for Aeronautics (RTCA) of Federal Aviation Administration (FAA), the prototype was submitted to constrained acceptance test conditions. The purpose of these tests is to define standard environmental test conditions and applicable test procedures for airborne equipment. The tests followed several RTCA/DO-160G [4] categories, including effects of the prototype temperatures on the aircraft system, effects of altitude, *e.g.* loss of cabin pressure on the testing device and support equipment as power supply and data acquisition system, as well as RF emission and susceptibility.

3.3.2 Test methodology

Experiments were performed under on-ground and in-flight conditions. Table 4 summarizes the main parameters of the experiments. On the ground, natural convection takes place in the fuselage condenser while heat is removed in the air conditioning duct by forced convection. In flight, forced convection acts in both condensers. The on-ground test took 1 h 30 min, and the flight lasted 2 h 30 min. The electrical heater input power ranged from 0 to 850 W. Further experimental details are given below.

Table 4 – In-flight and on-ground parameters.

Parameters	Flight	Ground
Cabin temperature, [ºC]	16 to 27	27
Input power range, [W]	0 to 850	0 to 850
Test time, [h]	2.5	1.5
Maximum Mach number	0.78	-
Altitude, [km]	0 to 12	-
Static air temperature, [ºC]	-56 to 27	27
AC air inlet temperature, [ºC]	10 to 50	10
AC air inlet velocity, [m/s]	10	10

3.4 EXPERIMENTAL RESULTS

3.4.1 Description of in-flight test

The in-flight test conditions were as follows. True air speeds of up to 878 km/h were registered, corresponding to a flight Mach number,

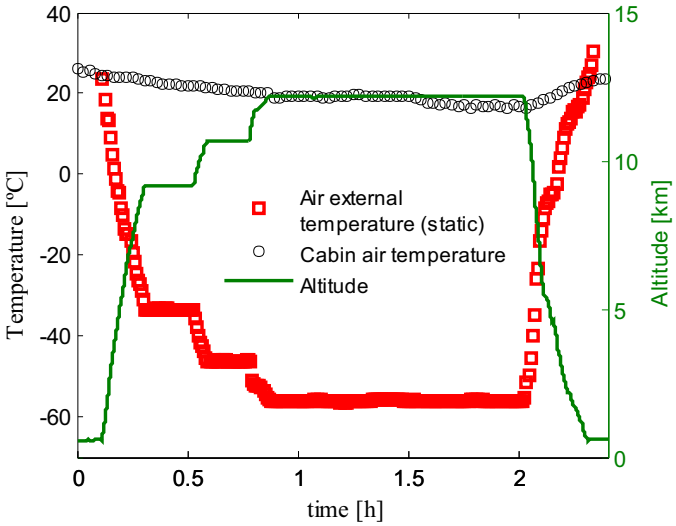

Figure 22 – Temperature profiles for the cabin and external static air during the flight.

M, of 0.78 at 8 km above sea level. The aircraft speed was varied above this height to keep the Mach number roughly the same. A static air temperature, T_∞, of -56 ºC was observed at 12 km altitude. The cabin air temperature ranged from 27 ºC on the ground to 16 ºC during the flight. These flight conditions are representative of commercial flights. The input power to the evaporator, q_{in}, varied in the range $0 < q_{in}[\mathrm{W}] < 850$ during the flight, which lasted 2 h 30 min. Fig. 22 shows the temperature profiles for the aircraft cabin and the external static air. The flight altitude is shown on the RHS.

Fig. 23 shows the flight attitude and the Cartesian coordinate system adopted. The X-axis is aligned with the aircraft nose, while the Y-axis is aligned with the wingspan and the Z-axis is orthogonal to the other two axes. Pitch, roll and yaw rotations are assumed for the Y-, X- and Z-axis, respectively.

The aircraft roll and pitch angles, angular velocities and accelerations are shown in Figs. 24, 25, 26, in that order. Pitch and roll angles ranged from -8º to 24º and -60º to 60º, respectively. Angular velocities alternated from -2.5 to 5 deg/s (pitch rate), -10 to 10 deg/s (roll rate), and -7 to 10 deg/s (yaw rate). The aircraft accelerations ranged from -0.83g to 0.27g (Z-axis), -0.14g to 0.14g (Y-axis), and -0.20g to 0.37g (X-axis). As shown in this chapter, the roll angle, angular velocities and aircraft

acceleration had little effect on the behavior of the heat exchanger. The pitch angle, however, did notably affect the heat exchanger performance.

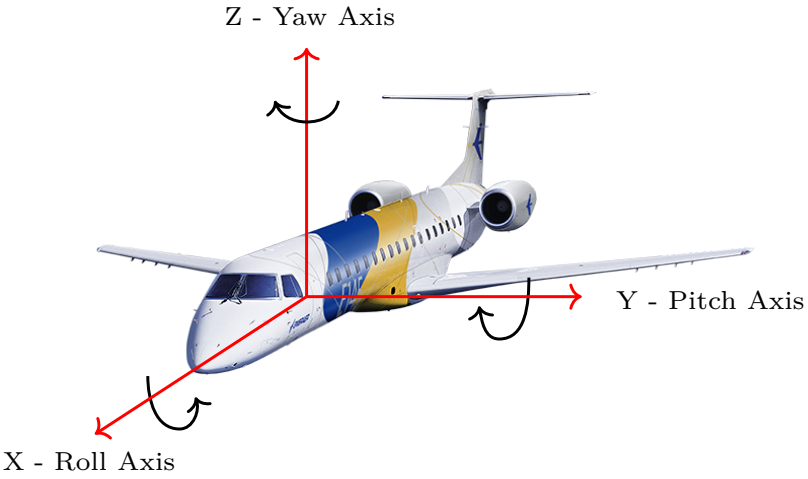

Figure 23 – Pitch, roll and yaw rotations represented in a cartesian coordinates system. The z-axis is anti-parallel to the acceleration due to gravity.

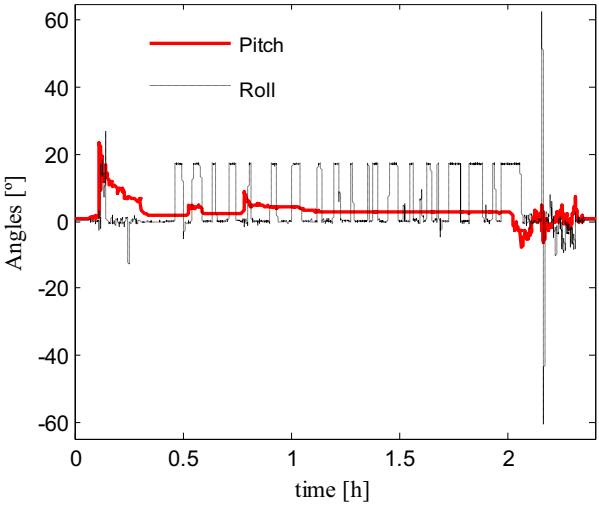

Figure 24 – Aircraft pitch and roll angles as a function of time.

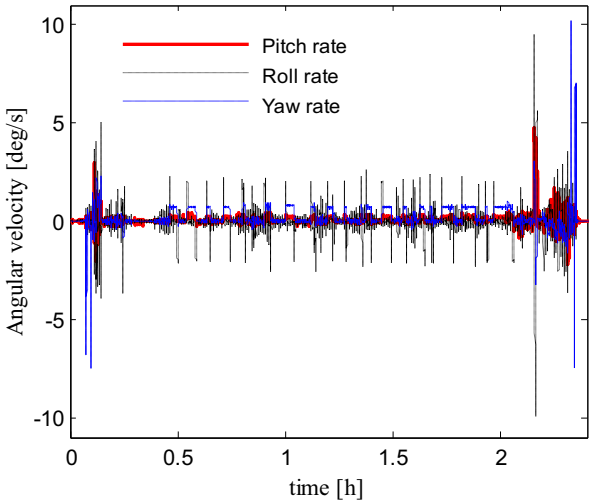

Figure 25 – Aircraft pitch, roll and yaw angular velocities as a function of time.

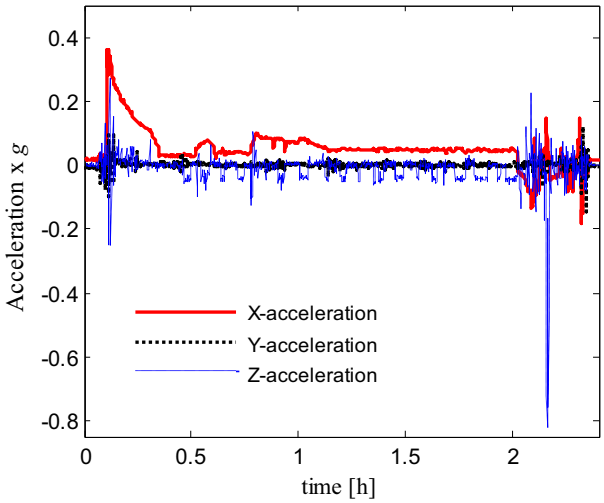

Figure 26 – Aircraft acceleration as a function of time.

3.4.2 In-flight results

3.4.2.1 Temperature distribution

The thermal performance of the evaporator is shown in Fig. 27. The input power was set at 850 W during takeoff at time ≈ 0.2 h. During the ascent, evaporator temperatures at points A and B (see Fig. 21) increased by over 100 ºC within a few minutes (see squares and triangles in Fig. 27), whereas evaporator temperatures at points C, D and E remained at approximately 45 ºC. Owing to pitch angles as high as 24º (see the solid line at time ≈ 0.2 h in Fig. 24) the electrical resistance at points A and B was not submerged and the evaporator region, where thermocouples C, D and E were installed, was flooded with water due to the liquid displacement. Therefore, the temperature of the vapor at points A and B increased quickly by 18 ºC/min. For safety reasons, the electrical resistance was turned off at time ≈ 0.25 h. When the pitch angle was less than 10º and the temperatures at points A and B were below 40 ºC at time ≈ 0.37 h, the input power was readjusted to 850 W. For time lags over 0.37 h, the pitch angle variations did not promote temperatures over 57 ºC at any point of the evaporator. Roll angle, pitch, roll and yaw rates, and X-, Y- and Z- aircraft accelerations did not affect the thermal behavior of the heat exchanger.

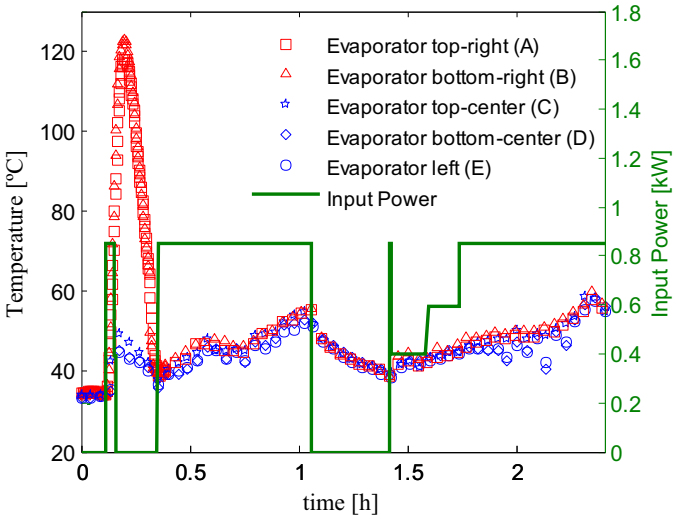

Figure 27 – Effects of input power and flight conditions on the thermal behavior of the evaporator.

It should be noted that the input power provided by the cartridge resistance varied during the flight, as represented by the solid line in Fig. 27. Variations in altitude (Fig. 22) allowed the heat exchanger to be evaluated at different static air temperatures and with different heat transfer coefficients. Even with the changes in the input power and in the external heat sink conditions, all points on the evaporator were kept at between 40 and 57 ºC for a time of over 0.37 h.

The vapor line temperatures are shown in Fig. 28. When the electrical power supply was readjusted to 850 W at time ≈ 0.37 h, temperatures along the AC vapor line (from points F to H in Fig. 21) were kept roughly at the same level as the evaporator temperatures (compare the curves in Figs. 27 and 28). An exception to this was that during the ascent, the resistance was turned off for safety reasons.

During the time interval between 1.05 h and 1.35 h, the power supply was turned off. During this time lag, the flight was kept at an altitude of approximately 12 km. Without input power the water inside the fuselage condenser became frozen, as the external surface of the aluminum block was subjected to static air temperatures of -56 ºC at Mach number of 0.78. The thermocouple located in the Fus inlet manifold close-end (point Q) registered temperatures below -6 ºC (see circles in Fig. 28).

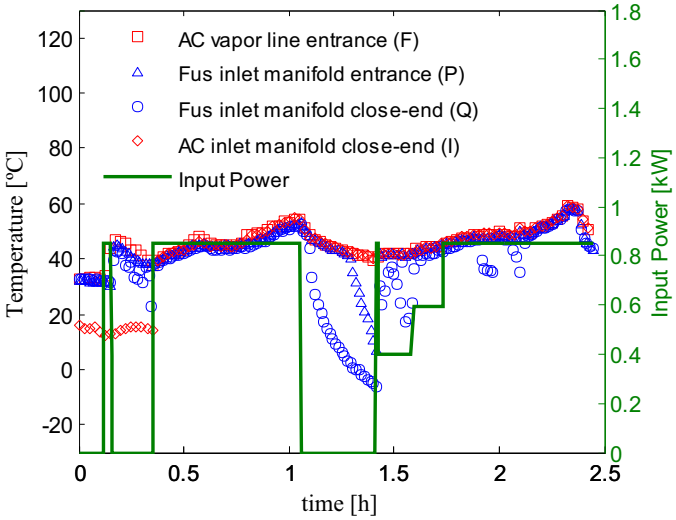

Figure 28 – Effects of input power and flight conditions on the thermal behavior of the vapor lines.

When the input power was adjusted to 400 W at time ≈ 1.4 h, water vapor was able to recirculate through the fuselage inlet manifold, which can be observed from the increase in the temperatures at points P and Q from approximately -5 to 35 ºC. When the input power was adjusted to 600 W at time ≈ 1.6 h, the temperatures along the fuselage inlet manifold (P and Q) were found to be similar to those of the evaporator.

Fig. 29 shows the thermal behavior of the liquid lines. For the period between 0 and 1.1 h, significant temperature differences between the AC inlet and outlet manifolds (red curves in Figs. 28 and 29) can be observed. After 1.1 h, temperatures in the AC inlet approach temperatures in the AC outlet manifold. The influence of the evaporator is detected in the conduit leaving the AC outlet manifold (point K). Temperatures at the center of the AC liquid line and at the AC liquid line return (points L and M, respectively) were similar to the temperatures of the evaporator (see triangles in Fig. 29) and thus, for the sake of simplicity, the temperatures of thermocouple L (see Fig. 21) are not shown.

The thermal behavior of the fuselage liquid line differs from that described above. When the power from the cartridge resistance was inactivated for the period between 1.1 h and 1.4 h, temperatures as low as -10 ºC were observed at the Fus outlet manifold (point S). The freezing process also occurred in the vapor line of the Fus condenser; see blue

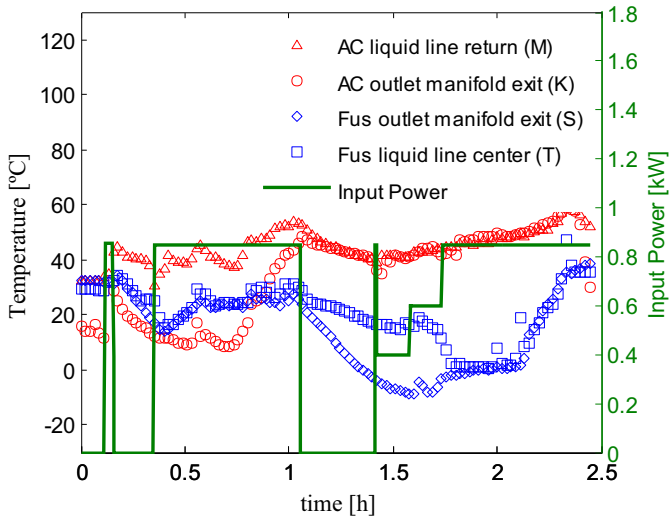

Figure 29 – Effects of input power and flight conditions on the temperatures of the liquid lines.

symbols in Fig. 28. The input power of 400 W at 1.4 h promoted melting in the Fus liquid line (thermocouple T). The Fus manifold temperatures (points S and T) were found to be above 0 ºC only at 1.8 h and with 600 W. It appears that the melting process is concluded when the temperature in the Fus liquid line central point (T) quickly decreased from 15 ºC to 0 ºC in the time period between 1.7 h and 1.8 h. This means that the vapor-liquid loop was reestablished in the fuselage circuit: cold water reached the central point of the liquid line and returned to the evaporator. It can be noted in Figs. 28 and 29 that the fuselage inlet and outlet manifolds show significant temperature differences. This is a clear indication that the fuselage condenser can easily handle input powers of over 850 W under the conditions tested.

3.4.2.2 Heat transfer at the air conditioning system

Measurements of air temperature and speed within the AC duct, as a function of the flight time, are shown in Fig. 30. Owing to cabin comfort requirements, the air stream temperature varies according to the external flight settings. During the airplane ascent and at low altitudes, the air stream temperature is kept between 10 ºC and 15 ºC. At time ≈ 1 h the altitude is approximately 12 km and the static air temperature is close to -56 ºC (see Fig. 22). Under these conditions, the air stream can enter the AC duct at over 50 ºC.

In the steady state, the heat flux to the AC air stream, q_{AC}, can be computed by:

$$q_{AC} = \dot{m} c_p (T_{out} - T_{in}); \tag{3.1}$$

where $\dot{m}$, c_p, T_{out} and T_{in} stand for average mass flow rate, specific heat at constant pressure and mean temperatures at the duct outlet and inlet, respectively. Considering the air mean velocity as 10 m/s, the air mass density as 1.21 kg/m^3 and the duct cross-section area as 0.007 m^2, $\dot{m}$ is roughly 0.085 kg/s. The specific heat for air is known to be approximately 1 kJ/(kg·K), and an estimation of q_{AC} is thus possible by considering the values of T_{out} and T_{in} given in Fig. 30. However, T_{out} and T_{in} matched within the measurement error. The error propagation of the temperature difference, $\Delta T = T_{out} - T_{in}$, is ±0.99 ºC. Therefore, only an estimation of the order of magnitude of q_{AC} can be provided. Assuming ΔT = 1 ºC, q_{AC} is approximately 85 W. Although this is a rough estimation, it suffices to show that only a small fraction of the input power was transferred to the AC duct.

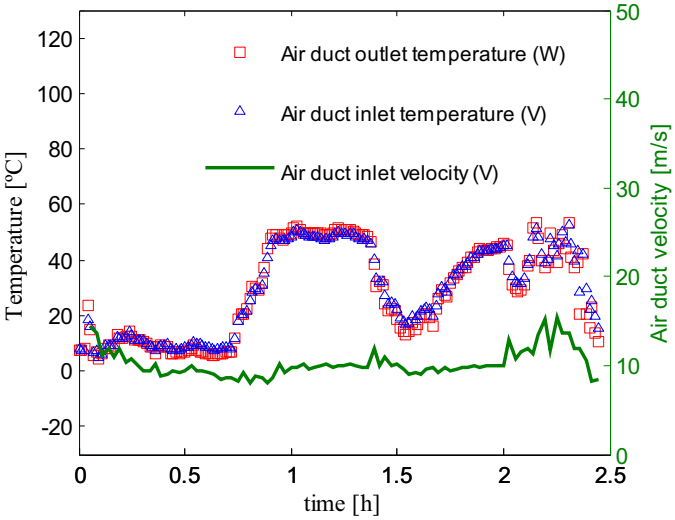

Figure 30 – Air stream conditions within the AC system. Symbols stand for temperature (LHS Y-axis) and solid line denotes the mean air velocity in the AC duct inlet (RHS Y-axis).

3.4.2.3 Heat transfer at the fuselage

Based on the flight results shown so far, it is possible to assess the fuselage heat transfer coefficients using the following equation, which represents the heat balance of the tested prototype:

$$q_{in} = q_{AC} + q_{Fus} + q_{TRAN}; \tag{3.2}$$

where q_{in}, q_{AC}, q_{Fus} and q_{TRAN} stand for, respectively, input power from the electrical resistance, heat removed from the air conditioning system, heat removed from the fuselage, and transient operation effects (sensible and latent heat). The external surfaces of the prototype were insulated and subjected to natural convection within the cabin; therefore, this heat parcel was neglected. Due to the low temperatures of the external surfaces of the apparatus, the radiation heat losses to the environment were also neglected. In this way, it can be admitted that all the heat added to the evaporation section is removed in the condensation section, either at fuselage or at the air conditioner. Note that after 1 h the heat input varied considerably and thus the vaporization and condensation could not be well balanced (see Figs. 27, 28 and 29). During this period, the following phase change mechanisms occurred: condensation, vaporization, freezing and melting.

On the other hand, during the time interval between 0.5 h and 1 h the input power was kept constant at 850 W and no freezing or melting occurred. In this period, the altitude was varied from 9 to 12 km and the external static air temperature varied from -35 ºC to -56 ºC (see Fig. 22), while the Mach number was approximately 0.78. By ignoring the transient effects, one can assume that the prototype is able to adapt instantly to the changes in the heat sink conditions. Note that the q_{AC} value for the in-flight period was estimated as a minor quantity in the previous section and therefore q_{Fus} is the only significant parcel on the RHS of Eq. (3.2). Based on these hypotheses and calculations, it is possible to compute the heat transfer coefficient for the external convective stream by:

$$q_{Fus} = hA\left(\overline{T}_{Fus} - T^*\right); \tag{3.3}$$

where h, A and $\overline{T}_{Fus}$ stand for, respectively, the convective heat transfer coefficient, the aluminum area exposed to the external air and the mean temperature at the external fuselage surface. The aluminum area can be approximated as 0.1 m^2 and q_{Fus} was calculated as 765 W. The conductive thermal resistance from the external aluminum area to the location where condensation occurs within the fuselage heat sink is unimportant, and therefore $\overline{T}_{Fus}$ can be approximated as the average temperature between the fuselage inlet and outlet manifolds. T^* is a characteristic temperature of the air stream and, as recommended in the ASHRAE handbook [15], it is defined as:

$$T^* = \frac{T_{AW} + T_\infty}{2} + 0.22(T_{AW} - T_\infty); \tag{3.4}$$

where T_{AW} is the adiabatic wall temperature or recovery temperature on the outer fuselage, which should be higher than the static air temperature (T_∞) due to the ram effect during flight; see Zhang *et al.* [14]. Therefore, T_{AW} can be evaluated as:

$$T_{AW} = T_\infty\left(1 + r\frac{\gamma - 1}{2}M^2\right); \tag{3.5}$$

$$r = Pr^{1/3}; \tag{3.6}$$

where r is the recovery factor for the turbulent boundary layer, γ the ratio of the specific heats, M is the aircraft Mach number, and Pr the Prandtl number. Values for the air properties as a function of height can be obtained from Cengel and Boles [42], and the aircraft instrumentation measurements of T_∞ are given in Fig. 22.

An estimation of the coefficient h is provided in Fig. 31. The effect of altitude on the heat transfer coefficient is evaluated for a Mach

number of 0.78 in the time period between 0.5 h and 1 h. The altitude and the air static temperature are also given together with the temperatures in the fuselage inlet and outlet manifolds (points Q and R).

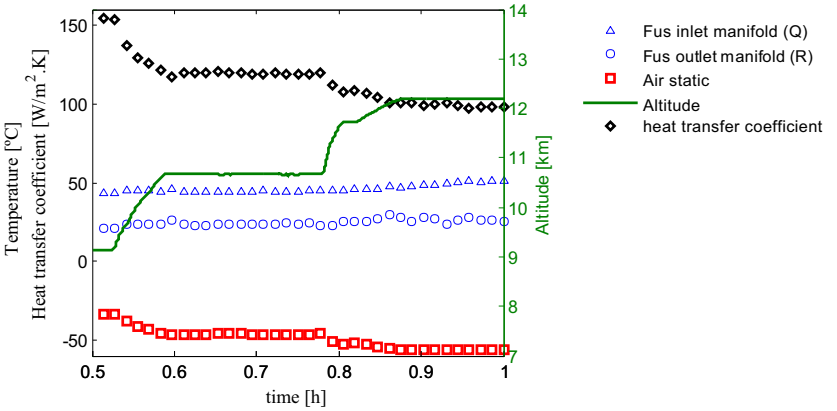

Figure 31 – Effects of altitude on the fuselage heat transfer coefficient for a Mach number of 0.78. Squares, triangles and circles stand for temperatures, and diamonds denote the heat transfer coefficient (LHS Y-axis). The solid line stand for altitude (RHS Y-axis).

It can be noted that the heat transfer coefficient drops from 155 W/(m^{2}K) at an altitude of 9 km to 97 W/(m^{2}K) at 12 km. In the computations of h via Eqs. (3.3) to (3.6), the uncertainty in h is most dependent on the heat input uncertainty, which was observed to be 3%. Error propagation for the heat transfer coefficient indicates uncertainties of order ± 6 W/(m^{2}K). The reduction in h is a direct consequence of the decrease in the air density. At an altitude of 9 km the air density is 0.467 kg/m^3 and at 12 km it is 0.312 kg/m^3. The mass density ratio, ρ_{9km}/ρ_{12km}, is approximately 1.5, while the ratio h_{9km}/h_{12km} is 1.6. Notice that both the static air temperature and the heat transfer coefficient decrease with increasing altitude (see Fig. 31). The variation of the heat removal capacity for a given fuselage condenser area, $hA\Delta T$, is to a certain extent kept constant. The reduction on h is balanced by the increase in temperature difference between the fuselage and static air, ΔT.

The coefficient h can be estimated from the formula recommended by the ASHRAE handbook [15]:

$$h_x = 0.185 \rho c_p u \left(\log_{10} Re_x\right)^{-2.584} Pr^{-2/3}; \tag{3.7}$$

$$Re_x = \frac{\rho u x}{\mu}; \tag{3.8}$$

where h_x is the local convective heat transfer coefficient at a distance x from the aircraft nose, c_p the specific heat at constant pressure, u the aircraft speed, Re_x the local Reynolds number, and μ the dynamic viscosity. Eq. (3.7) is only valid for $10^7 < Re_x < 10^9$. Taking x as 17 m, estimates of h for 9 Km and 12 km are 124 W/(m^{2}K) and 108 W/(m^{2}K), respectively. Note that the dynamic viscosity, for 9 km and 12 km, corresponds, respectively, to $1.493 \cdot 10^{-5}$ kg/(m·s) and to $1.422 \cdot 10^{-5}$ kg/(m·s). The ratio μ_{9km}/μ_{12km} is 1.049 and hence the effect of μ on h is not expected to be as relevant as the effect of mass density. Computations of h were performed with air properties given with static temperature equal to -35 ºC at 9 km and to -56 ºC at 12 km. The ASHRAE procedure can therefore be used as a first-order approximation; however, a decrease proportion to the mass density ratio is expected. Note that the ratio, h_{9km}/h_{12km}, for these estimations yields 1.15.

3.4.3 Ground results

3.4.3.1 Temperature distribution

The thermal performance of the heat exchanger prototype was evaluated on the ground and the results of this study are shown in this section. The following test conditions were selected: the external aluminum heat transfer area of the fuselage heat sink was exposed to ambient air at 27 ºC and cooled by natural convection; the input power to the evaporator, q_{in}, was varied between 0 and 850 W during the ground test, which lasted 1 h 30 min; the fan pumping power to the AC system duct was initially off and only activated at 0.5 h; the mean air velocities were approximately 10 m/s for the period between approximately 0.5 and 1.5 h.

The effects of the input power and ground conditions on the thermal behavior of the prototype are shown in Figs. 32, 33 and 34. Temperature measurements taken at several locations of the evaporator (Fig. 32) and the vapor (Fig. 33) and liquid (Fig. 34) lines are shown on the LHS Y-axis. The input power is shown on the RHS Y-axis of these figures.

At time $\approx$ 0.2 h, the input power, q_{in}, was adjusted to 500 W and at time $\approx$ 0.4 h it was raised to 850 W. For the period between 0 h and 0.5 h, both AC and Fus heat sinks were exposed to ambient air and, consequently, heat was only removed by natural convection. Temperatures at the evaporator, Fig. 32, and at the vapor lines, Fig. 33, increased from

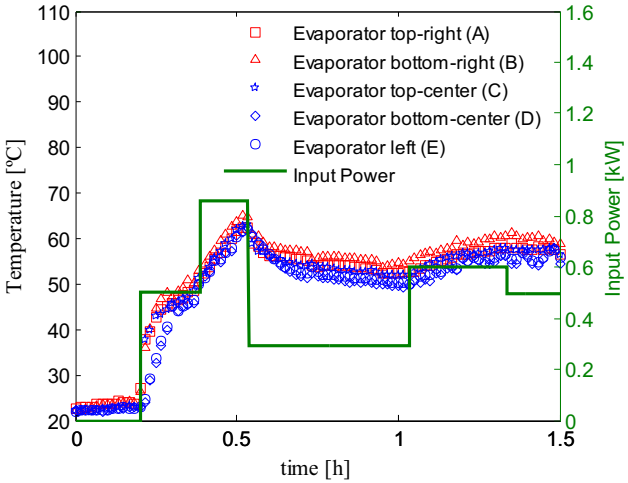

Figure 32 – Effect of input power and ground conditions on the evaporator of the prototype.

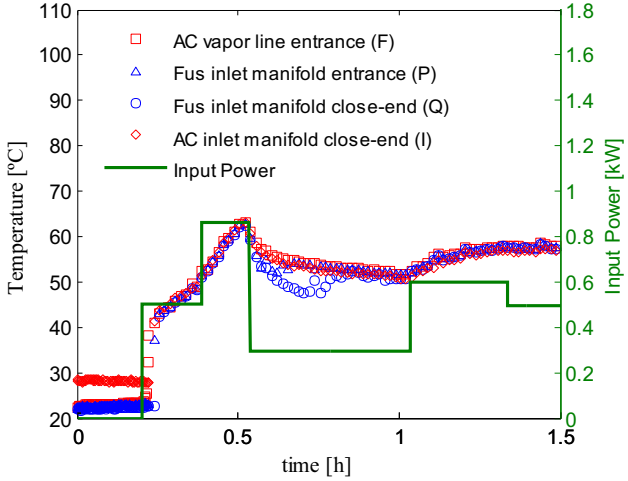

Figure 33 – Effect of input power and ground conditions on the vapor lines of the prototype.

27 ºC to 65 ºC in the interval between approximately 0.2 h and 0.5 h. The thermal resistance of the vapor was low and therefore temperatures at the evaporator and vapor lines are similar. This behavior continued for the rest of the experiment, as can be seen by comparing the temperatures

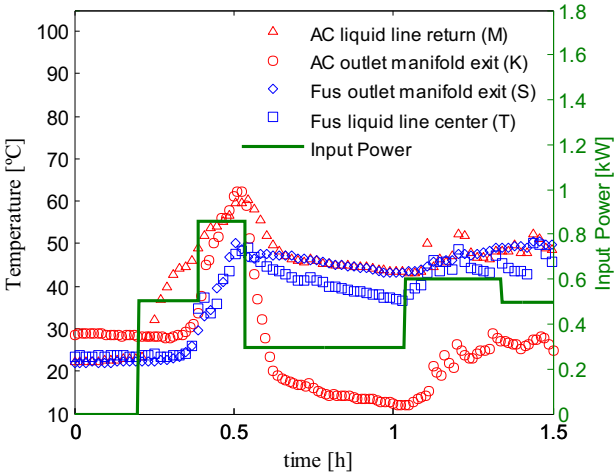

Figure 34 – Effect of input power and ground conditions on the liquid lines of the prototype.

in Figs. 32 and 33. At time ≈ 0.5 h, the temperatures of the liquid lines were slightly lower due to the heat removed by the AC and Fus heat sinks (see Fig. 34).

After a period of 0.5 h, the fan pumping power to the AC system was provided and air (at a mean velocity of 10 m/s) was blown into the AC system duct. The q_{in} value was readjusted to 300 W during the interval between 0.5 h and 1.0 h. With these settings, mean temperatures in the evaporator, vapor lines and Fus liquid line dropped by approximately 5 to 10 °C, while the temperature in the AC outlet manifold exit (point K) dropped by approximately 50 °C (from 61 to 11 °C). The heat transfer in the AC system was sufficient to maintain temperature levels in the prototype evaporator at approximately 50 °C.

After 1.0 h, the q_{in} value was readjusted to 600 W and, at time ≈ 1.3 h, to 500 W. Temperature levels in the prototype evaporator were kept below 60 °C despite the increase in q_{in}.

3.4.3.2 Heat transfer rates

Air temperature and speed measurements within the AC duct are shown in Fig. 35. Air speed velocities of approximately 10 m/s occurred after 0.5 h. When the pumping power was available for the ground tests, the air stream was blown at 10 °C and left the AC condenser at 13-14 °C.

The heat flux to the AC air stream, q_{AC}, is computed by Eq. (3.1).

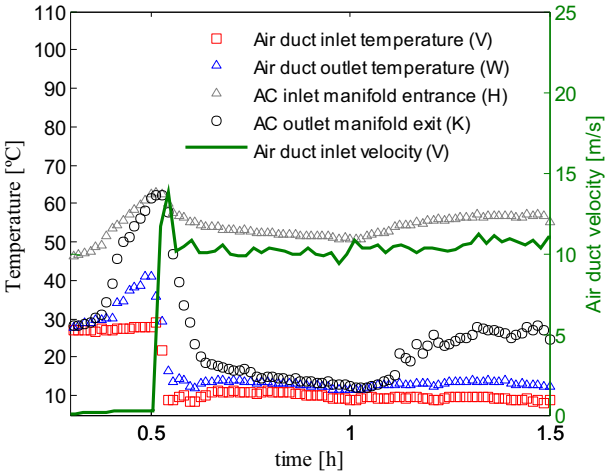

Figure 35 – Thermal conditions within the air conditioning system. Symbols stand for temperatures (LHS Y-axis) and the solid line denotes the mean air velocity in the AC duct inlet (RHS Y-axis), Temperatures in the AC inlet (H) and outlet manifolds (K) are also shown.

Following the above procedure, an estimation of q_{AC} is possible by considering the T_{out} and T_{in} values, shown in Fig. 35 by W and V, respectively. In the interval between 0.6 h and 1 h, $T_{out} - T_{in}$ was 3 ºC and a heat transfer rate of 255 W was estimated. It can be noted in the RHS Y-axis of Fig. 32 that the input power amounts to 300 W within this interval and, therefore, most of the input power to the evaporator was transferred to the AC duct, as expected. Since the remaining external area of the prototype is considerable (0.3 m^2), heat losses to the environment are expected. Heat transfer coefficients of approximately 3.5 W/(m^2K) have been reported for natural convection at vertical plates by Raithby and Hollands [16], while mean heat transfer coefficients for the bottom and top of horizontal plates of 1.5 and 5 W/(m^2K), respectively, were observed by Nellis and Klein [17]. For rough heat transfer modeling, it is convenient here to assume an h value of 3.5 W/(m^2K) for the rest of the prototype. Temperatures for the evaporator, fuselage vapor and liquid lines were obtained from Figs. 32, 33 and 34. The ambient temperature was approximately 27 ºC. The heat transfer to the environment by natural convection was roughly estimated as 35 W. Therefore, the estimation of q_{AC} is reasonable for the time interval between 0.6 and 1 h, since the sum of heat losses and q_{AC} matches the input power within the measurement error.

The assessment of the mean heat transfer coefficients for the AC system is not a straightforward procedure. In Fig. 35 it can be noted that the temperature at the inlet manifold entrance (point H) is approximately 55 ºC for the time period between 0.6 and 1 h, while the temperature at the outlet manifold exit (point K) approaches 16 ºC. In this interval, the air stream velocity (≈10 m/s) and the input power (≈300 W) did not vary. Latent and sensible heat were transferred from the AC condenser to the air stream in the AC duct. It is not possible to compute a mean heat transfer coefficient through a logarithmic mean temperature difference. The AC condenser area where condensation occurs is not known. However, an estimation can be performed by considering the mean temperatures for the AC condenser and the air stream in the duct, through the expression:

$$q_{AC} = h_{AC} A_{AC} \left(\overline{T}_{condenser} - \overline{T}_{stream} \right); \tag{3.9}$$

where h and A stand for the heat transfer coefficient and the external area of the condenser, respectively, the subscript AC denotes air conditioning, $\overline{T}_{condenser}$ denotes the mean temperature of the AC system (mean of points K and H) and $\overline{T}_{stream}$ stands for the mean temperature of the air stream (mean of points V and W). Considering q_{AC} and A_{AC} values of 255 W and 0.1 m^2, respectively, a rough estimation of the h_{AC} value, approximately 65 W/(m^2K) is obtained. Clearly this analysis must be treated with caution, but the result seems to be of the correct order of magnitude, as typical heat transfer coefficients for forced convection in air vary from 10 to 100 W/(m^2K); see Refs. [23, 24].

3.5 DISCUSSION

The prototype consists of one evaporator connected to two condensers in parallel. Independent liquid and vapor lines create two loop-thermosyphons as observed in Fig. 21. Vacuum is applied in the entire system and a filling ratio (working fluid volume / evaporator volume) of 80% ensures that the cartridge heater is immersed in the working fluid with the evaporator positioned horizontally. The heat flux to the evaporator promotes high temperatures and pressures. Vapor is formed at the top of the evaporator. The heat sink conditions (temperatures and heat transfer coefficients) control the vapor flow within the prototype. In-flight, the fuselage heat sink presents lower temperatures and higher heat transfer coefficients than the air conditioning heat sink (differences between heat sink temperatures in-flight can be as high as 100 ºC). In this circumstance, vapor flows preferentially to the fuselage condenser owing to the low pressure created at this condenser. The difference between evaporator and air conditioning pressures is low, reducing vapor flux

to this condenser and hence reducing the heat removal capacity there. On ground, there is an opposite trend: the air conditioning heat sink presents lower temperatures and higher heat transfer coefficients than the fuselage heat sink. In this circumstance, vapor flows preferentially to the air conditioning condenser owing to the low pressure created there. The difference between evaporator and fuselage condenser pressures is low, reducing vapor flux to the fuselage. Natural convection acts externally to the fuselage condenser. It is concluded (and shown experimentally) that the system is self-regulated. Although the insertion of valves (which is commented at the patent [13]) could avoid the use of the air conditioning heat sink during flight (which is an expensive heat sink), it is shown that most of the heat input (approximately 90%) is removed from the prototype at the fuselage. In addition, the use of valves can impose difficulties in the manufacturing process, facilitating working fluid leakage.

Changes in the roll angle, angular velocities (pitch, yaw and roll rates) and aircraft acceleration were shown to have little effect on the thermal behavior of the prototype when the flight attitude is varied within a range and over a timescale characteristic of commercial flights, as described above. Note in Fig. 26 that the aircraft was accelerated in z-direction in the range -0.8g to 0.25g (coordinates as given in Fig. 23). Once the prototype start-up occurs (approximately 300 W), heat is efficiently transported towards the heat sinks. The prototype thermal resistance (which is not affected by characteristic accelerations of a commercial flight) is negligible once startup occurs. The high thermal resistance of the insulation applied over the evaporator assures that the evaporator heat losses are very small, so that the applied heat is able to reach the condenser. The prototype performance is therefore mostly subjected to the heat sink conditions (namely, temperature and heat transfer coefficients), which cannot be reproduced in laboratory environment.

Therefore, for practical purposes, the gravity effect can be neglected in a prototype thermal resistance model. Only the effect of the heat sinks is of primary importance on the prototype performance. However, the pitch angle can affect the heat transfer performance of the prototype, as observed during the take off. The temperature increase at a rate of 18 ^{o}C/min in certain areas of the evaporator could damage electro-electronic equipment, which requires constant refrigeration. Therefore, the evaporator must be designed to be flooded at the input heat region, for any attitude angle occurring during the flight. Note that limit operating temperatures of electrical-electronic avionic devices approximately ranges between 70 and 100 ^{o}C. Temperature records in Figs. 27 and 32 confirm that temperature requisites of avionics are satisfied and so the actual design is suitable for avionics cooling either at ground or in-flight.

To the best of our knowledge, passive heat pipe technology has never been tested in circumstances where freezing can occur within a thermosyphon, especially considering aerospace applications. When the voltage supply was turned off during the flight, freezing was noted in the fuselage circuit. When the input power was adjusted to 400 W, the possibility of a sharp temperature increase at the evaporator was a concern. The loop-thermosyphon tested showed negligible thermal resistance when melting and evaporation occurred at the condenser and evaporator, respectively, under the design constraints. It is possible that heat removal at the fuselage condenser could be reduced due to the vapor flow being obstructed by the presence of ice, increasing the temperatures of the evaporator and vapor lines. This could lead to the electro-electronic equipment connected to the evaporator base being damaged. However, freezing of the working fluid at the fuselage condenser did not promote high temperatures in the evaporator or malfunctioning of the heat exchanger for low input power ($\approx$400 W) and the period involved ($\approx$12 min). Increasing the input power to 600 W allowed the evaporator and the fuselage condenser to work as a stable loop-thermosyphon once more.

Structural failure was also a concern during freezing. Due to safety requisites, local stresses resulting from water solidification should not damage the copper pipes. The internal volume of the heat exchanger is filled on the ground with water in the liquid phase, which occupies only a fraction of the evaporator volume. The vapor lines and condensers are mostly occupied with vapor. Therefore, the propagation of solidification can easily be directed to the pipe in a streamwise direction in cases where the entire cross-section at a given fuselage location is completely frozen. Vapor does not offer significant resistance to ice propagation. This is expected to ensure that local damage of the copper pipes at the fuselage does not occur. Besides avoiding a significant pressure drop, the selection of copper pipes with a relatively large diameter ($e.g > 20$ mm) can avoid complete freezing for a given pipe cross-section. Once the ice layer increases towards the pipe center, the freezing process is slowed by the poor heat conduction through ice. It is not trivial to analyze the process above with classical Neumann problems for heat conduction and to compute a typical timescale for the ice front propagation (Cheng and Seki [43] and Cho and Sunderland [44]), because water melting, vaporization, condensation and solidification occur simultaneously, and the boundary conditions at two-phase fronts are unknown. Therefore, freezing conditions were previously tested in the laboratory to assure structural and thermal consistency.

Convective heat transfer coefficients were estimated for the air conditioning on the ground and on the outside of the fuselage at high

altitudes (*e.g.* 10 km above sea level) for a Mach number of approximately 0.78. The h_{Fus} value was found to be 2 to 3 times higher than the h_{AC} value for mean air velocities of ≈ 10 m/s within the AC system duct. When the pumping power was applied in the ground tests, the air stream was blown at 10 ºC. At altitudes of 10 km, static air temperatures can be lower than -50 ºC and therefore air streams as hot as 50 ºC can be blown into the cabin duct through the air conditioning system to keep the cabin environment under comfortable thermal conditions. Intensive refrigeration through the AC system was not possible at high altitudes, due to the prototype AC condenser limitations. The heat transfer is governed by the heat transfer coefficient and by the mean temperature difference between the air streams and the surfaces of both condensers. Thus, it can be concluded that the heat removal capacity of the fuselage heat sink is largely dominant during the flight, representing over 90% of the input power, when the mean temperature of each condenser is approximately 60 ºC.

3.6 SUMMARY AND CONCLUDING REMARKS

A cooling system prototype was tested in an aircraft on the ground and on an experimental flight, which included conventional commercial flight maneuvers. The heat exchanger prototype consists of loop-thermosyphons with two condensers and a common evaporator. An electrical resistance cartridge inserted in the evaporator simulated the heat transfer from ordinary aircraft cabin electronic equipment. The air conditioning system and the fuselage served as heat sinks for the condensers.

True aircraft air speeds of up to 878 km/h were registered, corresponding to a flight Mach number of 0.78, at 8 km above sea level. The aircraft speed varied above this height to keep the Mach number roughly the same. Static air temperatures of approximately -56 ºC were reached at 12 km of altitude. Input powers of up to 850 W were applied to the evaporator. The flight time was 2 h 30 min and tests on the ground lasted 1 h 30 min. On the ground and at low altitudes, the air stream temperatures within the air conditioning system ranged between 10 ºC and 15 ºC. At high altitudes, air streams of 50 ºC can be admitted into the air duct with speeds of ≈10 m/s.

The main conclusions of this study are:

- The prototype is able to promote the refrigeration of heat sources, such as electronic equipment, in the aircraft cabin air on the ground or in-flight by means of a non-hazardous refrigerant, such as water. In-flight, the heat removal capacity of the fuselage heat sink is

largely dominant (over 90%). Therefore, the tested technology can improve the aircraft refrigeration capacity by reducing the cooling loads of the aircraft air conditioning system.

- Passive heat pipe technology can work efficiently in circumstances where freezing of the refrigerant can occur. Freezing of the working fluid at the fuselage condenser did not promote high temperatures in the evaporator or any structural failure.

- Variations in the roll angle, angular velocities (pitch, yaw and roll rates) and aircraft acceleration characteristic of commercial flights were shown to have little effect on the thermal behavior of the prototype, with the exception of the pitch angle.

- For the external side of the fuselage, the convective heat transfer coefficients at high altitudes (*e.g.* 10 km above sea level) can be 2 to 3 times higher than those observed for the air conditioning system, when the mean velocity of the air blown into the duct is approximately 10 m/s. The mean temperature difference between the air stream and the condenser surface can be 10 times greater at the fuselage. Therefore, it can be concluded that the heat removal capacity of the fuselage heat sink is largely dominant during the flight.

- The convective heat transfer coefficient at the fuselage reduced linearly from a height of 9 km to 12 km, due to the decrease in air density. The application of the heat exchanger system with only the fuselage condenser can be alternatively used to determine heat transfer coefficients with precision, replacing flat plate correlations commonly used in aerospace applications; *e.g.* ASHRAE handbook procedure [15].

4 GEYSER BOILING PHENOMENON IN TWO-PHASE CLOSED LOOP-THERMOSYPHONS

The content of this chapter is based on the following manuscript:

- TECCHIO, C.; OLIVEIRA, J. L. G.; PAIVA, K. V.; MANTELLI, M. B. H.; GANDOLFI, R.; RIBEIRO, L. G. S. Geyser Boiling in Two-Phase Closed Loop-Thermosyphons. Submitted to: International Journal of Heat and Mass Transfer, in November, 10, 2016.

4.1 INTRODUCTION

Although still not mentioned in the results reported in Chapters 2 and 3, a particular unstable phenomenon, known as geyser boiling, was observed at the heat exchanger setup during the experiments in certain working conditions. This instability is related to abrupt vapor expansion that occurs within the thermosyphon evaporator, characterized by long periods of quietness followed by scattered, sudden and blistering vapor nucleation. Typically, the average geyser frequency is lower than 0.1 Hz and the bubbles have the size of the tube inner diameter [45]. During the experiments, geyser occurrence was inferred by noteworthy vibration of the evaporator structure due to the vapor expansion impact on the tube end caps.

Geyser boiling may be observed in different thermosyphon arrangements. An attempt to distinguish geyser boiling phenomenon in axial conventional and loop-thermosyphons is performed with the aid of Figs. 36 and 37. Vapor bubbles are formed at the evaporator wall when the liquid pool becomes superheated. In conventional thermosyphons a bubble, which dimensions are of the order of the pipe inner diameter, abruptly leaves the evaporator towards the condenser after detachment. Liquid on the bubble top is propelled towards the condenser end. A characteristic sound is produced owing to the liquid impact at the condenser end cap. The liquid is then cooled and flows back to the evaporator.

In loop-thermosyphons, the geyser boiling phenomenon can be affected by several aspects such as the evaporator geometry, the evaporator location in the two-phase flow circuit and the amount of working fluid. Here, emphasis is provided to cases where the evaporator dimensions are larger than the pipeline diameter of the adiabatic region and the liquid fills the evaporator container partially. In these cases, the propelled liquid mainly collapses at evaporator walls and it is entrapped there. Coalescence of bubbles prior to detachment can play an important role [46]. The geyser

boiling effects on the condenser and adiabatic lines are dependent on the loop geometry and boundary conditions.

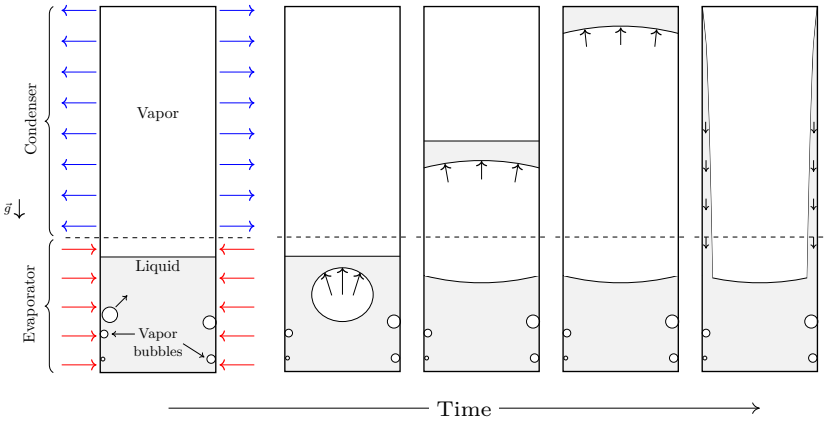

Source – Adapted from Faghri [47].

Figure 36 – Illustration of the geyser boiling phenomena within a typical coaxial thermosyphon.

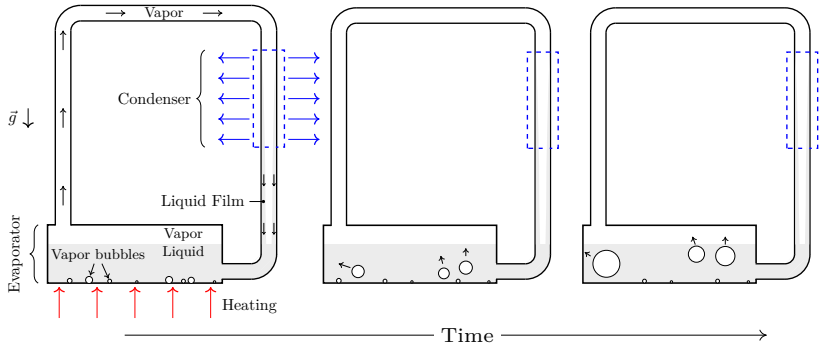

Figure 37 – Illustration of the geyser boiling phenomena within a loop-thermosyphon.

According to Jafari *et al.* [48], in general sense, there are no restrictions on thermosyphon thermal performance due to geyser boiling phenomenon. However, it must be avoided in order to prevent premature failure since structural vibrations induced by geysering occurrence can damage welding points, promoting vacuum leakage. Bezrodnyi and Beloivan [49] suggested performance limitations of thermosyphons with

high amount of working fluid. In this chapter an experimental analysis of geyser boiling phenomenon is conducted in the two-phase closed loop-thermosyphons presented in Section 2.3.

This study aims to investigate the effects of variable thermal conditions in both condensers, filling ratio, heat flux and vapor pressure on geyser boiling phenomenon. The thermal behavior of each condenser is analyzed with and without geyser occurrence in the evaporator. A criterion for geyser boiling occurrence is established based on abrupt oscillations in vapor pressure within the adiabatic line. Acceleration measurements of the evaporator axial axis allow to evaluate the geyser boiling influence on evaporator structural vibration.

The present study is motivated as follows:

- To the best of our knowledge geyser boiling phenomenon has been only analyzed by thermal aspects. However, the main concern during geyser boiling occurrence is the device structural integrity. High frequency and amplitude vibrations can induce the device failure by damaging junctions such as welding points. The present work aims to quantify the geyser boiling influence on the evaporator vibration;

- Evaluation of the geyser boiling phenomenon in a wide range of operating thermal conditions was poorly investigated. Particularly, results are unknown for large temperature differences (*e.g.* 60 ºC) along the heat pipe investigated;

- Most of previous investigations studied geysering effects in straight or coaxial thermosyphons. However, geyser boiling on complex geometries such as loop-thermosyphons was never extensively investigated. As a consequence, the results reported herein can differ from usual geyser boiling studies, as the vapor expulsion is directly propelled to the condenser section.

4.2 LITERATURE REVIEW

Geyser boiling effects on thermosyphons have been studied even before Boure *et al.* [50] used the term geysering for periodical rapid expulsions of a boiling liquid and its vapor in a tube. Griffith [51], for example, already studied geysering phenomenon characterized by cycles of a quiet condition and violent vapor expulsion at the liquid surface level. In this study, the main scientific contributions are summarized for two-phase closed and evacuated thermosyphons.

Casarosa *et al.* [52] evaluated the geyser boiling effects in conventional thermosyphons positioned vertically. The frequency of geyser

occurrence was shown to increase with increasing heat flux in the evaporator at a nearly constant condenser pressure. However, in these conditions, the geyser intensity remained almost constant. Moreover, they found that by keeping the heat flux constant and by increasing the condenser pressure, the geyser occurrence falls progressively until it disappears completely.

The critical heat flux in thermosyphons, considering developed boiling and the geyser effect, was studied by Imura *et al.* [53]. They proposed an equation for the ideal filling ratio (FR), according to the magnitude of the critical heat flux and the operating conditions. An optimum FR between 0.18 and 0.22 was reported. Larkin [54], Imura [55] and Harada *et al.* [56] also suggested similar ranges, as ideal filling ratios.

Niro and Beretta [45] presented experimental results and an analytical model for boiling regimes in thermosyphons. Unsteady operation occurred when the prototype was filled with medium and large working fluid quantities. Bubble dimensions mainly relied on liquid superheating and vapor mass density. The authors classified the boiling regime based on the bubble nucleation frequency and on the ratio of bubble to device diameter.

The experimental study conducted by Mantelli *et al.* [57] showed geyser boiling occurrence in thermosyphons developed for bakery oven applications. Results indicated that geyser boiling period decreases with increasing heat flux at the evaporator. A noteworthy physical discussion of how geyser boiling affects the temperature field along the thermosyphon is provided by the authors. The phenomenon has been widely noted in conventional thermosyphons mainly during the start-up.

Lin *et al.* [58] investigated geyser boiling effects in vertical annular thermosyphons. Their experimental results indicated that the geyser boiling phenomenon occurs more frequently with high heat loads, short evaporator lengths and small filling ratios. The amplitude of temperature oscillations decreased with decreasing evaporation length and filling ratios. The geyser boiling period was reduced for low condenser temperatures.

By using a thermosyphon made of glass to allow two-phase flow visualization, Kuncoro *et al.* [59] revealed that the temperature field within the setup may play an important role on geyser boiling occurrence. When the superheated liquid is the driving force for geyser onset, the phenomenon may still occur even with an increase in the evaporator pressure.

The effects of filling ratio, thermosyphon inclination and coolant mass flow rate on geyser boiling characteristics were investigated by Emami *et al.* [60]. They observed that the geyser period as well as the temperature oscillation amplitude in the condenser end cap were reduced

by decreasing the thermosyphon inclination angle regarding the horizontal axis. Moreover, geyser did not occur for inclination angles less than 15º. With increasing filling ratio the temperature oscillation magnitude was increased. They state that coolant mass flow rate in the jacket device show unimportant effect on geyser boiling phenomenon.

Khazaee *et al.* [61] conducted a series of experiments to investigate the influence of many parameters on geyser boiling. Methanol was chosen as the working fluid. They observed that geyser boiling frequency increased with increasing heat load and aspect ratio (defined as the ratio of evaporator length to inside pipe diameter) and decreased with increasing filling ratio. A correlation for the period of geyser boiling phenomenon was proposed based on their experimental data.

More recently, a three-dimensional numerical study was performed by Jouhara *et al.* [62] in order to predict the geyser boiling phenomenon within a thermosyphon. They used the volume of fluid (VOF) model and user defined functions (UDF's) to add source terms in the flow governing equations. Their numerical results allowed a visualization of the complex two-phase flow during the geyser boiling occurrence. A similar two-phase behavior during geyser occurrence was experimentally observed by Chen *et al.* [46].

4.3 EXPERIMENTAL APPARATUS AND PROCEDURE

The experimental setup consists of loop-thermosyphons with two parallel condensers and a common evaporator, as already presented in Chapter 2, Section 2.3. For the sake of brevity, the setup description and working principle are not repeated here. The prototype was instrumented as illustrated in Fig. 38. Red dots numbered from 2 to 9 indicate thermocouple positions. The evaporator temperature, $\overline{T}_{evap}$, is a mean value of several measurement points along the evaporator.

The mean velocity at the air duct is denoted by $\bar{v}_{AC}$. Inlet and outlet air duct temperatures are represented by $T_{AC,in}$ and $T_{AC,out}$, respectively. The heat transfer coefficient in the Fus-condenser is adjusted by setting different thermal bath temperatures, T_{tb}, and coolant mass flow rates, $\dot{m}$. The fluid temperatures at the calorimeter entrance and exit are denoted by $T_{Fus,in}$ and $T_{Fus,out}$, in that order. Water is used as refrigerant fluid for $T_{tb} > 0$ ºC, whereas ethyl alcohol is used for $T_{tb} \leq 0$ ºC. When $\dot{m}$ is set to 0.000 kg/s, heat exchange by natural convection occurs between the calorimeter and the ambient air, whose temperature is kept at approximately 25 ºC.

The prototype instrumentation is similar to that description given in Chapter 2, Section 2.3, and for this reason it will not be repeated

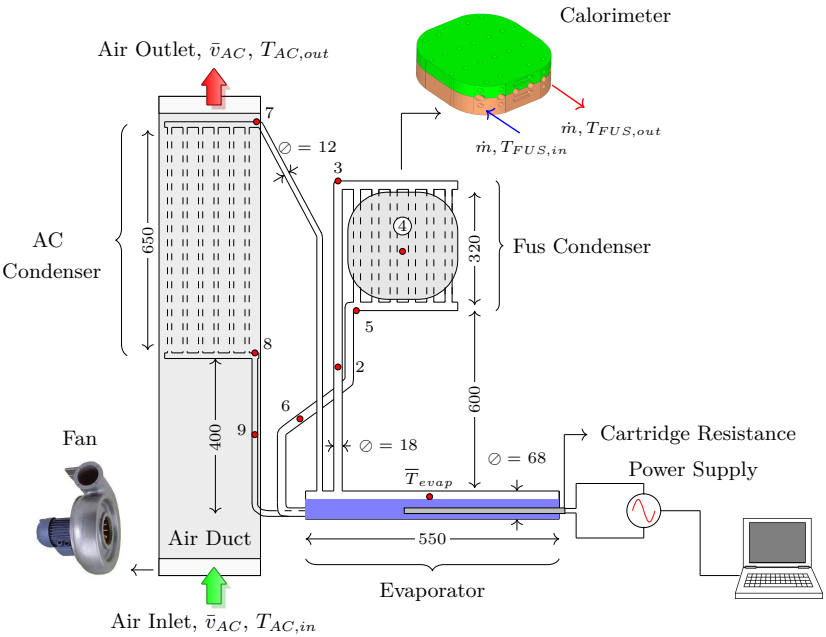

Figure 38 – Illustration of loop-thermosyphons prototype with AC- and Fus-condensers in parallel sharing the same evaporator. Red dots indicate temperature measurements by thermocouples (TC). Dimensions are shown in millimeters.

here. In order to investigate the geyser boiling effects on the prototype structural integrity, a Brüel & Kjaer type 4517 accelerometer was used to measure the evaporator acceleration. Previous experiments performed by Oliveira *et al.* [63, 64] indicate that noteworthy evaporator vibrations can occur due to geyser occurrence in the evaporator, particularly in its axial direction. The accelerometer was positioned in the evaporator left face (see point O in Fig. 39). The acceleration signal is measured along the AB axis with the aim of evaluating the main trend of the evaporator vibration. The accelerometer frequency and measuring range are 1 Hz to 20 kHz and ± 4900 m/s^2 peak, respectively.

Experiments were performed as follows. The prototype was tested under 15 different conditions as summarized in Table 5. The cooling fluid temperature was adjusted at the calorimeter heat sink by ranging T_{tb} from 40 to -20 ºC and $\dot{m}$ from 0.000 to 0.040 kg/s. Mean air velocities of up to 6.1 m/s were reached at the AC entrance with temperature $T_{AC,in}$

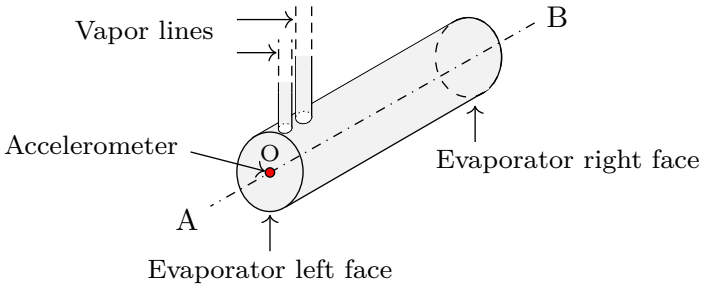

Figure 39 – Accelerometer located at point O in the evaporator left-face measures the structure accelerations along the AB axial axis. Positive accelerations are in direction OA and negative, OB.

kept at approximately 25 ºC. Input power ranged from 100 to 850 W with increments of 150 W. Each input power step was kept constant during 30 min and then increased. Natural convection occurred at the AC-condenser for cases C1, C2, C3, C4 and C13 (see that $\bar{v}_{AC} = 0.0$ m/s). Forced convection at the AC-condenser and natural convection at the Fus-condenser took place in cases C14 and C15. In cases C5 to C12, heat was removed by forced convection from both condenser by varying the mean air velocity at the AC-condenser and the mass flow rate of the coolant fluid at the Fus-condenser. Filling ratios of 0.5 and 0.9 were employed. As it will be shown in the next section, cases C1 to C13 represent loop-thermosyphons working in quasi-steady regime, whereas, in cases C14 and C15, a transient behavior is observed.

4.4 RESULTS

4.4.1 Identification of geyser boiling occurrence

In order to identify the geyser boiling occurrence within the evaporator, the pressure rate acting in the adiabatic lines, $G(t)$, defined as:

$$G(t) = \frac{\mathrm{d}}{\mathrm{d}t}\left[p_{sat}(T_v)\right] \ ; \tag{4.1}$$

was evaluated. In this expression, the RHS of Eq. (4.1) is the time-variation of the saturated vapor pressure, p_{sat}, at the adiabatic tube temperature (T_v). It is assumed that T_v corresponds to the thermocouple measurements at TC2 (see Fig. 38).

The choice of the adiabatic line instead of the evaporator to

Table 5 – Summary of experiments. The input power was raised from 100 to 850 W with increments of 150 W.

Case	$\bar{v}_{AC}$(m/s)	Calorimeter settings			FR	Working Condition
		$\dot{m}$(kg/s)	T_{tb} (ºC)	Coolant Fluid		
C1	0.0	0.040	40	water	0.5	
C2	0.0	0.040	20	water	0.5	
C3	0.0	0.021	0	alcohol	0.5	
C4	0.0	0.017	-20	alcohol	0.5	
C5	3.8	0.040	40	water	0.5	
C6	3.8	0.040	20	water	0.5	
C7	3.8	0.021	0	alcohol	0.5	Quasi-Steady
C8	3.8	0.017	-20	alcohol	0.5	Regime
C9	6.1	0.040	40	water	0.5	
C10	6.1	0.040	20	water	0.5	
C11	6.1	0.021	0	alcohol	0.5	
C12	6.1	0.017	-20	alcohol	0.5	
C13	0.0	0.040	40	water	**0.9**	
C14	3.8	0.000	25	ambient air	0.5	Unsteady
C15	6.1	0.000	25	ambient air	0.5	Regime

evaluate $G(t)$ is justified because, as the temperature histories at different locations on the evaporator wall are not similar, different mean and fluctuating temperature values are observed. In Fig. 40, five temperature histories (A, B, C, D and E, for thermocouples located at different positions, see evaporator schematic in Fig. 40) are presented for case C1. Therefore, analysis of the temperature field within the evaporator is rather complex: liquid and vapor phases can occur at the same location in different time-steps affecting the temperature history. Besides, the vapor temperature in the adiabatic section usually characterizes the thermosyphon (and other heat pipe related technology) as stated in Mantelli [65]. So, the geyser boiling analysis in the present prototype is evaluated using the temperature measurements in the adiabatic line, where, actually, liquid is hardly expected.

When geyser boiling occurs within the evaporator, vapor mass flux is abruptly increased in every adiabatic line entrance, yielding a dynamic pressure behavior. Fig. 41a shows a typical behavior of $p_{sat}(T_v)$ at the adiabatic line. The sudden increase in $p_{sat}(T_v)$ at time $\approx$ 72.4 and 73.6 min promotes pressure rates, $\Delta[p_{sat}(T_v)]/\Delta t$, up to 350 Pa/s and is characteristic of geyser boiling occurrence. Minor pressure rates do

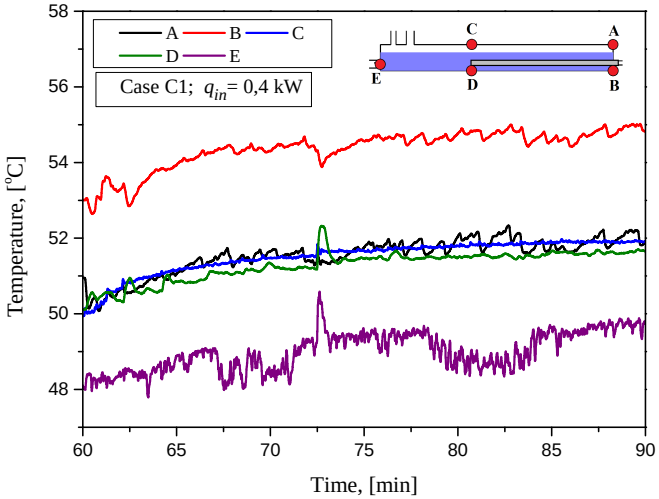

Figure 40 – Temperature histories on the evaporator wall for $q_{in} = 0.4$ kW in case C1.

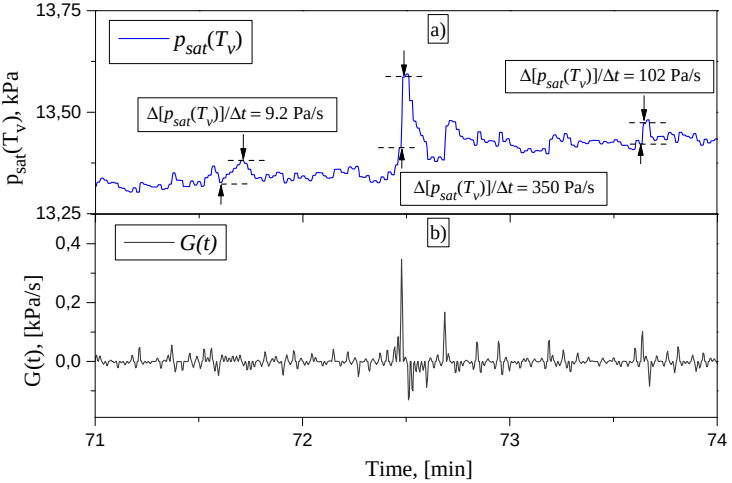

Figure 41 – a) Vapor pressure at adiabatic line and b) pressure rate for $q_{in} = 0.4$ kW in case C1.

not represent abrupt vapor expansion and therefore are not considered geysering phenomenon, as, for example observed at time $\approx$ 71.6 min, where the pressure rate is 9.2 Pa/s. The geyser boiling occurrence is then characterized by sharp peaks in time of $p_{sat}(T_v)$, which is clearly

indicated by the $G(t)$ function in Fig. 41b. In previous works concerning conventional thermosyphons, the magnitude of $p_{sat}(T_v)$ was sufficient to explain geyser boiling phenomenon. In the present case, the change in time of $p_{sat}(T_v)$, $G(t)$, is also necessary for a systematic and more accurate analysis.

4.4.2 Loop-thermosyphons in quasi-steady regime

Results for case C1 are presented in Fig. 42. The bath temperature is set to 40 ºC, whereas natural convection acts in the AC-condenser; $\bar{v}_{AC} = 0.0$ m/s. Input power is shown in the RHS ranging from 0.1 to 0.85 kW with increments of 0.15 kW. In the LHS prototype temperatures, pressure rate, $G(t)$, and evaporator acceleration, $a(t)$, are shown in Figs. 42a, 42b and 42c, respectively.

In Fig. 42a, the increase in $\overline{T}_{evap}$ from 24 to 45 ºC is roughly linear during the first input power level ($q_{in} = 0.1$ kW). The sharp increase in T_{adiab} at time ≈ 20 min indicates the system startup. For $q_{in} > 0.1$ kW, $\overline{T}_{evap}$ and T_{adiab} show an increase rate less than 0.2 ºC/min for a given input power, indicating a quasi-steady regime. The peaks in $G(t)$ indicate the occurrence of geyser boiling phenomenon; see Fig. 42b. However, the first peak at time ≈ 20 min occurs during the system startup and therefore does not represent quasi-steady state geyser occurrence. Although absolute pressure rates, $|G(t)|$, below 0.25 kPa/s are dominant, $|G(t)|$ over 0.5 kPa/s occur for $q_{in} \geq 0.55$ kW. The maximum value of $|G(t)|$ is approximately 1.1 kPa/s when $q_{in} = 0.85$ kW.

The evaporator accelerations induced by geyser phenomenon are presented in the LHS of Fig. 42c. The peaks in $a(t)$ ranging from -9.9 to 111 m/s^2 occur for $0.55 \leq q_{in}[\text{kW}] \leq 0.7$. Acceleration sign is in accordance to Fig. 39. Significant values of $|a(t)|$, over 2 m/s^2, only occur if $|G(t)|$ is higher than approximately 0.1 kPa/s. This thresholding in $|G(t)|$ is therefore used as a reference for geyser boiling occurrence for the present work and loop geometry. One should note that other geyser boiling definitions can be adopted to other geometries and operation conditions. Note, however, that unimportant evaporator accelerations happen for elevated values of $|G(t)|$ in most of the experiment. For example, at time $t \approx 175$ min, $|a(t)|$ is 0.1 m/s^2 with $|G(t)|$ 1.1 kPa/s. It is speculated that the increase in vapor mass flux at the evaporator can usually achieve the adiabatic lines. This can yield the fluctuation of $G(t)$, but not necessarily the evaporator acceleration. To accelerate (shake) the evaporator casing, the momentum transfer from the bubbles movement to the liquid pool must be high enough to surpass the evaporator structural inertia. This remark is further discussed in Section 4.5.1.

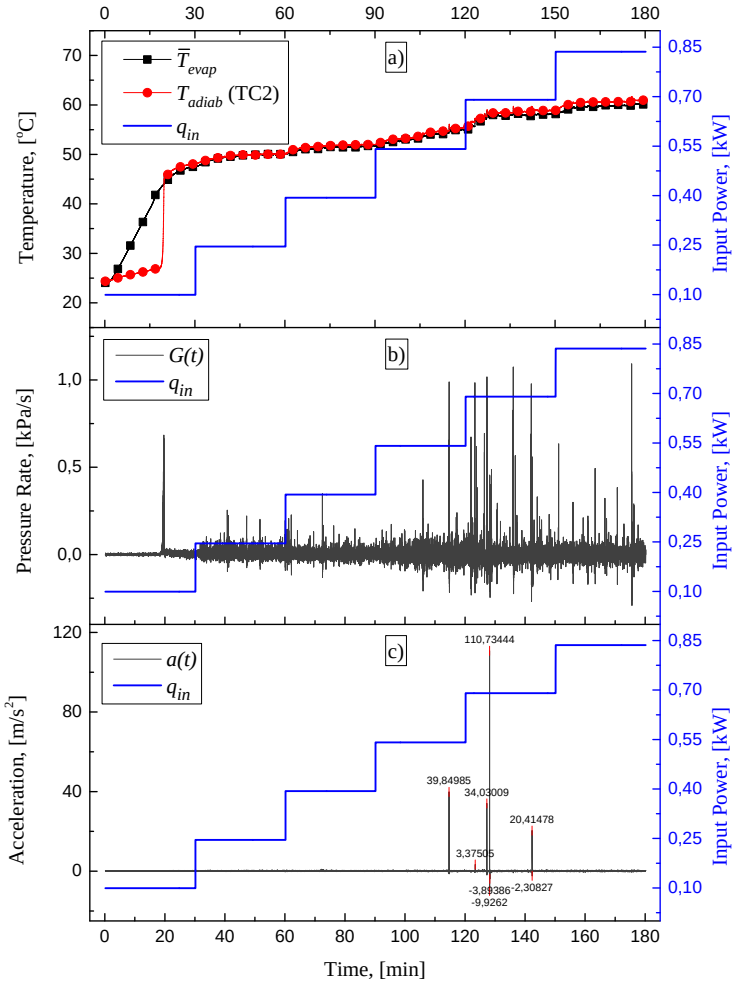

Figure 42 – Effect of input power on the loop-thermosyphons for case C1. a) $\overline{T}_{evap}$ and T_{adiab} (TC2); b) Pressure rate $G(t)$; c) Acceleration $a(t)$.

The maximum axial velocity of the evaporator structure at the acceleration peak, v_{max}, is obtained by:

$$v_{max} = \int_{t_0}^{t_0+\Delta t} a(t)dt; \tag{4.2}$$

where t_0 is the time when the peak in acceleration is initiated and Δt is the

time interval, typically 1 second. In case C1, $|a(t)|_{max}$ is approximately 111 m/s^2 at $t \approx 128$ min whereas v_{max} corresponds to 33.4 m/s.

The time-histories of $G(t)$ and $a(t)$ are shown in Fig. 43 for case C4. Similarly to case C1 natural convection occurs at the AC-condenser, whereas heat is removed from the Fus-condenser by forced convection. The thermal bath temperature is set to -20 ºC. The temperature measurements in the evaporator and in the adiabatic lines in cases C1 and C4 are qualitatively similar to those observed in Fig. 42a and do not yield new information. Peaks in $G(t)$ in case C4 are mainly meaningful with $q_{in} \geq 0.4$ kW (see Fig. 43a). $G(t)$ reaches 1.1 kPa/s at time ≈ 97 min. Nevertheless, significant vibrations of the evaporator are not observed: $|a(t)|_{max}$ is 1 m/s^2 at time ≈ 92 min corresponding to v_{max} of 1 m/s.

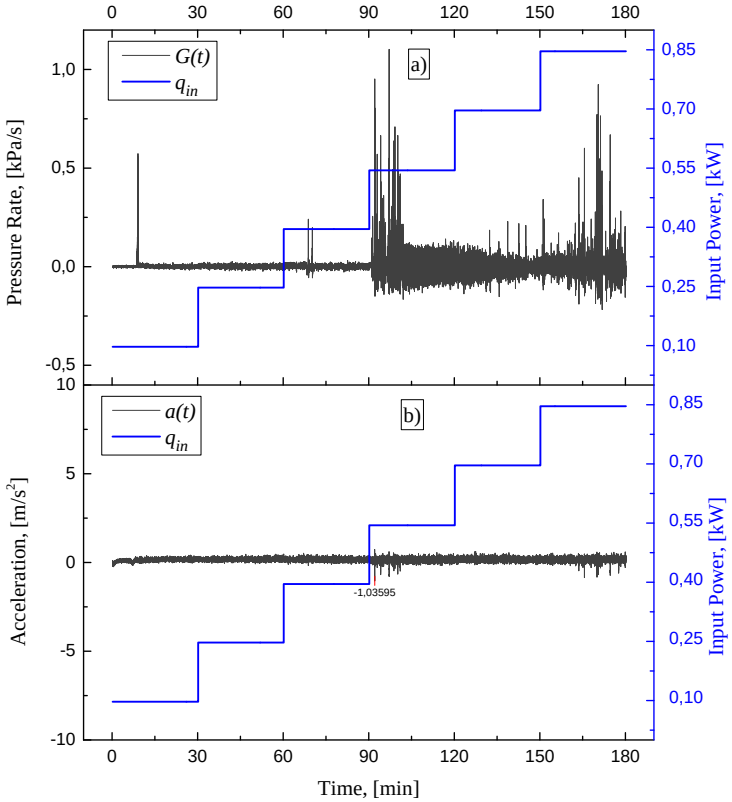

Figure 43 – Effect of input power on the a) $G(t)$ and b) $a(t)$ for case C4.

The main features of geyser boiling phenomenon when loop-thermosyphons work in quasi-steady regime (cases C1 to C13) are sum-

marized in Table 6. The maximum values of acceleration and pressure rate, $|a_{max}|$ and $G(t)_{max}$, are presented together with the experimental settings ($G(t)^{\boldsymbol{i}}$ and $q_{in}^{\boldsymbol{i}}$) for the first geyser boiling occurrence and $G(t)^{\boldsymbol{ii}}$ and $q_{in}^{\boldsymbol{ii}}$ for the maximum acceleration.

In cases C1 to C12, $G(t)^{\boldsymbol{i}}$ ranged from 0.12 to 0.85 kPa/s and the first geyser boiling occurrences were observed when $q_{in}^{\boldsymbol{i}}$ was set to 250 or 400 W, respectively. Noteworthy, evaporator accelerations ranged from 35.2 to 113.4 m/s^2 and occurred in cases C1, C2, C5 and C6. $G(t)^{\boldsymbol{ii}}$ ranged from 0.45 to 1.14 kPa/s, for $q_{in}^{\boldsymbol{ii}} \geq 400$ W when $|a_{max}|$ occurred. The heat sink performances of tests C1, C2, C5 and C6 presented different hydrodynamic behaviors when the loop-thermosyphons worked in quasi-steady regime; this remark will be analyzed in Section 4.5.1. Although typical values of $G(t)_{max}$ are 1.1 kPa/s, values as high as 6.51 kPa/s were observed for case C5. One should note, in Table 6, that values of $G(t)_{max}$ do not necessarily correspond to $|a_{max}|$.

4.4.2.1 Effect of filling ratio on geyser boiling

The effect of filling ratio (FR) on geyser boiling phenomenon is investigated, analyzing the behavior of cases C1 and C13 data. With exception of case C13, where the FR was 0.9, all the other tested configurations presented FR of 0.5. The other conditions for C13 were set at the same level as in case C1 (see Table 5). The time-histories of $G(t)$ and $a(t)$ for case C13 are shown in Figs. 44a and 44b, respectively.

Geyser boiling occurred with low input power when FR=0.9. Values of $G(t)$ up to 0.75 kPa/s were noted with $q_{in} = 0.1$ kW. For $q_{in} \geq 0.4$ kW, magnitude of $G(t)$ was as high as 1.6 kPa/s. The geyser frequency increased with increasing filling ratio; compare Figs. 44a and 42b where the number of occurrences of $G(t) \geq 0.1$ kPa/s increased in case C13. Accelerations occurred for $q_{in} \geq 0.25$ kW with higher magnitudes and frequencies; compare Fig. 44b and 42c. As depicted in Table 6 $|a_{max}|$ increased by a factor 10 when the FR was increased from 0.5 to 0.9. Increasing FR the amount of liquid available to be thrown against the evaporator walls also increases, yielding $|a_{max}|$ up to 1080 m/s^2.

4.4.3 Loop-thermosyphons in transient regime

In cases C14 and C15, the loop-thermosyphons work in transient regime. $\overline{T}_{evap}$ and T_{adiab} show an increase rate higher than 0.2 ^{o}C/min for a given input power, indicating an unsteady working condition. Heat is removed from AC- and Fus-condensers by forced and natural convection, respectively; see Table 5.

Table 6 – Main features of geyser boiling phenomenon for loop-thermosyphons working in quasi-steady regime (C1-C13).

Case	$G(t)^{i}$ [kPa/s]	q_{in}^{i} [W]	$\lvert a_{max}\rvert$ [m/s^2]	$G(t)^{ii}$ [kPa/s]	q_{in}^{ii} [W]	$G(t)_{max}$ [kPa/s]
C1	0.12	250	110.7	0.45	700	1.10
C2	0.79	400	113.4	0.84	400	1.31
C3	0.85	400	1.1	0.65	550	1.14
C4	0.24	400	1.0	0.95	550	1.10
C5	0.33	250	35.2	1.14	850	6.51
C6	0.13	400	41.6	0.63	850	1.00
C7	0.34	400	3.4	0.81	850	0.83
C8	0.25	400	1.6	0.61	550	1.22
C9	0.68	250	7.6	0.70	850	1.12
C10	0.44	250	5.4	0.80	850	1.22
C11	0.83	400	3.6	0.84	850	1.11
C12	0.29	250	2.4	0.63	400	1.27
C13^{iii}	0.25	100	1080.0	0.73	400	1.61

^{i} Experimental settings for the first geyser boiling occurrence.
^{ii} Experimental settings in $\lvert a_{max}\rvert$.
^{iii} Filling ratio was increased from 0.5 to 0.9 in case C13.

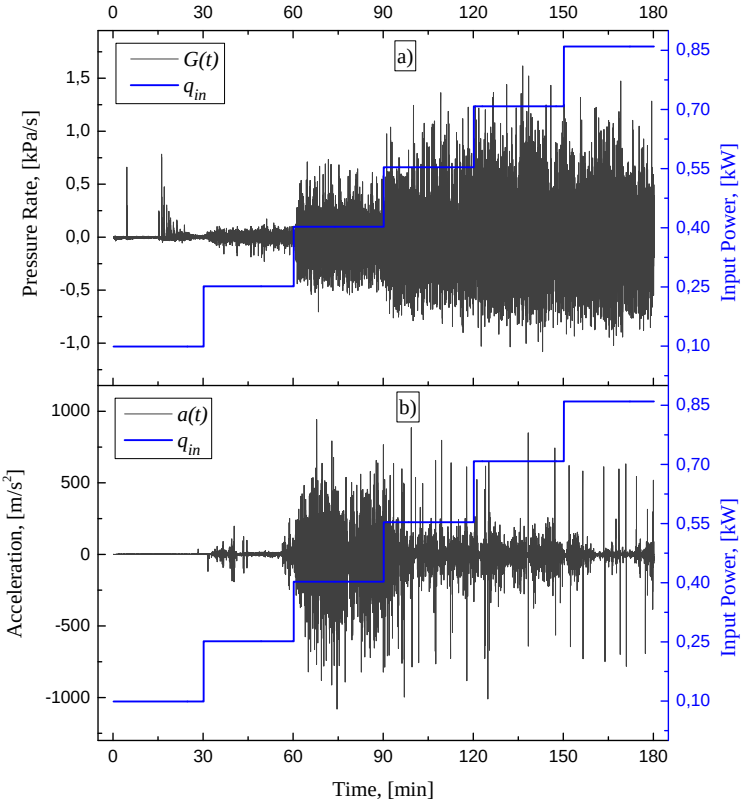

Figure 44 – Effect of input power on a) the pressure rate $G(t)$ and b) the evaporator acceleration $a(t)$ for case C13 (FR=0.9).

In Figs. 45 and 46 the temperature histories and $G(t)$ signal for case C14 are presented, in that order. The temperatures of the evaporator ($\overline{T}_{evap}$), AC and Fus returning lines (TC6 and TC9), and the outlet manifolds (TC5 and TC8) (see Fig. 38) are representative of the increasing temperature behavior of the device in C14 test conditions. Results for case C15 are similar and, therefore, not shown. Input power ranged from 0.1 to 0.7 kW with increments of 0.15 kW. Due to safety requirements, tests were interrupted when $\overline{T}_{evap}$ reached 100 ºC with q_{in} set to 0.7 kW. It can be observed in Fig. 45 that the temperature distribution on time becomes roughly linear for $q_{in} \geq 0.25$ kW, showing that actually the system works in unsteady-state. The first geyser boiling occurrence is identified when $G(t) \approx 0.31$ kPa/s at time ≈ 45 min. Amplitudes of $G(t)$ are particularly pronounced when q_{in} is set to 0.4 kW, reaching

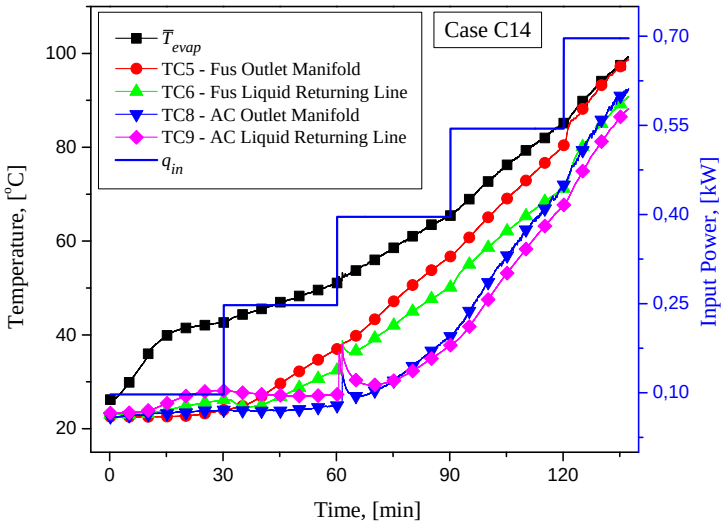

Figure 45 – Temperature histories of the loop-thermosyphons for case C14.

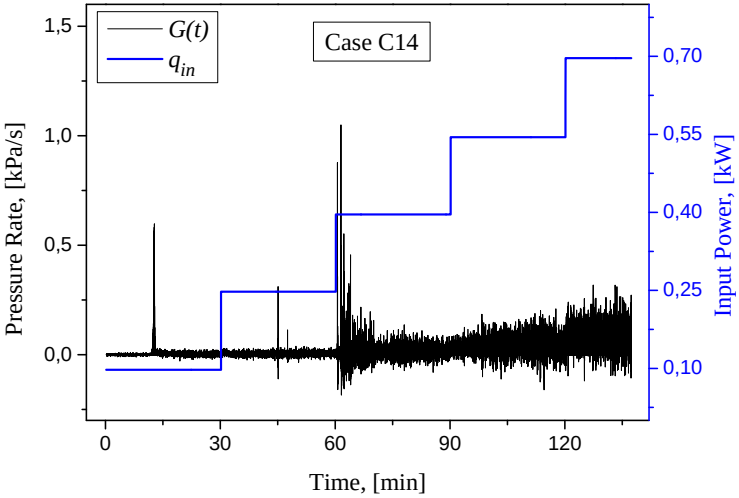

Figure 46 – Transient effect on pressure rate, $G(t)$, for case C14.

approximately 1.1 kPa/s. Reduction of $G(t)$ occurs for $t \geq 65$ min.

The main features of geyser boiling phenomenon when the system works in unsteady regime are summarized in Table 7. Although $G(t) \geq 1$ kPa/s occur within the adiabatic lines, the evaporator accelerations are small. Note that values of $|a_{max}|$ up to 1.3 m/s^2 were reached. In

cases C14 and C15, $G(t)^{i}$ is 0.31 and 0.65 kPa/s, respectively, and occurs with q_{in}^{i} = 250 W. Values of $G(t)_{max}$ can reach up to 1.3 kPa/s. A vapor pressure analysis will assist explaining these results, as presented in Section 4.5.2.

Table 7 – Main features of geyser boiling phenomenon for loop-thermosyphons working in unsteady regime (C14 and C15).

Case	$G(t)^{i}$ [kPa/s]	q_{in}^{i} [W]	$\lvert a_{max}\rvert$ [m/s^2]
C14	0.31	250	1.3
C15	0.65	250	1.2
Case	$G(t)^{ii}$ [kPa/s]	q_{in}^{ii} [W]	$G(t)_{max}$ [kPa/s]
C14	0.31	700	1.1
C15	0.25	700	1.3

^{i} Experimental settings for the first geyser boiling occurrence.
^{ii} Experimental settings in $|a_{max}|$.

4.5 ANALYSIS

4.5.1 Evaporator accelerations induced by geyser boiling

The last section shows results where significant evaporator accelerations, *i.e.* above 10 m/s^2, are observed, in a time-scale of approximately 1 second, for cases C1, C2, C5 and C6, for filling ratio of 0.5. These meaningful accelerations were coincidental with values of pressure rate above 0.25 kPa/s. Although the geyser occurrence is presumably associated to these events, the physical phenomena still need to be elucidated, which is done with the aid of the analysis of heat sink thermal conditions observed externally to both condensers.

Temperatures of each condenser pipe-lines are considered constant in this thermal analysis, since condensation occurs in a significant part of the condensers. The wall temperature at the orifice within the calorimeter can be approximated by thermocouple measurements at TC4 (see Fig. 38) owing to the negligible conductive thermal resistance of the aluminum blocks, $\mathcal{O}(10^{-3})$, and due to the low heat transfer rates from the Fus-condenser to air ambient by natural convection. The thermal resistance associated with natural convection is of order $\mathcal{O}(10^{0})$. This assumption is not precise at the bottom part of the calorimeter (close to the outlet manifold) where sensible heat exchange occurs. The surface

external to the air stream within the duct was nearly the same as the temperature at point TC7 (AC inlet manifold). This was verified by thermocouple measurements at the AC-condenser walls not shown in Fig. 38. Actually, the nearly isothermal condition at the AC-condenser is particularly noted a few minutes after geyser boiling is initiated.

At this point of the analysis, it is important to define the ratio of external convective thermal resistances acting on AC- and Fus-condensers, denoted as $R_{h,AC}/R_{h,Fus}$. When heat is removed from both condensers by forced convection (cases C5 to C12), the thermal resistance ratio is given by:

$$\frac{R_{h,AC}}{R_{h,Fus}} = \frac{\Delta T_{ln,AC}/q_{AC}}{\Delta T_{ln,Fus}/q_{Fus}} \; ; \tag{4.3}$$

where the heat transfer rate is represented by q and ΔT_{ln} stands for the logarithmic mean temperature difference expressed as

$$\Delta T_{ln} = \frac{T_{in} - T_{out}}{\ln\left(\frac{T_w - T_{out}}{T_w - T_{in}}\right)} \; ; \tag{4.4}$$

where T_w, T_{in} and T_{out} stand for temperatures at the wall in contact with the cooling fluid, inlet and outlet cooling fluid, respectively. Actually, T_{in} and T_{out} stand for the temperatures $T_{AC,in}$ and $T_{AC,out}$ at the air duct, and $T_{Fus,in}$ and $T_{Fus,out}$ at the calorimeter; see Section 4.3. T_w was estimated as explained above. The heat transfer rates q_{AC} and q_{Fus} were determined by energy balances, and so, expressed as

$$q = \dot{m} c_p \left(T_{out} - T_{in}\right); \tag{4.5}$$

where $\dot{m}$ represents the mass flow rate and c_p the specific heat at constant pressure of the cooling fluid.

A heat transfer coefficient for natural convection of 3.5 W/(m^{2}K) acting at the AC-condenser provides a rough estimation of $R_{h,AC}$ in cases C1 to C4; see Raithby and Hollands [16]. Here, it is verified that $q_{in} \approx q_{Fus}$. For quasi-steady cases C1 to C12, the energy balance for the system, $q_{in} = q_{AC} + q_{Fus}$, was verified and matches with the input power within experimental uncertainty.

The maximum accelerations, $|a_{max}|$, which occurred for cases C1 to C12 (see Table 6) as a function of the ratio of $R_{h,AC}/R_{h,Fus}$ are shown in Fig. 47. Noteworthy evaporator accelerations were only observed for resistance ratios higher than 150. $|a_{max}|$ increases exponentially with increasing $R_{h,AC}/R_{h,Fus}$ for values over 100. The quality of the fitting curve is demonstrated with a high value of the parameter r^2; approximately 0.94.

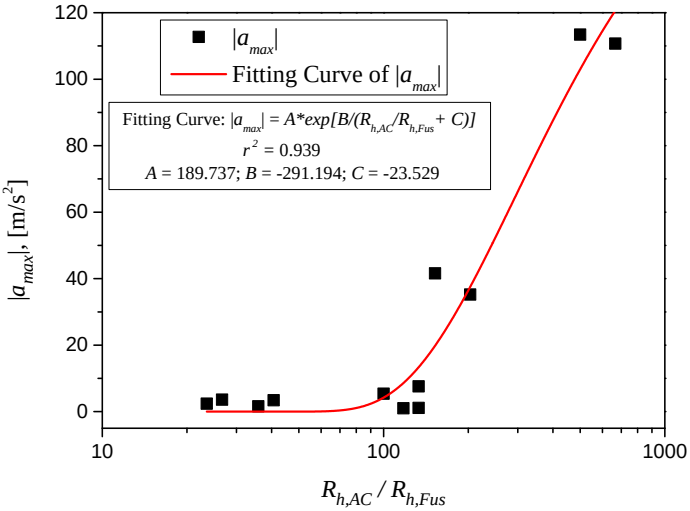

Figure 47 – Effect of convective thermal resistances on $|a_{max}|$.

The maximum evaporator accelerations became more intense once the heat transfer at the AC-condenser was negligible as compared to the one at the Fus-condenser. It is speculated that the vapor flux hardly achieved the AC-condenser when $|a_{max}|$ occurred for $R_{h,AC}/R_{h,Fus}$ over 150. With one condenser nearly disabled, intense vapor fluxes characteristic of geyser boiling could only be directed to the Fus-condenser. In cases where the pressure rate was higher than 0.25 kPa/s, it is possible that significant vapor produced at the evaporator could not flow towards the Fus-condenser owing to vapor blockage promoted by liquid content or a coincidental high pressure acting at the vapor line of the Fus-condenser. If that was the case, the energy associated with the sudden vapor expansion would be dissipated in the form of vibration of the evaporator structure. The description above could explain why high values of $G(t)$ can occur with minor evaporator accelerations.

4.5.2 Effects of heat flux and vapor pressure on geyser boiling

The effect of heat flux on geyser boiling can be evaluated by analyzing the magnitude of $G(t)_{max}$ in experiments with loop-thermosyphons in quasi-steady regime. In Fig. 48, $G(t)_{max}$ is plotted as a function of the heat flux, $q" = q_{in}/A$, for cases C1 to C4. Experiments C5 to C12 are similar and therefore not presented.

Values of $G(t)_{max}$ over 0.1 kPa/s occur when the heat flux, $q"$,

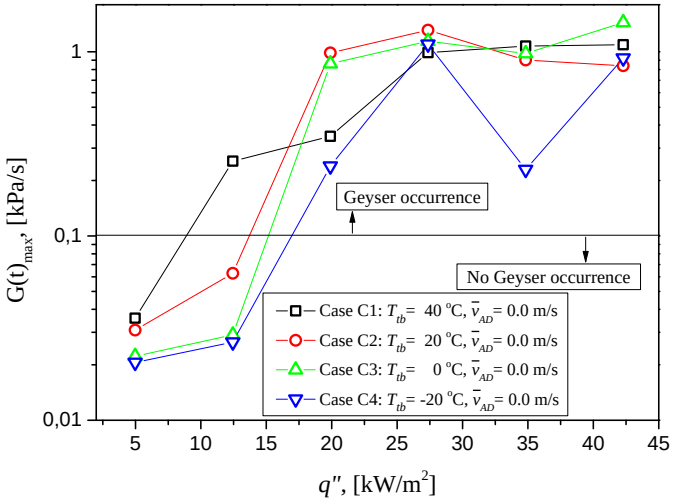

Figure 48 – Effect of heat flux on the maximum pressure rate, $G(t)_{max}$.

is higher than 12.5 kW/m^2 for case C1 and 20 kW/m^2 for C2 to C4. With q" $\geq$ 25 kW/m^2 $G(t)_{max}$ achieves a plateau for the measured heat flux range. Values of $G(t)_{max}$ do not overcome 1.1 kPa/s.

The effect of vapor pressure on geyser boiling can be depicted by comparing the pressure rate in experiments with loop-thermosyphons in quasi-steady and transient regimes. Cases C1 and C14 are sufficient for this appraisal. In Fig. 49, values of vapor pressure and $G(t)$ higher than 0.25 kPa/s are presented as function of time. One should remember that the input power is raised from 0.1 to 0.85 kW in case C1 and from 0.1 to 0.70 kW in case C14. The heater was turned off in the last case due to safety requisites.

At time $\approx$ 45 min the input power is set to 250 W and the vapor pressure in the adiabatic lines is roughly 15 kPa in both cases. With q_{in} set to 700 W and in time $\approx$ 135 min the vapor pressure is roughly 17 kPa in C1 and 100 kPa in C14. The vapor pressure magnitude is dependent on the heat sink capacity, which is reduced in C14. Note that values of $G(t) \approx 1.0$ kPa/s only occur for vapor pressures less than 25 kPa. The geyser boiling intensity is therefore decreased with increasing vapor pressure. This results is in accordance to Casarosa *et al.* [52] who investigated geyser boiling occurrence in a thermosyphon filled with water. They noted less pronounced geyser effects for vapor pressures above 25 kPa.

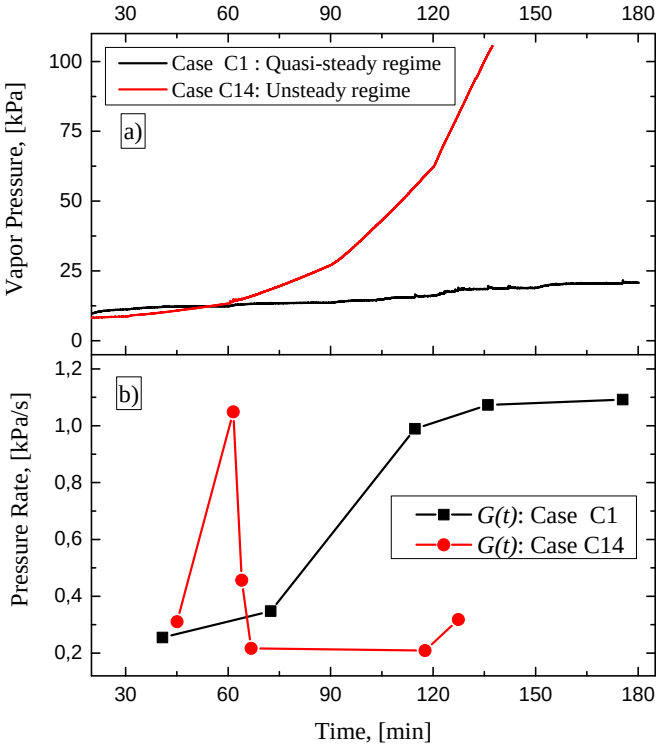

Figure 49 – Effect of vapor pressure on geyser boiling occurrence.

4.5.3 Geyser boiling influence on loop-thermosyphon temperatures

The geyser boiling effect on the temperature of condensers and liquid returning lines is analyzed when the loop-thermosyphons operate in quasi-steady and transient regimes. Only one experiment is sufficient to depict the main temperature trends for each regime.

The pressure rate and the evaporator acceleration are presented in the LHS and RHS of Fig. 50 for quasi-steady case C2. Dashed vertical lines distinguish three different loop-thermosyphon working conditions in intervals I1 ($50 \leq t[\text{min}] \leq 63.5$), I2 ($63.5 \leq t[\text{min}] \leq 71.2$) and I3 ($71.2 \leq t[\text{min}] \leq 100$). The input power ranges from 250 to 550 W for the given time interval. Geyser boiling and evaporator accelerations do not occur in the range I1. Values of $G(t)$ up to 0.8 kPa/s confirm geyser boiling occurrence in I2, but evaporator accelerations do not happen. In interval I3 geyser boiling often occurs and occasionally promote significant evaporator accelerations. Values of $a(t)$ up to 110 m/s^2 are observed.

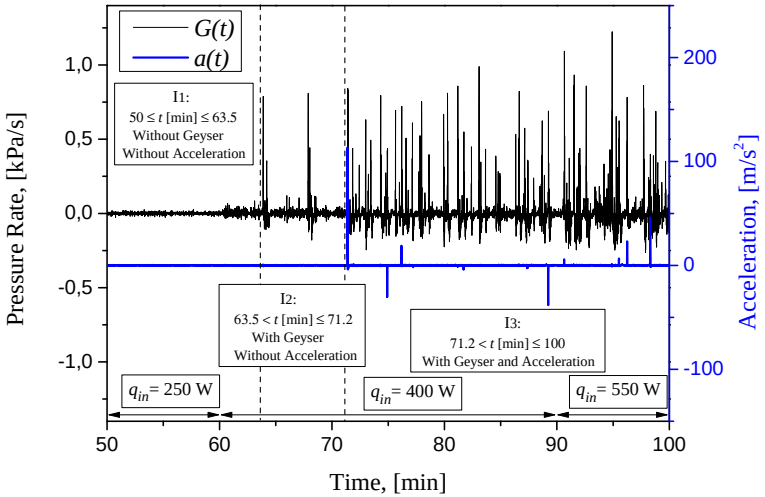

Figure 50 – $G(t)$ and $a(t)$ for case C2. Dashed vertical lines delimit regions I1, I2 and I3 regarding peaking occurrences in $G(t)$ and $a(t)$.

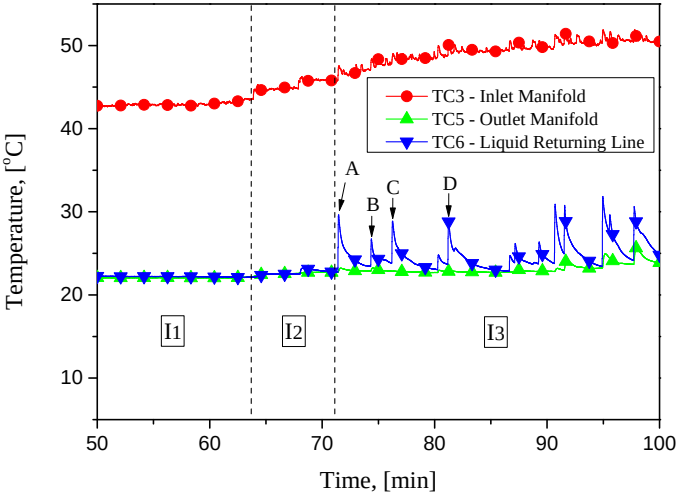

Figure 51 – Geyser effect on temperatures of the Fus-condenser pipelines for case C2.

The effects of the temperatures of the liquid returning line (TC6), inlet (TC3) and outlet (TC5) manifolds on the geyser effect is presented in Fig. 51 for the pipelines of the Fus-condenser. In interval I1, temperatures TC3, TC5 and TC6 are constant. In interval I2 peaks in $G(t)$ of approxi-

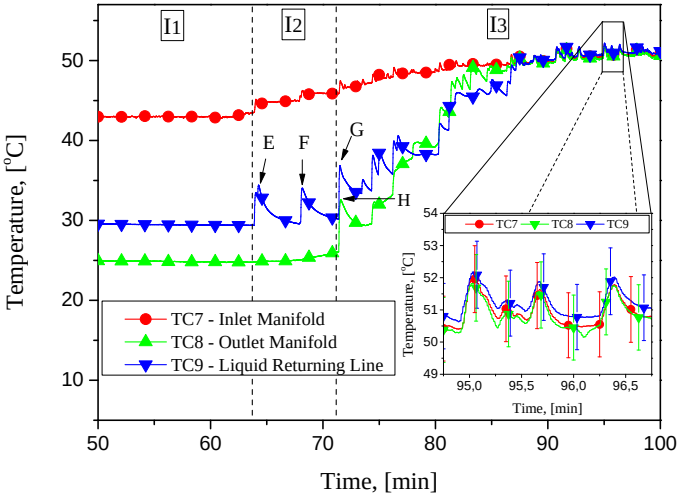

Figure 52 – Geyser effect on temperatures of the AC-condenser pipelines for case C2.

mately 0.8 kPa/s are coincident with the increase in temperature TC3 of 1.5 °C. TC5 and TC6 temperatures do not show important oscillations in I2. Peaks in $G(t)$ are also coincident to the increase in temperature TC3 for interval I3, whereas TC5 is slightly modified. A new feature occurs in interval I3: the abrupt raise in temperature TC6 of 7 °C at the liquid returning line (see points A, B, C and D in Fig. 51, for example). A mean temperature difference of 20 °C between the inlet and outlet manifolds throughout the time interval indicates that heat is properly removed at the Fus-condenser even during geyser boiling occurrence.

Similarly, corresponding temperatures for the pipelines of the AC-condenser are presented in Fig. 52. The inlet manifold temperatures at Fus- and AC-condensers, TC3 and TC7, in that order, present similar behaviors. Peaks in $G(t)$ are also coincident with the increase in temperature TC7. In interval I2, the liquid returning line temperature (TC9) is abruptly increased in approximately 4.4 °C (see points E and F in Fig. 52), while the outlet manifold temperature (TC8) remains roughly constant. A different thermal behavior occurs in interval I3: the outlet manifold temperature TC8 raises and oscillates as the temperature at TC9 (see points G and H). With increasing heat flux at the evaporator and limited heat removal capacity at the AC-condenser, the temperature difference between TC7 and TC8 becomes minor for $t > 87.5$ min. The strong correlation in time presented by temperatures TC7, TC8 and TC9 (see the inset-graph in Fig. 52) suggests that the vapor flows along the AC-condenser without

complete phase-change.

The geysering effect on loop-thermosyphons transient operation can be analyzed with the aid of Fig. 45 for case C14. Experiment C15 is similar. Heat is removed by forced convection from the AC-condenser and by natural convection from the Fus-condenser. Sharp temperature oscillations are only meaningful when $q_{in} = 0.4$ kW at $t \approx 61$ min at the AC and Fus liquid returning lines, and at the AC outlet manifold (TC8). When the loop-thermosyphons work in transient state, the temperature difference between the inlet manifolds (which scale with $\overline{T}_{evap}$) and TC6 and TC9 is roughly 10 ºC with input power of 0.7 kW at time ≈ 130 min. Vapor pressure increases with increasing system temperature. No sharp temperature raise in the liquid return lines occurs with pressure rates less than 0.25 kPa/s for time ≥ 65 min; see Fig. 46.

4.6 SUMMARY AND CONCLUDING REMARKS

Geyser boiling phenomenon was experimentally investigated in loop-thermosyphons for variable thermal conditions. The setup consists of two parallel condensers and a shared cylindrical evaporator in horizontal. The heat exchanger was tested in steady-state and transient regimes. Heat was removed from each condenser by several combinations of natural and forced convection. Filling ratios of 0.5 and 0.9 were used. Input power of up to 0.85 kW was provided to the evaporator. Axial accelerations of the evaporator and temperature histories in several prototype locations have been measured. The effects of vapor pressure and heat flux on geyser boiling occurrence were analyzed. Explanations of how this phenomenon affects condenser temperatures were also provided.

The main remarks of this study are:

- For the prototype studied, when loop-thermosyphons work in steady-state regime, geyser boiling occurs if the heat flux is higher than 12.5 kW/m^2. Typical pressure rates in the adiabatic lines are approximately 1 kPa/s. This occurred for vapor pressures below 25 kPa;

- When loop-thermosyphons work in transient regime the vapor pressure is increased with increasing heat flux, suppressing geyser boiling intensity. Pressure rate is only significant, *i.e.* 1 kPa/s, for heat fluxes less than 20 kW/m^2 and vapor pressures less than 25 kPa;

- Geyser boiling can eventually yield intense evaporator accelerations. Maximum accelerations were affected by the ratio of thermal resistances acting at each condenser. For ratio of condenser thermal

resistances over 150, evaporator accelerations up to 110 m/s^2 happened with filling ratio of 0.5, and up to 1100 m/s^2 with filling ratio of 0.9.

5 THERMAL PERFORMANCE OF THERMOSYPHONS IN SERIES CONNECTED BY THERMAL PLUGS

The content of this chapter is based on the following manuscript:

- TECCHIO, C.; OLIVEIRA, J. L. G.; PAIVA, K. V.; MANTELLI, M. B. H.; GANDOLFI, R.; RIBEIRO, L. G. S. Thermal Performance of Thermosyphons in Series Connected by Thermal Plugs. Submitted to: Experimental Thermal and Fluid Science in, December, 20, 2016.

5.1 INTRODUCTION

In the previous chapters the thermal performance of a heat exchanger system (HES) consisting of two loop-thermosyphons was experimentally evaluated. In these tests heat sources were simulated by means of cartridge resistances inserted in the evaporator casing. In fact, these fictitious heat sources represent several independent electronic devices, which, in practical situations, are located in different positions inside the aircraft cabin. In this work, thermosyphons were used as intermediary heat transfer elements (IHTEs) between independent heat sources and the evaporator of HES. The IHTEs and HES were coupled in series through cylindrical or conical shaped plugs. A schematic of this arrangement is presented in Fig. 53. Tests were performed to evaluate the effects of filling ratio, inclination angle, input power and condenser geometry on the ITHEs thermal performance.

The arrangement in Fig. 53 is recommended for applications where several independent heat sources need refrigeration; *e.g* avionics equipment inside an aircraft. The idea is making an analogy with electrical net, plugs and domestic appliances of a house, that the heat exchanger evaporator works as a "heat sink net", that "energizes" the several "heat sink thermal plugs". In this case, one common HES can be responsible for collecting the heat through its evaporator and removing it to a major heat sink while the IHTEs are responsible for collecting the individual heat and conducting it to the HES evaporator. Of course one single thermosyphon could handle this job, but it would be quite complex. Thermosyphon technologies applied to complex geometries can demand several weldings in different locations, which can favor air infiltration. Besides, the vacuum quality which is a necessity for proper thermosyphon operation is facilitated in simpler geometries. If the contact thermal

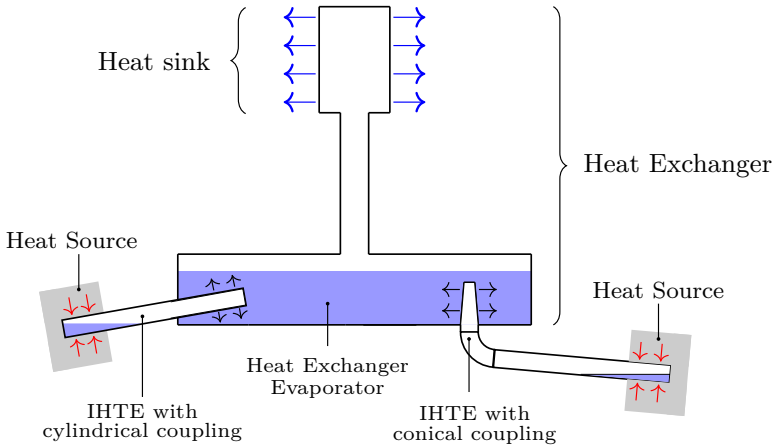

Figure 53 – Intermediary heat transfer elements (IHTEs) connected in series with a common heat exchanger. Heat is transported from independent heat sources to the heat sink through conical and cylindrical couplings.

resistance between the IHTE and the HES loop thermosyphons is minor, the use of two thermosyphons in series can be a feasible solution.

Many parameters affect the thermosyphon thermal performance, such as: working fluid properties, inclination angle, geometry, inner vacuum level and filling ratio (FR), defined as the volume ratio of working fluid to evaporator, FR $= V_w/V_{evap}$ [47], where V_w and V_{evap} stand for volumes of the working fluid and evaporator casing, respectively. These parameters must be defined carefully in order to avoid the thermosyphon to reach typical operating limits such as dryout, flooding and boiling, which impose restrictions to the maximum heat transfer rate [47,48,66,67].

The objectives of the present chapter are:

- To propose a new heat transfer device configuration, composed by two thermosyphon connected in series, able to give more layout flexibility, to be applied in equipments of intricate geometry;
- To propose and study the mechanical and thermal behavior of two easy to assemble mechanical fitting geometries (conical and cylindrical couplings);
- To investigate the thermal performance of thermosyphons connected in series; particularly, the design parameters of the intermediary heat transfer thermosyphons;

- To evaluate the whole operation range of intermediary thermosyphons from the start-up to the dryout limit.

One should note that the two-phase flow transport mechanism within thermosyphons is gravity driven, and so, more efficient if compared to the flow transport mechanism in capillary driven heat pipes. Thermosyphon assessment is performed in challenging operation conditions regarding low inclination angles (less than or equal to 5º with respect to the horizontal axis). Filling ratios higher than or equal to 0.6 were used. Geyser boiling occurrence was observed and its effect on thermal performance was analyzed.

5.2 LITERATURE REVIEW

Design features of thermosyphons were extensively investigated through experiments and numerical simulations in the last decades. The effects of filling ratio, inclination angle, working fluid properties and device geometry on thermal performance have been systematically analyzed [65]. In this section, literature results concerning the subject of the present study are reviewed.

The heat transfer performance of an inclined thermosyphon was experimentally investigated by Negishi and Sawada [68]. Water and ethanol were used as working fluids. They observed that, in steady state regime, the overall heat transfer coefficient increased with increasing the operating temperature. For water, they suggested for best device performance, inclination angles and filling ratios between 20-40º and 25-60%, respectively.

Imura *et al.* [53] investigated the ideal filling ratio for thermosyphons vertically oriented, according to the magnitude of the critical heat flux and operating conditions. Best results were achieved with FR in the range 0.18-0.22. Imura [55], Larkin [54] and Harada *et al.* [56] suggested similar ranges for ideal filling ratios.

Wang and Ma [69] developed a semi-empirical correlation to predict the optimum condensation heat transfer coefficient within inclined thermosyphons. The ideal inclination angle increased from 20 to 50º by increasing the filling ratio from 0.10 to 0.33.

The ratio of heat transfer rates between inclined and vertical thermosyphons, q/q_{90}, was investigated by Payakaruk *et al.* [70], who observed that the ratio q/q_{90} was hardly affected by filling ratio modifications. On the other hand, the ratio q/q_{90} increased with decreasing latent heat of vaporization of the working fluid at inclination angles ranging from 20 to 70º. By using water as the working fluid, q/q_{90} achieved its maximum value with an inclination angle of 50º. Zuo and Gunnerson [71]

stated that the optimum inclination angle may vary according to the operating conditions and device geometry.

The critical heat flux for dryout occurrence in thermosyphons with small filling ratios was studied by Cohen and Bayley [72], Strel'tsov [73], Andros and Florschuetz [74]. Results of Cohen and Bayley model showed good agreement with the experimental results obtained by Shiraishi *et al.* [75] for filling ratios between 0.10 and 0.20. Faghri [47] and Park *et al.* [76] suggested that the critical heat flux is associated with the flooding limit, for filling ratios higher than 0.20.

Noie *et al.* [77] performed experiments to evaluate the thermal performance of water-filled thermosyphons, by modifying the inclination angle (from 5º to 90º) and the filling ratio (from 0.15 to 0.30). The heat transfer coefficients at the condenser region increased with increasing filling ratio and reached the highest values with inclination angles in the range 30 to 45º.

Shabgard *et al.* [35] proposed a numerical model to predict the transient operation of a vertical thermosyphons with various filling ratios, which optimum value was obtained considering that there is liquid film from the condenser to the evaporator end. They observed that, for this optimum filling ratio, the transient operation conditions were shortened. They suggested that a small amount of additional working fluid could prevent the breakdown of the liquid film.

Agostini *et al.* [78] evaluated the thermal performance of a prototype based on heat pipe technologies, aiming the thermal control of electronics. The setup consisted of two-loop thermosyphons connected in series. A mechanical fitting yielded the heat transfer from the condenser of the first loop to the evaporator of the second loop. The prototype dissipated approximately 1 kW with a mean operating temperature of 110 ºC.

5.3 EXPERIMENTAL SETUPS AND PROCEDURE

Thermosyphons with cylindrical and conical shaped plug condensers were designed and tested as intermediary heat transfer elements (IHTEs) between a fictitious heat source and the evaporator of the loop thermosyphons heat exchanger system (HES). To test the IHTEs with cylindrical evaporator shape, the HES presented in the last chapters was used. To test the conical shaped condenser a calorimeter was employed. The use of a calorimeter instead of the HES evaporator is justified as follows: due to space constraints and several welding points, air infiltration could occur in the HES evaporator. The vacuum procedure is not necessary by applying a calorimeter and, therefore, IHTE results are not

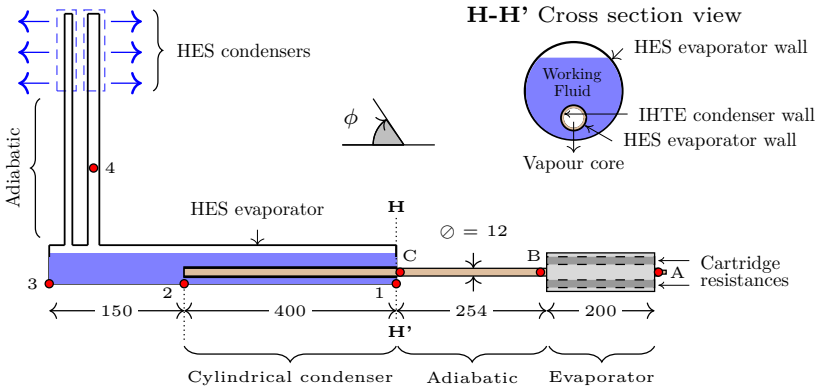

Figure 54 – Thermosyphon with cylindrical shaped condenser (in the illustration $\phi = 0$). The main dimensions are shown in millimeters. Red dots denote temperature recording points. The angle ϕ was varied from 0 to 5º. HES stands for a heat exchanger (loop thermosyphons) connected to end heat sink.

compromised by HES malfunctioning in a first evaluation. In next chapter, the calorimeter (Fig. 55) will serve as the HES loop thermosyphons evaporator. Schematics of the cylindrical and conical appliances are presented in Figs. 54 and 55, where main dimensions are presented in millimeters. Red dots indicate thermocouple positions.

The working principles of the tested devices are briefly described as follows. The input power to be removed from the heat source heats up the working fluid within the evaporator of the IHTEs, causing liquid to vapor phase change. The vapor flows from the IHTEs evaporator to the condenser, where condensation takes place, releasing latent heat of vaporization. The formed liquid returns to the evaporator by means of gravity. The same phase change phenomena drive the HES used to remove heat from the cylindrical shaped thermosyphon evaporator. As a result, the input power is transferred from a fictitious equipment to the heat sink through two thermasyphons in series.

The HES depicted in Fig. 54 and used for testing ITHE with cylindrical condenser consists of a closed loop-thermosyphon composed by two condensers in parallel and one common evaporator, as already described in Section 2.3. The HES condensers are not shown here to simplify the illustration. One should note that the objective of this chapter is to analyze the IHTE and so, only the HES evaporator (in thermal connection with the condenser of the IHTE) schematic suffices to analyze the present results. The IHTE shown in Fig. 54 consists of a

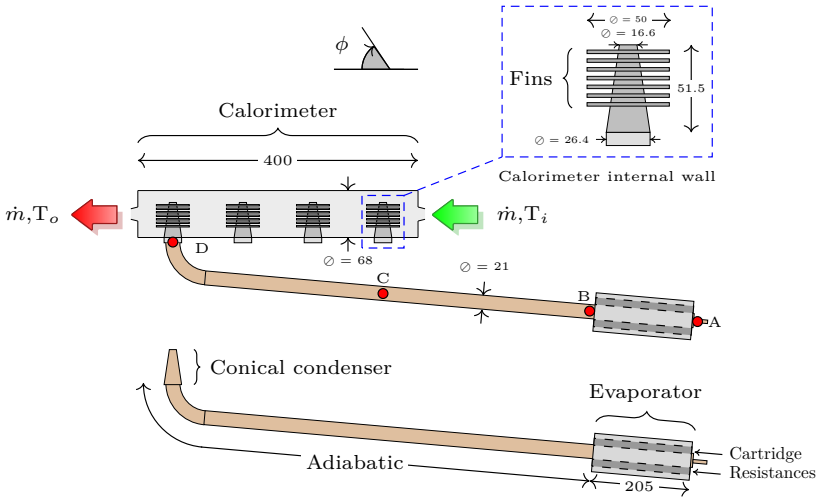

Figure 55 – Thermosyphon with conical shaped condenser. The main dimensions are shown in millimeters. Red dots (A-D) denote temperature recording points. The angle ϕ was kept in 5º. A calorimeter replaced the HES loop thermosyphons.

cylindrical thermosyphon with an outer diameter of 12 mm and a length of 854 mm. The condenser section has a length of 400 mm and is in direct contact with the HES evaporator wall (details of the mechanical fitting can be observed in the cross section view H-H' in Fig. 54). The inner area of the cylindrical shaped condenser is 0.0126 m^2. The mechanical coupling between the HES evaporator and the IHTE condenser was designed to assure practical fitting and low thermal contact resistance.

The thermal contact resistance observed in cylindrical contacts, such as the one shown in Fig. 54 can be quite high due to the low contact pressure. Therefore, other contact geometries should be considered; see Alvarenga [79]. The conical contacts are evaluated in this work since they can provide higher contact pressure than cylindrical plugs and, therefore, the thermal contact resistance can be reduced. The IHTE depicted in Fig. 55 comprises a thermosyphon with a conical shaped condenser. The evaporator and adiabatic sections are made of the same tube and so they have constant cross sections, with outer diameter of 21 mm. Four conical plugs, designed to match the IHTE conical shaped condenser, were welded in the calorimeter wall. The heat transfer area of the calorimeter conical wall within the calorimeter was increased by means of fins. The inner area of the conical shaped condenser is 0.0037 m^2. Cone and fin dimensions are presented in the expanded illustration in Fig. 55. A thermal bath

provides coolant mass flow rate to the calorimeter of up to $\dot{m} = 25$ L/min. Water was used as the coolant fluid at the calorimeter.

The heat sources were simulated by cartridge resistances inserted within aluminum blocks, which are in close contact with the evaporator of the IHTEs. Thermal grease reduced the thermal contact resistance between these elements. To avoid heat losses to the environment, ceramic fiber blankets covered the external area of the prototypes.

Distilled water was employed as the working fluid for the HES and for the IHTEs. Copper was chosen as the container material due to its compatibility with the working fluid (water), avoiding the formation of non-condensable gases. Before inserting the working fluid, the contaminants of the copper surfaces where removed and high vacuum procedures were performed to the containers.

The experimental setups were instrumented as follows. Temperatures were recorded by means of K-type thermocouples, disposed as presented in Figs. 54 and 55. A National Instrument NI cDAQ-9178 was used as the data acquisition system. The input power, q_{in}, was controlled via software Labview 2013 and adjusted by voltage control through a TDK Lambda power supply (GEN 300-5). A personal computer was employed for data storage and to control the experimental variables. The heat transfer conditions at the calorimeter were controlled by a Lauda Proline thermal bath. This equipment allows volumetric flow rates and temperatures ranging from 0 to 25 L/min and from -20 to 50 ºC. Uncertainties for temperature measurements and input power were ±1.1 ºC and 3%, respectively.

A summary of the parameter combination for the experiments performed in this work is presented in Table 8. One can see that the thermosyphon with cylindrical shaped condenser (see Fig. 54) was evaluated under 5 different conditions (D1 to D5) with the input power ranging from 100 to 700 W in 150 W increments. Inclination angles, ϕ, of 0º, 2º and 5º with respect to the horizontal axis and filling ratios of 0.8, 1 and 1.2 were employed in these cases. The aspect ratio (AR), defined here as

$$AR = \frac{l_{ad}}{d_{ad-in}} \; ; \tag{5.1}$$

was set to 25 for tests D1 to D5. In Eq. (5.1) l_{ad} and d_{ad-in} stand for adiabatic section length and inner diameter, in that order. The thermal performance of the thermosyphon with conical condenser plug (see Fig. 55) was evaluated in cases E1 to E6 with the input power ranging from 20 to 200 W in 20 W increments. The inclination angle was kept constant at 5º and two different aspect ratios were employed: 49 and 29. Three filling ratios (0.6, 0.8 and 1) were employed for each value of aspect ratio. In cases

E1 to E6, the mean coolant mass flow rate and the inlet temperature at the calorimeter were adjusted to 0.3 kg/s and 15 ºC, respectively. Each input power level for every experimental case was kept constant during 20 min and then increased. Due to safety requirements, tests were interrupted when the evaporator temperature of the intermediary thermosyphons reached 100 ºC.

Table 8 – Summary of experiments.

Setup	Case	Input power, Increment [W]	ϕ [º]	FR	AR
Cylindrical Plug (Fig. 54)	D1	100-700, 150	0	0.8	25
	D2	100-700, 150	2	0.8	25
	D3	100-700, 150	5	0.8	25
	D4	100-700, 150	5	1	25
	D5	100-700, 150	5	1.2	25
Conical Plug (Fig. 55)	E1	20-200, 20	5	0.6	49
	E2	20-200, 20	5	0.8	49
	E3	20-200, 20	5	1	49
	E4	20-200, 20	5	0.6	29
	E5	20-200, 20	5	0.8	29
	E6	20-200, 20	5	1	29

5.4 RESULTS

5.4.1 Thermosyphon with cylindrical condensers: effect of inclination angle on the thermal behavior

Temperatures of the IHTE and of the HES are shown for case D1 in the left hand side (LHS) axis of Fig. 56. The input power is presented in the right hand side (RHS) axis. Temperature recording locations are disposed as depicted in Fig. 54. In case D1, the inclination angle and the filling ratio were set to 0º and 0.8, respectively.

One can see in Fig. 56 a) that the evaporator temperature (A) of the IHTE increases linearly with the input power. The IHTE works in transient regime. The regime operating condition is defined in this work in accordance with the change rate of the IHTE evaporator temperature (represented here as point A in Figures 54 and 55): transient regime for values higher than 0.2 ºC/min and quasi-steady state regime otherwise. The test was interrupted when the operation limiting temperature (100 ºC) was achieved at time $\approx$ 26.5 min and with the input power set to 250 W. The temperature at the adiabatic section (point C) remained roughly

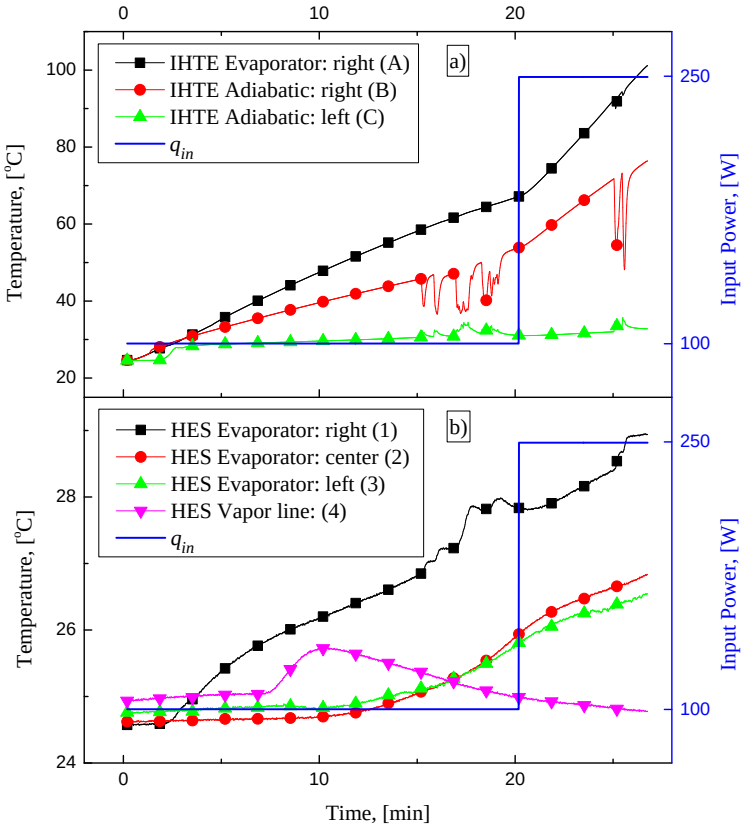

Figure 56 – Effect of input power on the thermal behavior of the a) intermediary thermosyphon with cylindrical condenser and b) heat exchanger system for case D1 ($\phi = 0^o$ and FR = 0.8). Symbols represent temperature recordings and the solid line, the input power.

constant at 31 °C for time $\geq$ 2.5 min. The large temperature difference between the thermosyphon locations A and C, over 60 °C for time $\geq$ 22 min, reveals that heat is not properly transferred from the evaporator to the IHTE condenser. As expected the thermosyphon performance is reduced when the inclination angle with the horizontal position is null ($\phi = 0^o$). Only a minor heat amount is transferred to the HES evaporator by heat conduction through the walls of the intermediary thermosyphon, while most of the input power is used to increase the internal energy of the IHTE casing.

Temperature histories of HES are shown in Fig. 56 b) for case

D1. The temperature in the right side of the HES evaporator (point 1, see Fig. 54) increases almost linearly for time $\geq$ 2.5 min. Similar behavior is observed for HES evaporator temperatures at locations 2 and 3 for time $\geq$ 12.5 min. The large temperature difference between the vapor line (point 4) and the HES evaporator (points 1, 2 or 3) exposes that vapor is hardly produced within the HES evaporator. Most of the energy released by the resistances heats up the IHTE element and only a fraction achieves the HES evaporator. This fraction is not sufficient to lead the HES to start-up.

The ITHE thermal performance was modified by increasing ϕ

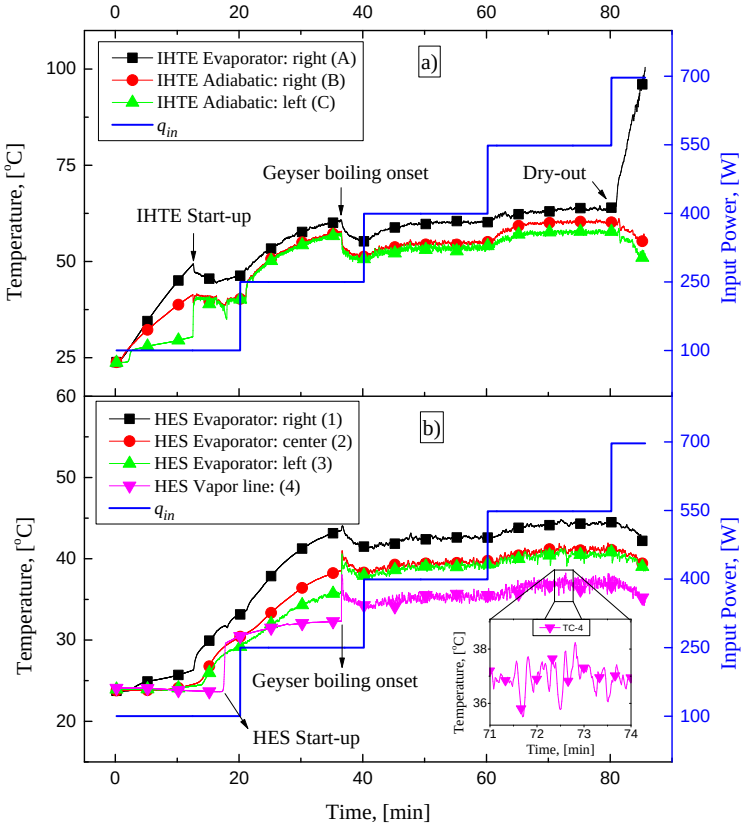

Figure 57 – Effect of input power on the thermal behavior of the a) intermediary thermosyphon with cylindrical condenser and b) heat exchanger system for case D3 ($\phi = 5^{o}$ and FR = 0.8). Symbols represent temperature recordings and the solid line, the input power.

from 0^o to 2^o or 5^o and keeping the filling ratio as 0.8. Start-up already occurs with $\phi = 2^o$. For the sake of brevity, only the results for case D3 are presented (see Fig. 57), where the temperature histories are shown on the LHS, and the input power, on the RHS. Results for the IHTE are shown in Fig. 57 a) and for the HES in Fig. 57 b). Four distinct patterns can be perceived in the IHTE thermal analysis of case D3: a transient regime, a transitional and unstable regime, a steady-state regime and a regime affected by dryout.

The IHTE thermosyphon works in transient regime for time $\leq$ 12.5 min; note the closely linear increase in evaporator temperature in Fig. 57 a) (point A). The abrupt increase in temperature at the adiabatic section (point C) at time $\approx$ 12.5 min indicates the thermosyphon start-up. The HES start-up only occurs at time $\approx$ 17.5 min; see the sudden temperature increase in the vapor line (point 4) in Fig. 57 b). This reduced interval of 5 minutes is an indication of low thermal contact resistance between the ITHE cylindrical condenser and the HES evaporator.

In the interval 12.5 $\leq$ time [min] $\leq$ 40 and with 100 $\leq q_{in}$ [W] $\leq$ 250, a transitional and unstable regime occurs. Although start-up already happened, the change rate in IHTE temperatures in points A, B and C is significant but less pronounced than in the transient regime. The IHTE evaporator and adiabatic temperatures decrease unexpectedly at time $\approx$ 36.5 min; see temperature profiles of points A, B and C in Fig. 57 a). This event coincides with a decrease in the HES temperatures; see Fig. 57 b). The temperature decrease is followed by an oscillatory behavior, which is also noted for higher input powers; see the inset graph in the same figure. This sort of fluctuation is characteristic of geyser boiling occurrence; see Casarosa *et al.* [52], Khazaee *et al.* [61] and Lin *et al.* [58], and apparently occurs more intensely in the HES device. The reduction in temperature at time $\approx$ 36.5 min is possibly associated to thermal resistance reduction at the HES evaporator induced by the geysering action.

For 400 $\leq q_{in}$[W]$\leq$ 550 corresponding to the interval 40 $\leq$ time [min] $\leq$ 80 the IHTE works in quasi-steady regime. The IHTE thermosyphon works with a mean operation temperature, T_o, below 60 ^{o}C. T_o is defined as the mean temperature value at the adiabatic section (mean of measurements at locations B and C; Fig. 54).

For input power equal to 700 W, the IHTE evaporator temperature (point A) increases almost linearly in a rate of 7.6 ^{o}C/min. At the same time temperatures in the adiabatic section (points B and C) slightly decrease. Actually, this effect shows that the IHTE thermal behavior is affected by dryout occurrence. The liquid film thickness reduces at the evaporator end cap. As a result, a dry region is created; see Faghri [47].

Since evaporation hardly occurs in this regime, the input power is mainly converted in sensible heat and the IHTE evaporator temperature increases sharply.

The thermosyphon thermal performance can be assessed with the aid of the overall thermal resistance concept, where R is defined as:

$$R = \frac{\overline{T}_{evap} - \overline{T}_{cond}}{q_{in}} \; ; \tag{5.2}$$

where $\overline{T}_{evap}$, $\overline{T}_{cond}$ stand for mean evaporator and condenser temperatures, in that order. $\overline{T}_{evap}$ is defined as the mean temperatures, red points A and B, and $\overline{T}_{cond}$, with the mean of points 1 and 2; see Fig. 54. Since Eq. (5.2) is only valid for quasi-steady regime, the apparent overall thermal resistance R_{ap} is shown in Fig. 58 along the whole IHTE operation for cases D1 to D3. Error bars for R are estimated with the aid of the standard error analysis within 95% confidence interval, following the procedure described by Holman [21] and Coleman and Steele [22].

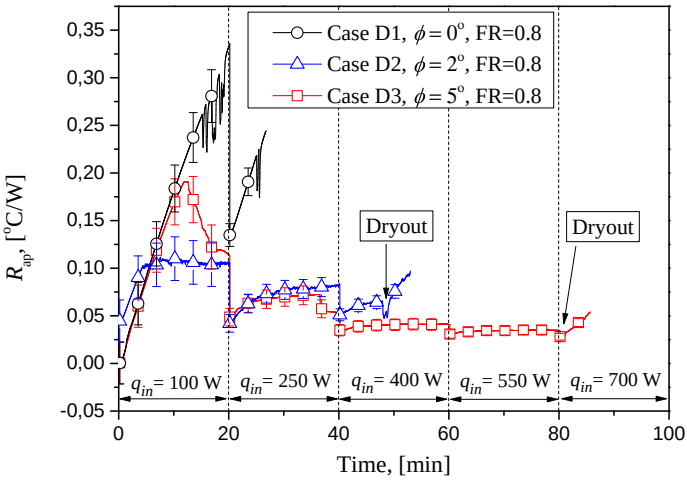

Figure 58 – Effect of inclination angle on the apparent overall thermal resistance, R_{ap}, of the intermediary thermosyphon with cylindrical condenser for cases D1, D2 and D3.

In Fig. 58 one can see that, when the IHTE start-up does not occur or the thermosyphon works in unsteady regime, the apparent overall thermal resistance increases almost linearly with the input power. That happened in case D1 for the whole operation range and in cases D2 and D3 before the start-up. Of course, the thermal resistance increases

with increasing operation temperature since the thermosyphon does not transfer heat properly in this condition.

Once the IHTE start-up occurs and in quasi-steady regime, the apparent resistance R_{ap} tends to reach a constant plateau, indicating that in these circumstances $R_{ap} \equiv R$. However, a sudden increase in R_{ap} happens if the input power is sufficiently high: this shows the onset of dryout. This is observed at time $\approx$ 48 min for case D2 and at time $\approx$ 80 min for case D3 with input powers of 400 W and 700 W, in that order. The critical input heat flux ($q" = q_{in}/A_{evap}$) for dryout occurrence is estimated as 53 kW/m^2 ($\phi = 2^o$) and as 92.8 kW/m^2 ($\phi = 5^o$). Here, $A_{evap} = \pi d_{evap-out} l_{evap}$, where $d_{evap-out}$ and l_{evap} stand for evaporator outer diameter and length, respectively. Therefore, the critical heat flux of the intermediary thermosyphon increases with increasing inclination angle. Values of R below 0.05 ^{o}C/W occur with $q_{in} = 400$ or 550 W for inclination angles of 5^o. However, these data shows that thermosyphons with cylindrical shaped condensers can work properly as intermediary heat transfer elements (IHTE) even at low inclination angles (*e.g.* ϕ from 2^o to 5^o).

5.4.2 Thermosyphon with cylindrical condenser: effect of filling ratio on the thermal behavior

The filling ratio (FR) influence on the thermal behavior of the ITHE with cylindrical plug is shown in Fig. 59 by plotting the IHTE operation temperatures in quasi-steady regime, as a function of the input power, for cases D3, D4 and D5. FR varied from 0.8 in case D3 to 1 and 1.2 in cases D4 and D5, respectively, whereas the inclination angle was kept equal to 5^o (see Table 8).

In Fig. 59, one can see that T_o increases almost linearly with the input power, in a rate of 0.025 ^{o}C/W, for the three FR cases studied. For a same input power, T_o increased of 20 and 40 ^{o}C by increasing the FR from 0.8 to 1.0 and 1.2, respectively. The filling ratio change also affects dryout occurrence. Note in Fig. 59 that the operation temperature for $q_{in} = 700$ W is not plotted for case D3 (FR=0.8), because dryout was reached. Therefore, while increasing filling ratios promote increasing operation temperatures, decreasing filling ratios facilitate dryout. The operating temperature uncertainty is estimated in $\pm$1.6 ^{o}C for a confidence interval of 95%.

5.4.3 Thermosyphon with conical condenser

Thermosyphons with conical shaped condensers were also tested as intermediary heat transfer devices, but as already justified, in this case

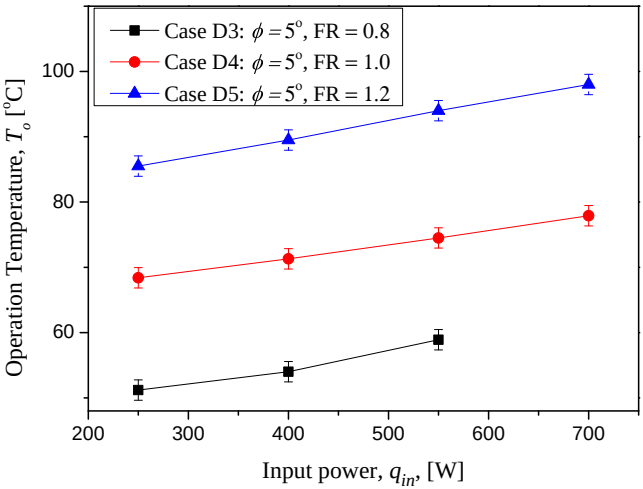

Figure 59 – Effect of filling ratio on the thermosyphon operation temperature as a function of the input power for cases D3, D4 and D5.

a calorimeter replaced the HES evaporator. The effects of filling ratio, input power and aspect ratio on the thermosyphon thermal performance are evaluated in cases E1 to E6; see Table 8. The inclination angle was set to 5^o in these cases.

Temperature histories for case E1 are presented in the LHS of Fig. 60. Measurements were performed at positions A, B, C and D as illustrated in Fig. 55. The input power provided to the IHTE evaporator is presented in the RHS.

In Fig. 60, two distinct patterns can be observed in the thermal analysis of case E1: a transient regime and a quasi-steady regime. The interval of transient operation, Δt_{to}, of approximately 63 min is indicated and represents the range where the change rate of the evaporator temperature (point A in Fig. 55) is higher than 0.2 °C/min. Note that the system start-up occurs at time $\approx$ 12.5 min with input power of 20 W, observed by the sudden raise in the adiabatic section temperature (point C). The evaporator temperature increases in a rate of 0.65 °C/min during this interval. For time $\leq$ 63 min condensation takes place along the adiabatic section owing to low input power levels ($q_{in} \leq 60$ W) and to the reduced vapor flux towards the condenser; note that the temperature difference between points C and D in Fig. 60 becomes minor only for $q_{in} \geq 80$ W.

The vapor produced in the evaporator hardly achieves the condenser. As a consequence, the operation temperature of the IHTE rises sharply. Only for time $\geq$ 63 min and $q_{in} \geq 80$ W the vapor transport to the

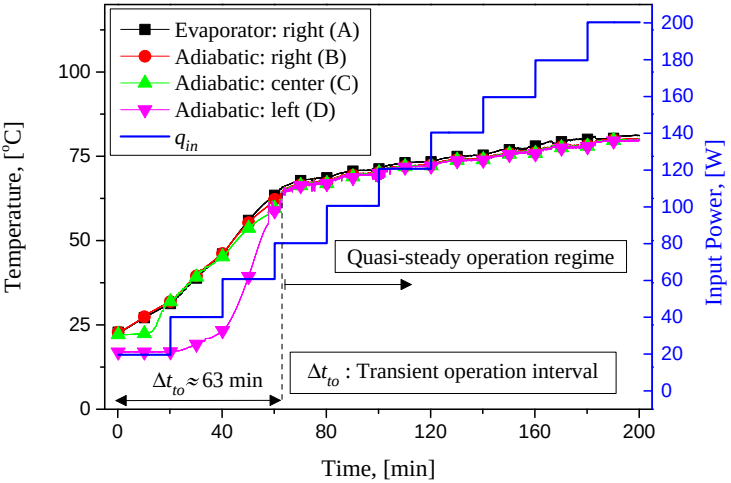

Figure 60 – Effect of input power on the thermal behavior of the intermediary thermosyphon with conical condenser plug for case E1 (FR=0.6; AR=49). Symbols represent temperature recordings and the solid line, the input power.

condenser is effective and the thermosyphon works in quasi-steady regime. The temperature difference along the thermosyphon (between points A and D) becomes minor. An operation temperature of approximately 80 ºC is achieved with an input power of 200 W.

The main thermal characteristics of thermosyphons with conical condenser (cases E1 to E6) are summarized in Table 9. The interval of transient operation, Δt_{to}, is presented together with the input power and the operation temperature in the transition from transient to quasi-steady operation regime, q_{in}^{i} and T_{o}^{i}, respectively, besides the operation temperature when the input power is modified to 200 W, T_{o}^{ii}. T_o is defined for these cases as the average temperature value at the adiabatic section (average of measurements at locations B, C and D; see Fig. 55).

Inspection of results in Table 9 reveals that T_{o}^{i} and Δt_{to} increase with increasing filling ratio for both aspect ratios. Decreasing filling ratios promote decreasing operation temperatures as expected: less heat is necessary to promote effective vapor transport towards the condenser. Of course, T_{o}^{i} and Δt_{to} increase with increasing aspect ratio: more energy at the evaporator is necessary to the vapor to surpass the additional pressure drop owing to a higher adiabatic section length. For cases with AR = 29 and FR = 0.6 or 0.8 (cases E4 and E5), the input power to promote the transition from transient to quasi-steady operation regime was 60 W, while q_{in}^{i} was 80 W for the remaining cases. Flor cases with

Table 9 – Main thermal features of thermosyphons with conical condensers (cases E1-E6).

Case (FR;AR)	Δt_{to}[min]	q_{in}^{i} [W]	T_o^{i} [^{o}C]	T_o^{ii} [^{o}C]
E1 (0.6;49)	63.0	80	64.4	80.1
E2 (0.8;49)	77.5	80	80.8	97.0
E3 (1.0;49)	77.6	80	82.8	98.7
E4 (0.6;29)	52.7	60	54.9	70.2
E5 (0.8;29)	53.8	60	56.3	70.6
E6 (1.0;29)	62.1	80	66.0	75.9

^{i} Values in the transition from transient to quasi-steady operation regime.
^{ii} Values when q_{in} reaches 200 W.

FR=0.6, when AR is reduced from 49 (case E1) to 29 (case E4) T_o^{ii} is decreased in approximately 10 ^{o}C, whereas for FR of 0.8 and 1.0 T_o^{ii} is decreased in approximately 24.5 ^{o}C.

The IHTE with conical condenser shows a higher operating temperature than the cylindrical one. Cases D3 and E5 assist this remark. These cases present the same FR and inclination angles and similar AR values; see Table 8. In case D3, the IHTE with cylindrical shaped plug was able to transfer 250 W with T_o of approximately 50 ^{o}C (see Fig. 59) whereas the IHTE with conical condenser transferred 200 W with T_o of approximately 71 ^{o}C in case E5 (see Table 9). This is expected owing to the small condenser area provided by the conical contact surface (3.4 times smaller than the cylindrical condenser). As a result, the heat transfer is not effective unless the temperature difference ($\Delta T = T_o - \overline{T}_{cond}$) is high enough. The IHTE operating temperature decreases with increasing condenser area in a rate of -0.24 ^{o}C/cm^2.

5.5 SUMMARY AND CONCLUDING REMARKS

Fictitious heat sources, mimicking electrical devices, were cooled by a heat sink via two thermosyphons associated in series. Thermosyphons with cylindrical and conical shaped condensers were experimentally evaluated as intermediary heat transfer elements. These arrangement assures practical mechanical assembly and a modularity concept for cooling of several independent heat sources. The effects of input power, filling ratio, inclination angle and aspect ratio of adiabatic section length to pipe diameter on the thermal performance of the intermediary thermosyphons

were investigated. The thermosyphon with cylindrical condenser was evaluated with inclination angles in the range 0 to 5º, filling ratios in the range 0.8 to 1.2, input power up to 700 W and constant aspect ratio of 25. The thermosyphon with conical plug was tested with filling ratios ranging from 0.6 to 1.0, input power up to 200 W and aspect ratios of 49 and 29, with a constant inclination angle of 5º. Critical heat fluxes for dryout and the input power for thermosyphon start-up have been determined.

The main concluding remarks of this study are:

- Thermosyphons with cylindrical shaped condensers can work properly as intermediary heat transfer elements even at low inclination angles (ϕ); *e.g.* 2º to 5º. In these conditions the critical input heat flux for dryout occurrence increased with increasing inclination angle, whereas the operation temperature increased with increasing filling ratio. The critical heat flux for dryout occurrence is estimated as 53 kW/m^2 for $\phi = 2º$ and as 92.8 kW/m^2 for $\phi = 5º$ with a filling ratio of 0.8. Decreasing filling ratios facilitate dryout.

- By increasing the aspect ratios from 25 to 29 or 49 and by reducing the condenser area from 0.0126 to 0.0037 m^2, the interval of transient operation and the working temperature in quasi-steady operation are increased for intermediary thermosyphons with conical shaped condenser. By decreasing the filling ratio, the intervals of transient operation and the working temperatures are decreased.

6 PASSIVE COOLING CONCEPT FOR ONBOARD HEAT SOURCES IN AIRCRAFTS

The content of this chapter is based on the following article:

- TECCHIO, C.; PAIVA, K. V.; OLIVEIRA, J. L. G.; MANTELLI, M. B. H.; GANDOLFI, R.; RIBEIRO, L. G. S. Passive cooling concept for onboard heat sources in aircrafts. Experimental Thermal and Fluid Science, v. 82, p. 402-413, 2017. DOI:10.1016/j.expthermflusci.2016.11.038

6.1 INTRODUCTION

In the last chapter, thermosyphons with cylindrical and conical shaped condensers were tested as intermediary heat transfer elements between independent heat sources and a common heat exchanger. The effects of filling ratio, inclination angle, input power, aspect ratio and condenser geometry on the operating characteristics of the intermediary thermosyphons allowed to assess the optimum design parameters for a given input heat load.

Based on the results reported in the last chapter four thermosyphons and a heat pipe were designed as intermediary heat transfer elements (IHTEs) between individual heat sources and the HES evaporator. In-flight experiments in an Embraer test aircraft were performed to certify the cooling concept (HES and IHTEs) during cruise conditions and conventional aircraft maneuvers such as roller coaster and G-load turn, which could not be achieved in laboratory conditions.

Avionics thermal behavior was simulated by employing electrical resistances with input power ranging from 40 to 850 W. Experiments were conducted with Mach numbers from 0.55 to 0.78 at altitudes of 4.5, 9.1 and 10.6 km, corresponding to air static temperatures of 0, -30 and -43 ^{o}C, respectively.

This chapter aims at:

- Verifying the thermal performance of the present passive cooling concept (HES and IHTEs) during a flight test in cruise conditions. Heat transfer from the heat sources to the evaporator of the IHTEs is tested by heat conduction and by forced convection. Although heat transfer by conduction is preferred because heat leakage is easily avoided and contact thermal resistance can be lowered, heat transfer via forced convection is also tested;

- Evaluating the positioning of heat source elements relative to the HES evaporator. A heat pipe and four thermosyphons are both tested as IHTEs. Although two-phase flow motion induced by gravity in thermosyphons improves the IHTE performance, the actual positioning of heat sources may not allow gravity induced flow motion. Therefore, a heat pipe in horizontal position relative to the HES evaporator is tested to evaluate the IHTE efficiency promoted by capillary induced flow motion;

- Assessing the HES evaporator design in order to allow practical mechanical fitting, namely here as "thermal bus". The efficacy of common basic fittings (cylindrical and conical shape plugs) is tested to evaluate contact thermal resistance between the HES evaporator and the IHTEs condensers;

- Assessing the IHTEs and HES performance in different heat sink conditions imposed by three different aircraft altitudes (4.5, 9.1 and 10.6 km), while input power from resistances are systematically varied from 40 to 850 W;

- Investigating the possibility of system malfunctioning under maneuvers such as roller coaster and G-load turn. Vertical load factors up to 2.0 were applied.

6.2 EXPERIMENTAL APPARATUS DESCRIPTION

In order to evaluate the thermal performance of the cooling system concept, all the IHTEs were developed and constructed at the Heat Pipe Laboratory facility, Labtucal/Lepten (Brazil), as well as the HES prototype. The complete passive cooling setup is described as follows.

6.2.1 Heat Exchanger System - HES

A HES schematic is shown in Fig. 61. The heat exchanger system has been extensively described in the previous chapters; see Chapter 2, Fig. 5. It is only reproduced here to show the temperature recording points, indicated by red dots numbered from 00 to 19. The evaporator outer diameter was increased from 68 to 102 mm to allow the mechanical assembly of the intermediary elements within the evaporator casing.

The HES external area was thermally isolated from the environment using a ceramic fiber for heat loss minimization. Temperatures along the HES are monitored by means of K-type thermocouples with uncertainty of ± 1.1 ºC, distributed according to Fig. 61. Velocity and temperature transmitters (two CTV 110 from KIMO Instruments) with

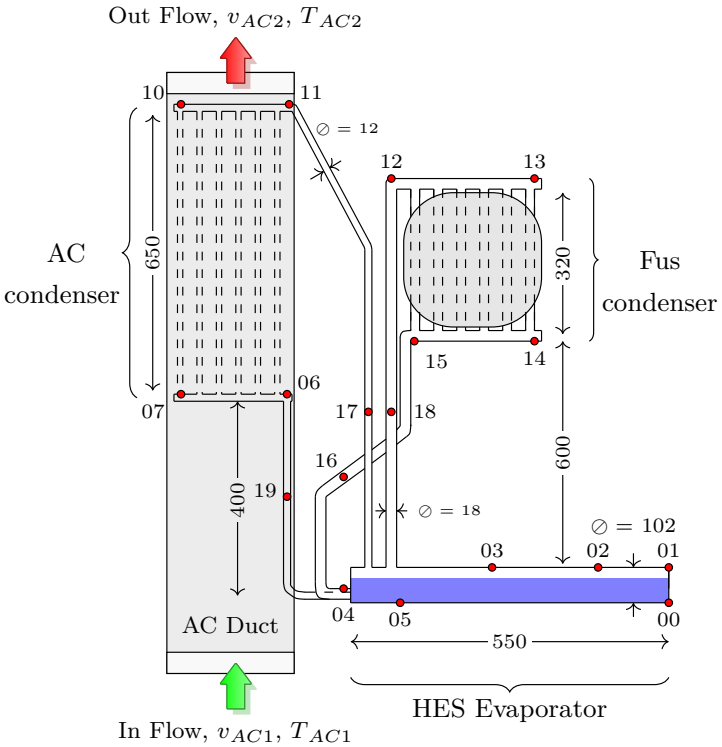

Figure 61 – Schematics of the heat exchanger system (HES). Red dots indicate thermocouple recording points.

hot-wire anemometry are used in the AC duct entrance (AC1) and exit (AC2) for velocity (v) and temperature (T) measurements. Uncertainties for v and T transmitter measurements were roughly $\pm 3\%$ and ± 0.3 ºC, respectively, of the actual measurements.

6.2.2 Intermediary Heat Transfer Elements - IHTEs

Heat pipe technologies (in this work one heat pipe and four thermosyphons) serve as intermediary heat transfer elements (IHTEs) between equipment inside the airplane and the HES evaporator. This arrangement is recommended for aerospace applications since several independent heat sources can be cooled down via IHTEs by a common heat exchanger connected to a heat sink. Note that the heat removal capacity of the fuselage HES condenser is of order 10 kW/m^2; see Oliveira *et al.* [13]. In addition, the layout strictness imposed by the limited

space for electronic equipment within aircrafts might not allow the use of thermosyphons (liquid return to the evaporator by gravity), so that the capillary pumping mechanism of heat pipes can be an alternative. For cases where the evaporator can be positioned below the condenser, the use of thermosyphons is preferable since the introduction of a wick structure represents an additional resistance to the liquid flow.

In this work, two types of shaped plugs (conical with fins and cylindrical) allow easy assembly between the IHTE condensers and the HES evaporator. These plugs were designed to reduce the contact thermal resistance between these elements and the evaporator wall. Schematics of these appliances are shown in Figs. 62 and 63. Thermosyphons (2, 3, 6-I and 6-II) and a heat pipe (4) transport heat to the HES evaporator (1). In order to simulate an electronic device operation, a heat conduction mechanism employing cartridge resistances is used to provide input power for thermosyphons (2 and 3) and heat pipe (4). A closed-loop system based on a forced convection mechanism (5) is used to provide input power to the finned thermosyphons (6-I and 6-II), as shown in Figs. 62 and 63. Heat is then transferred from these intermediate elements to the HES evaporator (1).

In Figs. 62 and 63, external and internal views of the convective system (5) are presented, respectively. The convective system is composed by a closed-loop box, an upper and a lower fan, aluminum blocks (7) and an air recirculation duct. Cartridge resistances provide heat power to the

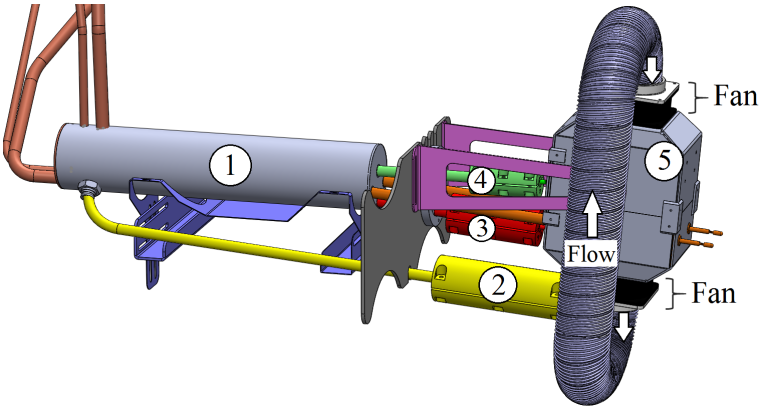

Figure 62 – Schematics of the thermal coupling apparatus. The HES system is completely independent from each IHTE. Each IHTE condenser is pressed against a metal coupling within the HES evaporator (1) with the same matching geometry.

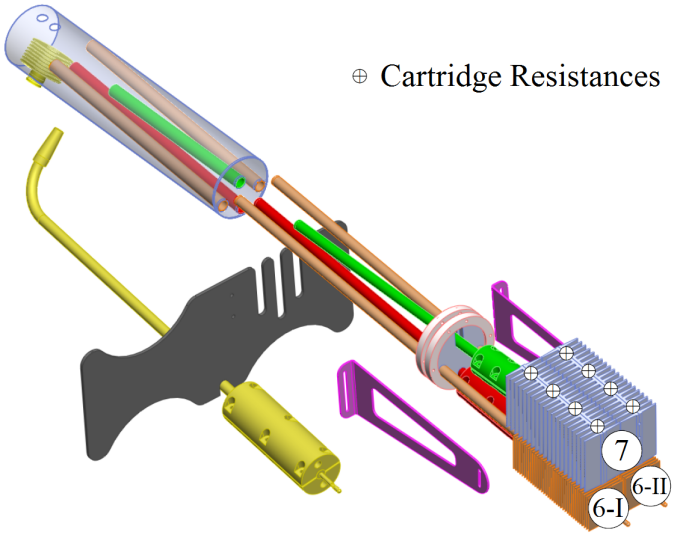

Figure 63 – Internal view of the convective system and HES evaporator. Thermosyphon evaporators contain fins (6-I and 6-II). Heat is transported from heated aluminum blocks (7) to the recirculating air by forced convection.

aluminum blocks (7), as it can be seen in Fig. 63. These blocks heat up the recirculating air within the convective system (5). To increase the heat transfer rate between the recirculating heated air and the thermosyphons, fins are welded to the evaporators of 6-I and 6-II.

Heat to the thermosyphon evaporators (6-I and 6-II) is delivered by air forced convection. The idea is to mimic cooling of actual equipment, when the original design of the heat source equipment cannot be modified to host the thermosyphon. In this case, the aluminum blocks represent a sort of avionics equipment. Air flow temperature of the convective system is monitored by Resistance Temperature Detectors (RTDs): Pt100 class 1/10 DIN sensor. Input power to the cartridge resistances is controlled virtually via Labview 2013. A TDK-Lambda GEN-300-5 programmable power supply allows voltage control.

Copper is the material used for construction of HES and IHTE devices. Besides compatible with water, this material presents high thermal conductivity. In order to ensure that condensate liquid within the thermosyphons returns to the evaporator section with the aid of gravity, the angle between horizontal and the axial axis of the intermediate thermosyphons is approximately 5º. The heat pipe is positioned horizontally as it does not depend on gravity to operate. IHTE dimensions and data

recording points are illustrated in Fig. 64. Thirty-six squared fins of 65.2 mm of length and 1.1 mm of thickness were welded to the thermosyphon evaporators (6-I and 6-II in Fig. 63) to increase the heat transfer area (namely, FTS thermosyphons), as shown in Fig. 64d. Similarly, the thermosyphon with a conical shaped condenser (namely, CTS thermosyphon) matches a conical plug within the HES evaporator with 8 fins. In this case the fins external radius is roughly 70 mm; see Fig. 63.

Water was applied as working fluid for each IHTE and for the HES. Filling ratios (FR) of 90% and 80% were used for the HES and intermediary thermosyphons, respectively. The filling ratio is defined as [47]:

$$FR = \frac{V_w}{V^*_{evap}} 100\% \ ; \tag{6.1}$$

where V^*_{evap} and V_w denote the evaporator effective volume and the working fluid volume, in that order. For thermosyphons V^*_{evap} is the inner evaporator volume (V_{evap}) given by $V_{evap} = \pi d^2_{evap} l_{evap}/4$; where d_{evap} and l_{evap} stand for the evaporator inner diameter and evaporator length, respectively. For heat pipes, $V^*_{evap} = V_{evap} - V_{ws}$; where V_{ws} stands for the wick volume at the evaporator. The choice of the applied filling ratio for the HES was affected by the presence of each IHTE condenser in the HES evaporator. A minimum filling ratio of 90% should be used to ensure that all IHTE condensers would be flooded by the working fluid, preventing the IHTEs malfunctioning. For the intermediary thermosyphons (CTS, TS and FTS), the filling ratios were selected based on a systematic assessment of the filling ratio influence on the thermosyphons performance. Filling ratios of 80% were chosen because critical heat fluxes for dryout were sufficiently high whereas operation temperatures were below typical failure values for avionics; *e.g.* 70 to 100 ^{o}C; see Chapter 5, Section 5.4.2.

A copper wire mesh screen was employed as the heat pipe wick structure. To increase heat transfer capacity, eight layers of a mesh number sixty-two were used. In order to fulfill with liquid the entire wick void, water volume corresponding to 110% of the wick structure void volume was selected. Premature failure by dry-out occurrence was then prevented. The water volume V_w can be written as:

$$V_w = 1.1 \varepsilon V_t \ ; \tag{6.2}$$

where ε and V_t stand for wick porosity and wick structure volume considered as a continuum medium, in that order. The porosity, ε, is given

by:

$$\varepsilon = 1 - \frac{1}{4}\pi S N d_w \ ; \tag{6.3}$$

where S, N, and d_w stand for the crimping factor (in general 1.05; see Marcus [80]) mesh number and wire diameter, respectively. The filling ratio for the heat pipe is 105%. The characteristics of the heat pipe wick structure are summarized in Table 10.

Table 10 – Characteristics of the heat pipe wick structure.

Wick material	Copper
Wick type	Wire mesh screen
Mesh Number, N, [inch^{-1}]	62
Number of layers	8
Wire diameter, d_w[mm]	0.16
Porosity, ε	68%

6.3 EXPERIMENTAL PROCEDURE

The experimental apparatus was installed and tested in an aircraft in several flight conditions. Since heat sink conditions vary with altitude, the HES and IHTEs thermal performance was evaluated in several different test settings.

6.3.1 Flight Description

Experiments were executed as follows. For tests in cruise conditions, a constant Mach number, M_∞, of 0.78 was set. The test windows were executed at altitudes, H_{sl}, of 9.1 and 10.6 km above the sea level, corresponding to air static external temperatures, T_∞, of approximately -30 and -43 ^{o}C, respectively; see Fig. 65. The thermal behavior of the IHTEs was also evaluated during roller coaster and G-load turn maneuvers with an approximated altitude of 4.5 km and Mach number of 0.55; see the time lag from 144 to 168 minutes in Fig. 66. Vertical load factors, $N_z = L/W$, of 0.5, 1.5 and 2.0 were experimented during aircraft maneuvers. Here, L and W are lift and aircraft weight, respectively.

(a) Heat pipe - HP.

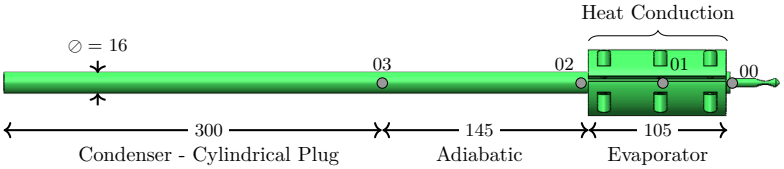

(b) Thermosyphon with cylindrical plug - TS.

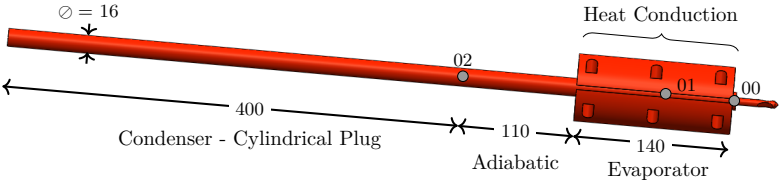

(c) Thermosyphon with conical plug - CTS.

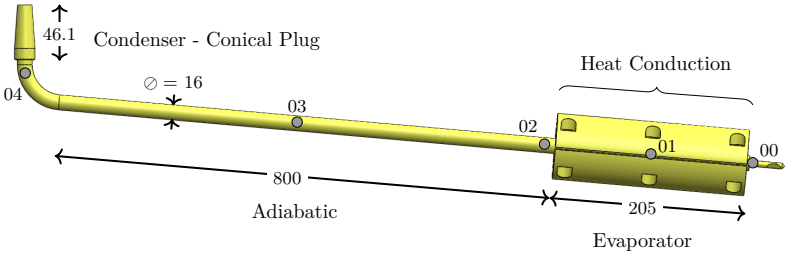

(d) Thermosyphon with fins welded to the evaporator - FTS.

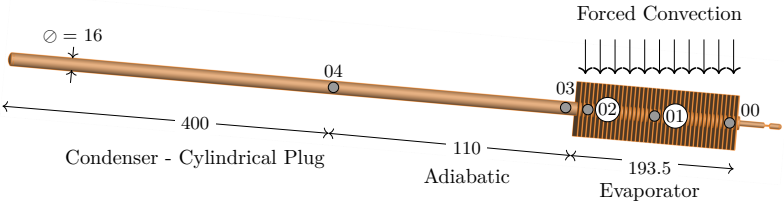

Figure 64 – IHTE dimensions in millimeters and temperature recording points, indicated by gray dots.

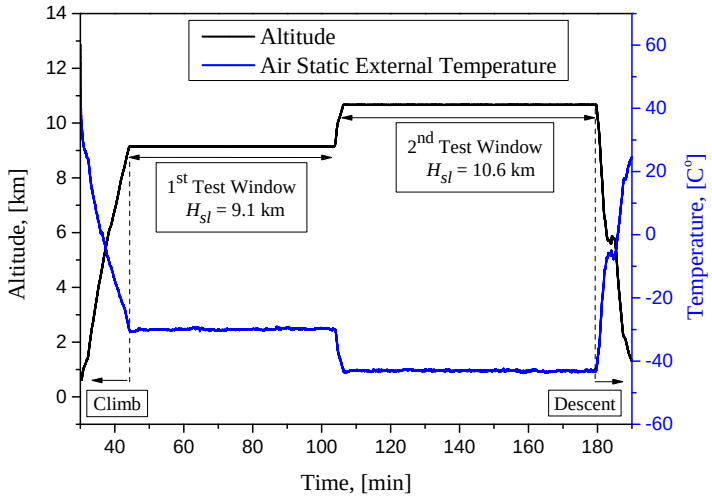

Figure 65 – Altitude, H_{sl}, and air static external temperature, T_{∞}, for the flight tests in cruise conditions.

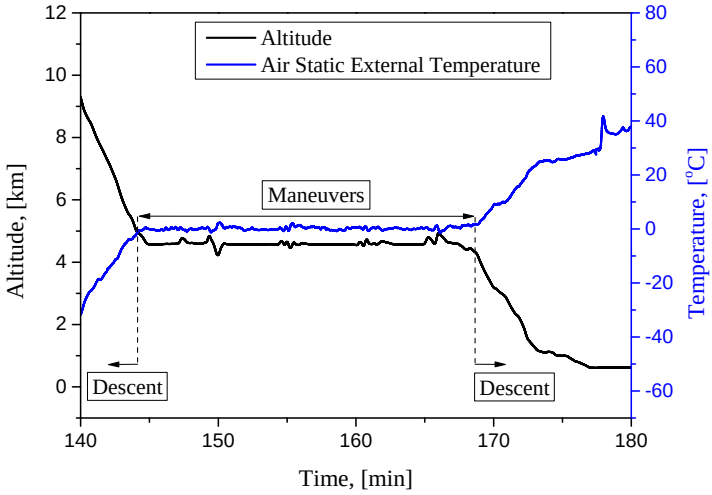

Figure 66 – Altitude, H_{sl}, and air static external temperature, T_{∞}, for the flight tests during roller coaster and G-load turn maneuvers.

6.4 RESULTS AND DISCUSSION

6.4.1 Heat pipe (HP)

The effect of the input power on the heat pipe thermal performance is presented in Fig. 67. Input power ranges from 40 to 120 W with an increment of 40 W. A period of 10 minutes in each power level sufficed to approach steady state operation. Note that the HP temperatures in the LHS of y-axis are approximately constant after 7-8 min once a test is initiated. The heat pipe was cooled down between the first and second test windows, corresponding to a total cooling time of 40 min (note that the time axis is shortened in Fig. 67 for better visualization).

With a given input power level, the heat pipe shows similar thermal operational conditions during the first and second test windows (altitudes of 9.1 and 10.6 km above sea level, in that order). The reduction of the air static external temperature from -30 to -45 ºC with increasing altitude barely modified the HES evaporator average temperature for a given level of input power (HES results are further presented in Fig. 72). Notice that the HES evaporator is the heat sink for every IHTE; see Figs. 62 and 63. Therefore, changes in the heat sink of the HES fuselage condenser promoted by modifying the aircraft altitude from 9.1 to 10.6 km weakly affect the heat pipe thermal performance.

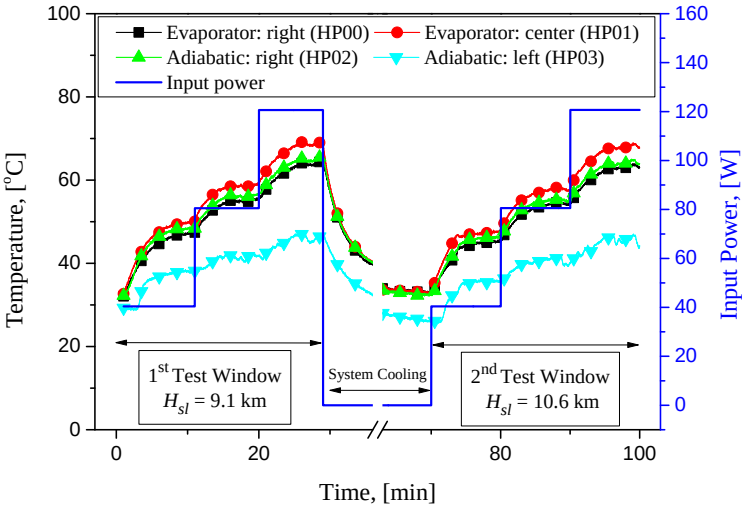

Figure 67 – Effects of input power and altitude on the heat pipe thermal response during a flight test in cruise conditions. The thermocouple positioning (00, 01, 02 and 03) as provided in Fig. 64a.

The HP evaporator temperature (HP01) in quasi steady-state regime increases with a ratio of 0.25 ºC/W for input power ranging from 40 to 120 W. The heat pipe start-up already occurs with 40 W in both altitude conditions. Maximum temperature, approximately 70 ºC, occurs at the heat pipe evaporator with 120 W. With the same power, a temperature difference of 15 ºC is observed between the HP evaporator (HP00) and the condenser entrance (HP03). The average temperature of the HES evaporator strongly affects the HP03 temperature. Dry-out occurrence is not evident during tests for the given experimental conditions.

The overall heat pipe thermal resistance, R_{HP}, including the thermal contact resistance between HES evaporator and HP condenser, can be written as:

$$R_{HP} = \frac{\overline{T}_{evap-HP} - \overline{T}_{evap-HES}}{q_{in}} \; ; \tag{6.4}$$

where q_{in}, $\overline{T}_{evap-HP}$ and $\overline{T}_{evap-HES}$ stand for input power, average temperature of the heat pipe evaporator and average temperature of the HES evaporator, respectively. A thermal resistance, R_{HP}, of 0.33 ºC/W was obtained in quasi-steady regime with $q_{in} = 120$ W. $T_{evap-HES}$ is roughly 30 ºC.

6.4.2 Thermosyphons with fins welded to the evaporator (FTS)

Thermosyphons with cylindrical shaped condenser and with fins welded to the evaporator (two FTS, Fig. 64d) were also tested in cruise conditions. In Fig. 68, the effect of the input power on the temperature field of the convective system containing two FTS is presented. T_{alum} stands for the aluminum blocks temperature and T_{air}, the air flow temperature. The fan outlet mean velocity is approximately 9.0 m/s for a constant rotation speed of 3600 rpm. Temperature measurements in the surface of the aluminum blocks (heated by resistances) presented minor variation and therefore only one result is presented in Fig. 68. This is expected owing to the negligible conductive resistance, R_k, as compared to the convective one, R_h. A Biot number, Bi, as defined by Eq. (6.5) assists this remark:

$$Bi = \frac{R_k}{R_h} = \frac{l/k_s}{1/h} \; ; \tag{6.5}$$

where l, k_s and h stand for a characteristic length, aluminum thermal conductivity and heat transfer coefficient. Here, $R_h >> R_k$ and therefore

$Bi << 1$, implying minor temperature variations in the aluminum block. A lumped system analysis is possible; see [81–84].

Between the first and second test windows, FTS-I and FTS-II are cooled down for approximately 45 minutes (note that the time axis is shortened between 55 and 100 min in Fig. 68 for better visualization). Input power ranges from 300 W to 850 W. Steady state operation is not evident for the intermediate heat transfer elements, FTS-I and FTS-II; they do not present a constant temperature level after 10 min in a given input power.

The intense fluctuations in temperature recordings are characteristic of geyser boiling phenomenon as already discussed in Chapter 4. This condition is observed by high amplitude and low frequency temperature oscillations, particularly for FTS04 thermocouples. Temperature oscillations in the condenser entrance are explained as follows. Bubbles grow abruptly in a short period, detach and leave the evaporator section. Thus, the vapor mass flux along the thermosyphon axis is instantly accelerated, corresponding to sudden overheating of the condenser. The heat flux to the FTS evaporator is not sufficient to keep the intense evaporation rate and cooling of the FTS condenser occurs. The description above is recurrent once a new abrupt evaporation event occurs.

FTS start-up takes place when the input power is set to 600 W and 300 W for the first and second window test, respectively, in both FTS elements. Notice the FTS temperature gradients are modified at time 45 min (first window) and at time 105 min (second window). In fact, the start-up for elements FTS-I and FTS-II is not simultaneous. The start-up difference in time is due to the non-symmetrical air flow inside the closed-loop forced convection system.

The air temperature, T_{air}, was monitored due to safety requirements: fans could not work above 100 ºC. Note in Fig. 68 a) that the input power is decreased when T_{air} reaches 90 ºC. Maximum temperature for the aluminum blocks, T_{alum}, was approximately 137 ºC when the input power was set to 850 W. Clearly, with this setup the convective heat transfer coefficient acting at the aluminum blocks need to be increased to keep T_{alum} (representing the avionics temperature) below 100 ºC. During the first test window T_{air} and T_{alum} continuously increased. In the second test window, reduction of the input power was necessary after time $\approx$ 121 min.

6.4.2.1 Analysis

Energy and fluid flow analyses of the convective system are provided as follows. For a control volume containing the aluminum blocks,

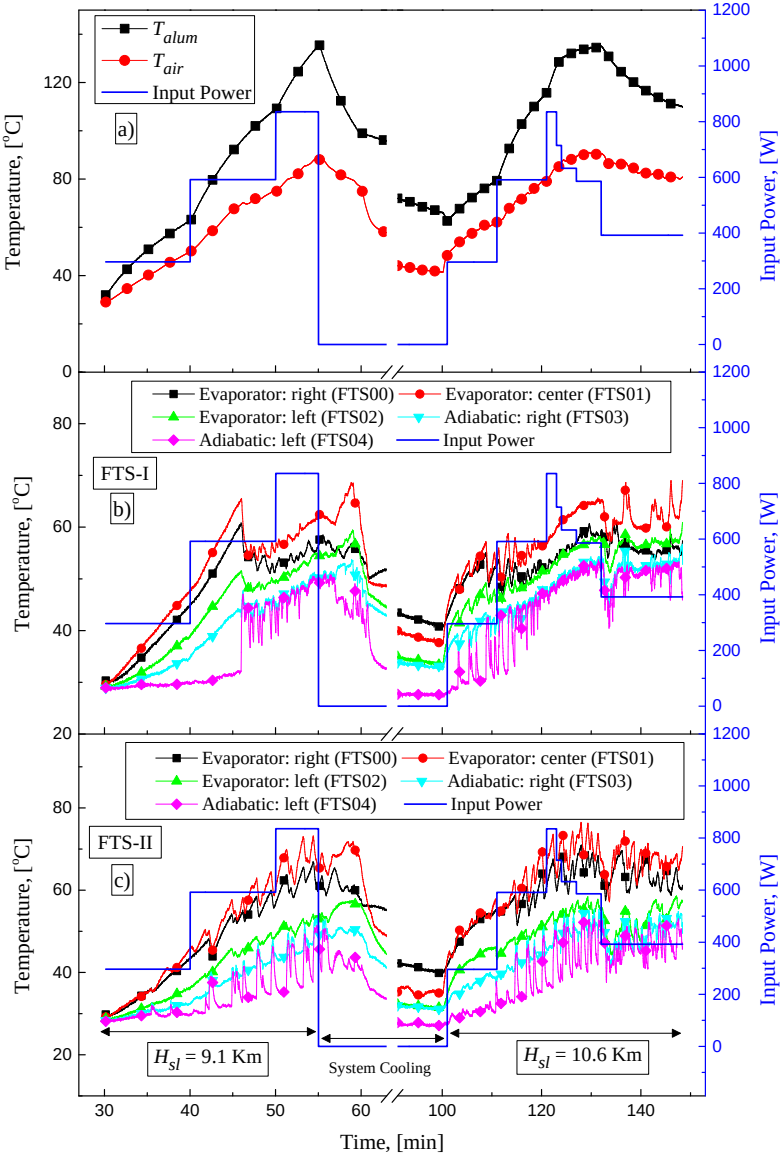

Figure 68 – Effects of input power and altitude on the thermal response of the convective system containing two FTS; temperature recordings of a) aluminum blocks, T_{alum}, and air flux, T_{air}; b) FTS-I and c) FTS-II. The thermocouple positioning (00, 01, 02 and 03) as provided in Fig. 64b.

the lumped system analysis ($Bi << 1$) assures that the energy released by the cartridge resistances, Q [J], in a time interval dt is equal to the sum of the energy transferred to the air stream and the change in internal energy of the aluminum blocks:

$$Q = \int q_{in} dt = \int hA_{alum} \left(T_{alum} - T_{air}\right) dt + \int m_{alum} c_{p,alum} dT_{alum} \ ; \tag{6.6}$$

where A, T, m and c_p stand for area, temperature, mass and specific heat at constant pressure. The fans are kept with the same rotation speed and assuming that the temperature influence on h is minor, it is reasonable to assume a constant mean h throughout the FTS experiment. The aluminum variables (A, m and c_p) are known a priori. Since input power and temperature measurements are shown in Fig. 68, estimation of h is possible. Solving Eq. (6.6) for h yields

$$h = \frac{q_{in}\Delta t - \left[mc_p \left(T_{t_0+\Delta t} - T_{t_0}\right)\right]_{alum}}{A_{alum} \int\limits_{t_0}^{t_0+\Delta t} \left(T_{alum} - T_{air}\right) dt} \ . \tag{6.7}$$

Values of h externally to the aluminum block were found to be approximately 31 W/(m^{2}K). Thus, the power transferred by forced convection from the aluminum blocks to the air stream is given by:

$$q_{alum-air} = hA_{alum} \left(T_{alum} - T_{air}\right) \ . \tag{6.8}$$

Assuming that the heat transfer coefficients on the FTS evaporators, h_{FTS}, are of same order of magnitude as the ones externally to the aluminum block, h, it is possible to compute the power absorbed by each FTS, $q_{air-FTS}$, and therefore the heat leakage to the cabin:

$$q_{air-FTS} = hA_{FTS} \left(T_{air} - \overline{T}_{evap-FTS}\right) \ . \tag{6.9}$$

In Fig. 69, the power transferred from the recirculating air stream to the evaporator of the finned thermosyphons by forced convection, $q_{FTS} = q_{air-FTS-I} + q_{air-FTS-II}$, is presented. In $46 \leq t[\text{min}] \leq 55$, 600 or 850 W are provided by the cartridge resistances to the aluminum block; see input power in Fig. 69. In this time lag, the power transferred to the recirculating air stream, $q_{alum-air}$, ranges roughly linearly from 400 to 700 W while the remaining power is used to increase the aluminum blocks internal energy. With Eq. (6.9), it is estimated that 84% of $q_{alum-air}$ is transferred to the evaporator of the thermosyphons and, as a consequence, the remaining power (16%) is leaked to the air cabin. Roughly 586 W

are transferred to the FTS thermosyphons in time ≈ 55 min. The FTS start-up was found to occur when each FTS received ≈ 150 W. Heat transfer coefficients were restricted by geometrical constraints in the aircraft setup. Values of h were found to be 40 W/(m^{2}K) in laboratory with the same fan outlet mean velocity; ≈ 9 m/s. Recirculating air in laboratory tests was subjected to a minor pressure drop within the air loop.

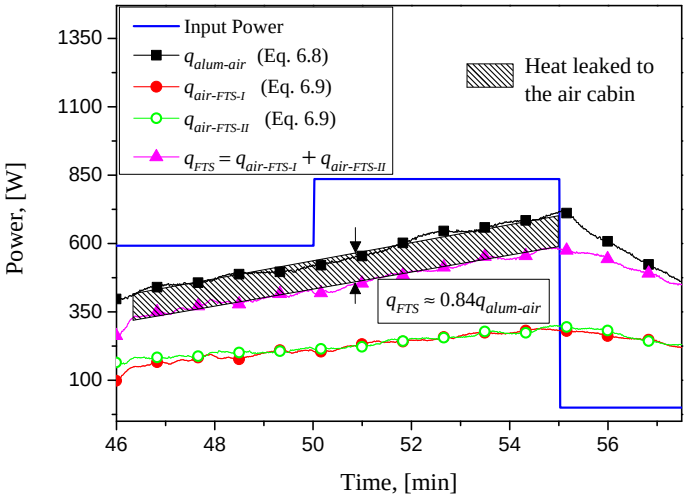

Figure 69 – Power transferred from the air stream to the thermosyphons with fins welded to the evaporator, q_{FTS}, and the heat leaked to the air cabin.

6.4.3 Thermosyphon with conical plug (CTS)

Thermosyphons with conical (CTS) shaped plugs were also evaluated as intermediary heat transfer elements; see Fig 64c. Values of aircraft altitude, 9.1 and 10.6 km above sea level, and air static temperatures, -30 and -45 ^{o}C, are approximately the same as the ones presented in Fig. 65. Effects of input power and altitude on the CTS thermal behaviors can be seen in Fig 70.

The input power was set to 100, 250 and 400 W in Fig. 70. Between the 1^{st} and 2^{nd} test windows, CTS heat sources are turned off and the system is cooled down for approximately 45 minutes (note that the time axis is shortened in Fig. 70).

Inspection of Fig. 70 reveals that the start-up only occurred when the input power was set to 250 W in both time windows. In time ≈ 13 and 87 min, the change in temperature gradient of the thermocouple

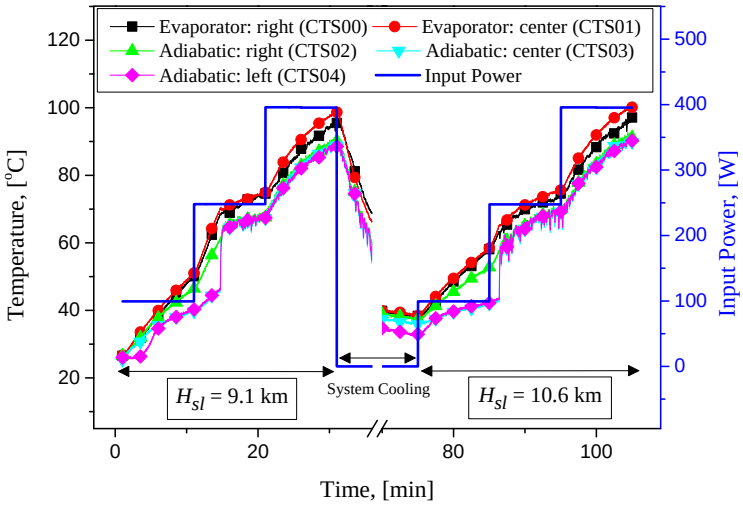

Figure 70 – Effects of input power and altitude on the CTS thermal performance. The thermocouple positioning (00, 01, 02, 03 and 04) as provided in Fig. 64c.

CTS04 supports this remark. Operation of the CTS thermosyphon tends to a steady state regime when kept longer at this power level. When the input power is increased to 400 W, transient regime operation is evident. The heat removal capacity in the CTS condenser is limited due to the elevated thermal resistance to the HES evaporator. Heat leaves the conical geometric shape with restricted area (2914 mm^2) followed by thermal contact resistance until reaching the plug with fins at the HES evaporator (55600 mm^2). Note that the heat path is facilitated in the HP, FTS and TS condensers (79100 mm^2 of area), followed by contact resistance and an approximated matching geometry at the HES evaporator.

Note that heat sink changes of the HES fuselage condenser (changes in the air static temperature and heat transfer coefficients) promoted by experiments at different altitudes, 9.1 and 10.6 km, hardly affect the CTS operation. Intermediate devices show similar thermal behavior during first and second test windows. Of course, the heat sink capacity of the Fus condenser is big enough to not affect the IHTE thermal behavior.

6.4.4 Thermosyphon with cylindrical plug (TS)

The thermal behavior of the thermosyphon with cylindrical plug (Fig. 64b) is shown in Fig. 71. The input power was set to 100, 300 and 500 W in both test windows. In each setting, the power level is

kept constant for 10 minutes, except for the last level in the second test window, which takes approximately 15 min. The test windows settings are in accordance with the flight description shown in Fig. 65.

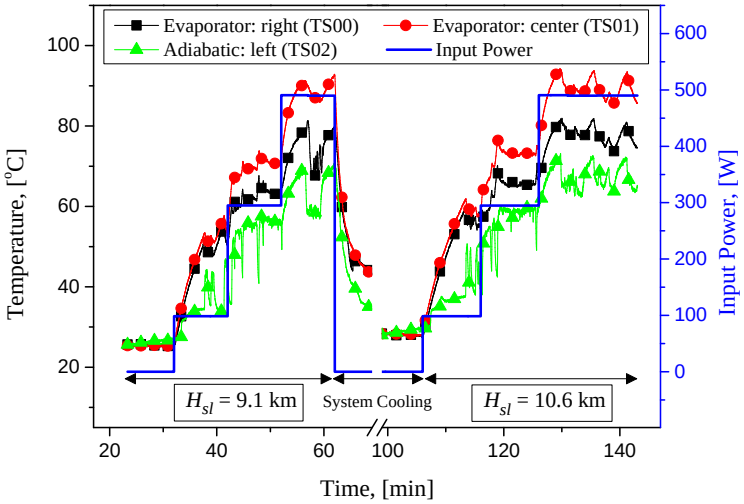

Figure 71 – Effects of input power and altitude on the CTS thermal performance. The thermocouple positioning (00, 01, 02, 03 and 04) as provided in Fig. 64c.

Start-up operation occurs with 100 W in both windows. As compared to the CTS operation, the lower resistance at the TS condenser facilitates the start-up. Although geyser boiling instabilities are observed (see the temperature oscillations in Fig. 71), the TS element is able to work properly with 500 W of input power. Mean temperature of the TS element is 75 ºC for input power of 500 W. Heat sink changes of the HES fuselage condenser promoted by different altitudes hardly affect the TS operation. Although not shown here, further increase in power promotes TS dry-out.

6.4.5 Thermal response of the heat exchanger system (HES)

The HES thermal behavior while the HP and FTS were active is presented in Fig. 72. Numbers denote the thermocouple positioning along the HES in accordance to Fig. 61.

Air flow velocity in the AC duct is approximately 2.5 m/s throughout the experiment with a mean temperature at the entrance section of 15 ºC. The HES evaporator receives heat from the HP or FTS intermediate elements. Temperature differences between vapor lines and exit manifolds in both Fus and AC condensers of the HES, evidenced by ther-

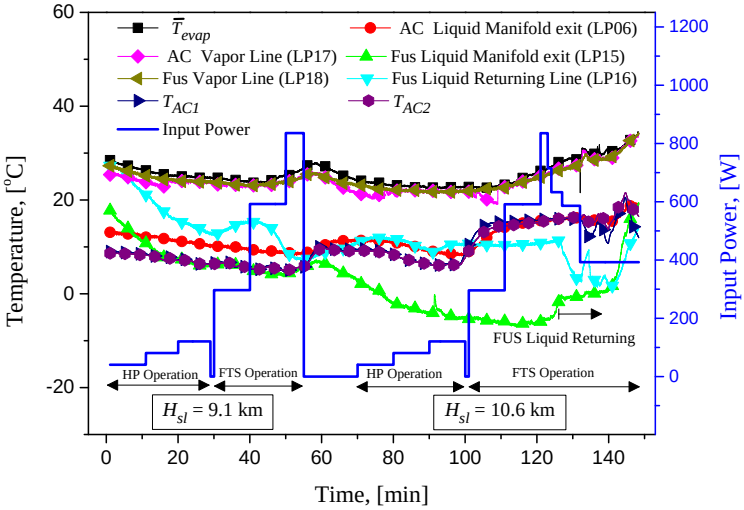

Figure 72 – Effects of input power and altitude on the HES thermal performance. Heat Pipe (HP) or two thermosyphons with fins at the evaporator (FTS) were used as IHTEs. The temperature recording points as given in Fig. 61.

mocouples LP17, LP18, LP06 and LP15 reveal that condensation process occurs in both condensers during the first test window ($H_{sl} = 9.1$ km). Freezing of water refrigerant occurred within the Fus condenser during the second test window ($H_{sl} = 10.6$ km) with $T_\infty \approx -43$ ºC.

During the 2^{nd} test window (after time ≈ 70 min), the HES and HP collective behaviors are explained as follows. Once heat is transferred from the HP to the HES evaporator, evaporation occurs and vapor is transported to both heat sinks. Condensation occurs at the AC condenser (it can be inferred by thermocouples LP06 and LP17 in Fig. 72). The energy carried by the vapor flux which achieves the Fus condenser is not enough to melt the frozen region at the Fus condenser (see the temperature recordings of LP15 in Fig. 72 and its positioning in Fig. 61). The heat removal capacity of the Fus condenser is rather dominant in-flight, 10 kW/m^2 at the fuselage and in the given conditions. Nevertheless, the experimental findings above only mean that the HES does not work as two closed loops with input power of order 120 W at the HES evaporator. From an engineering viewpoint, the heat sink capacity of the HES evaporator relative to the HP performance is sufficient to keep the temperature of the HP evaporator (which represents a sort of avionics) in tolerable levels.

After time ≈ 100 min, the HP is disabled and the FTS is ac-

tivated with 300 W of input power. The HES is still over-dimensioned for such power load. With the input power over 600 W, the temperature recording at the Fus exit manifold (thermocouple LP15 in Figs. 61 and 72) raises until becoming above 0 ºC. The energy content of the vapor flux which reaches the Fus condenser is enough to melt the refrigerant in the condenser lines and liquid returns to the HES evaporator. Temperature in the Fus liquid returning line (thermocouple LP16 in Figs. 61 and 72) decreases: cold liquid reaches the Fus return which was occupied with vapor prior to the melting process. The HES system works then as two closed loops.

From the description given above, it is demonstrated the HES heat removal capacity (particularly, the Fus condenser of the HES): temperatures of the HP and FTS evaporators (Figures 67 and 68) were kept in acceptable levels. Only a small part of the heat load which reaches the HES evaporator is dissipated in the AC condenser in-flight. Temperatures at the AC entrance, T_{AC1}, and at the AC exit, T_{AC2}, match within experimental uncertainty. The AC condenser is mainly suitable to assure cooling of intermediate heat loads (*e.g.* 350 W) on ground.

The HES thermal response when CTS and TS thermosyphons are working as IHTEs is shown in Fig. 73. The HES works as two closed loop thermosyphons for the first flight test window (note that the temperature in the Fus liquid manifold exit, thermocouple 15, is above 0 ºC). When the aircraft altitude reaches 10.6 Km ($T_\infty \approx -43$ ºC) and without input power to any IHTE, freezing of water refrigerant within the HES occurs at the Fus condenser. The fuselage condenser thermal condition does not allow liquid returning to the HES evaporator. With the CTS operation, the heat transfer rate is not sufficient to melt the refrigerant. That only happened when the input power was set to 500 W during the TS operation. Note that the temperature of the Fus liquid returning line (LP16) suddenly decreases from 15 ºC to approximately 0 ºC in time $\approx$ 130 min. At this point, cold liquid reached the return line of the evaporator, meaning that melting occurred.

6.4.6 Thermal response of the intermediary elements in maneuvers

Aircraft maneuvers may affect the IHTEs thermal performance and therefore were tested. Basic maneuvers as roller coaster and G-Load turn were performed. A pull-up with vertical load factor, $N_z = L/W$, of 1.5 and a push-over of 0.5 were employed for roller coaster maneuvers. G-load turns were performed with N_z of 2.0. Roller coaster and G-load turn maneuvers occurred in periods of 2 and 5 seconds, respectively.

IHTEs thermal behaviors are shown in Figs. 74 and 75 with the

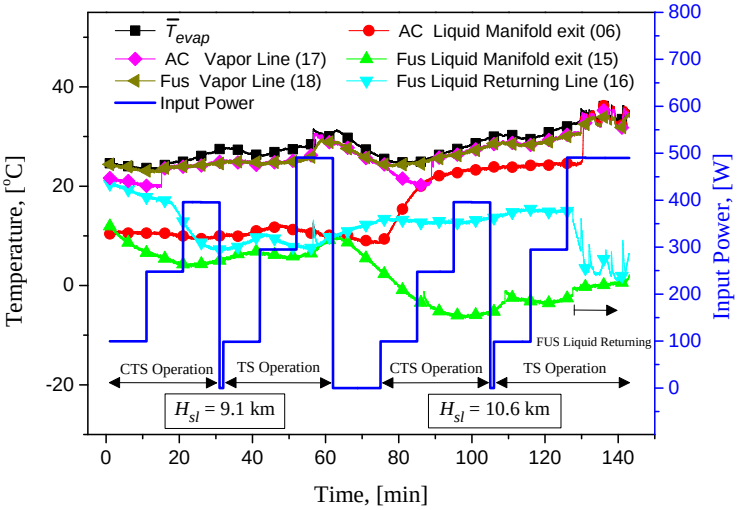

Figure 73 – Effects of input power and altitude on the HES thermal performance. Thermosyphons with conical (CTS) and cylindrical (TS) shaped plugs were used as intermediary elements.

vertical load factors during aircraft maneuvers. A constant input power for each IHTE is set during aircraft maneuver (120 W for HP; 500 W for TS; 400 W for CTS and 850 W for FTS). As thermosyphons FTS-I and FTS-II are similar only the results for FTS-I suffice to understand the main thermal features.

Roller coaster and G-load turn maneuvers can be considered unimportant for IHTE thermal performance. Note that the temperature recordings are not affected by the imposed vertical loads in Figs. 74a, 74c, 75a and 75c. Although accelerations could theoretically affect the HES and the IHTEs performance, the timescale in which they occur in aerospace applications are irrelevant to modify the two-phase flow behavior within heat pipe technologies and therefore their thermal behavior.

6.5 SUMMARY AND CONCLUDING REMARKS

A cooling system concept to manage heat sources in aircrafts was experimentally evaluated during conventional cruise conditions and maneuvers. A heat exchanger system - HES (consisting of two closed-loop thermosyphons), intermediate heat transfer elements - IHTEs (heat pipe and thermosyphons) and heat sources (simulating avionics) compose the setup. Heat conduction and forced convection were applied to transfer heat from the sources to the evaporators of IHTEs. Two types of shaped

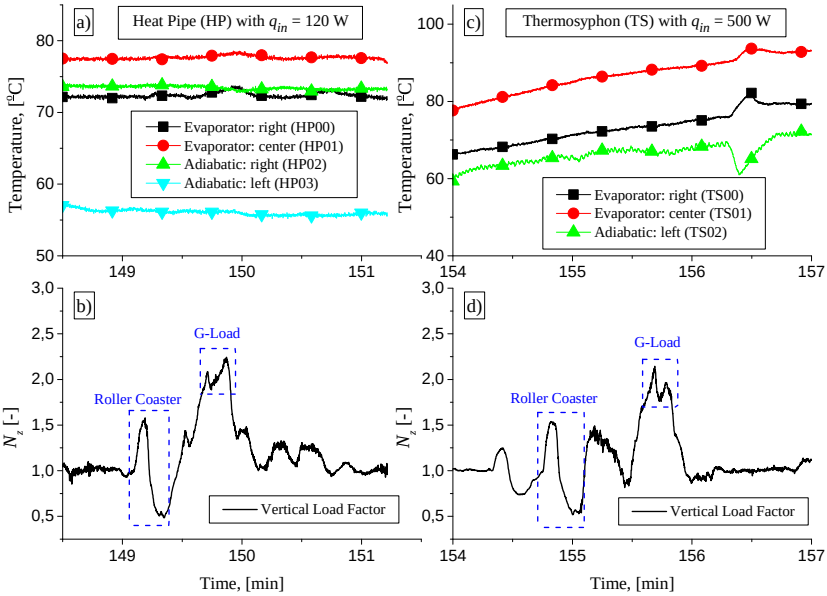

Figure 74 – Thermal response of the a) heat pipe (HP) and c) thermosyphon with cylindrical plug (TS) during b) and d) roller coaster and G-load maneuvers.

plugs were employed for thermal coupling between the IHTE condenser and HES evaporator: conical with fins and cylindrical. Heat is finally dissipated in the air conditioning system and mainly in the aircraft fuselage.

The main achievements of this work are:

- Heat sink changes of the HES fuselage condenser promoted by experiments at different altitudes, 9.1 and 10.6 km, hardly affect the IHTEs operation. The heat sink capacity of the fuselage condenser is large enough to not affect the IHTE thermal behavior and therefore assuring acceptable temperature levels for avionics;

- Thermal control of avionics at mean temperatures of 70 ºC can be achieved with 0.7 meter long heat pipes and thermosyphons dissipating 120 W and 500 W, respectively. With increasing thermal resistance in the thermosyphon condenser (thermosyphon with conical plug), dissipation may be limited to 250 W;

- Convective system is a heat dissipation alternative where heat conduction between avionics and IHTE evaporator is not possible. Increased evaporator area by fins and large heat transfer coefficients

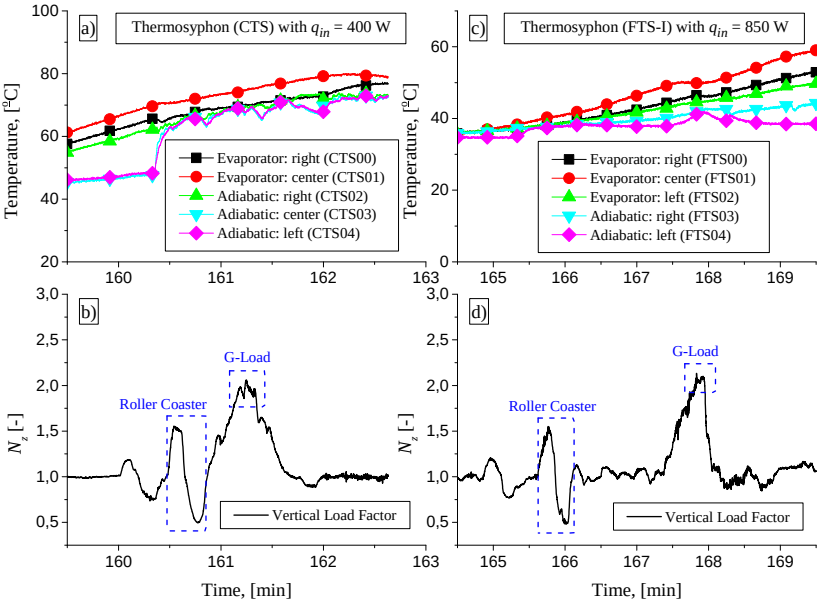

Figure 75 – Thermal response of the a) thermosyphon with conical plug (CTS) and c) thermosyphon with fins welded to the evaporator (FTS-I) during b) and d) roller coaster and G-load maneuvers.

can assure heat transport to the ITHE. Two thermosyphons with fins in the evaporator dissipated 586 W with the air temperature within the convective system of approximately 80 ºC. Nevertheless, power consumption by fans, sound noise, periodic maintenance and increased IHTE weight are major drawbacks of this solution;

- Timescale in which aircraft maneuvers occur are irrelevant to modify the thermal behavior of heat pipe technologies.

7 CONCLUSION

7.1 SUMMARY AND CONCLUDING REMARKS

Passive aircraft cooling systems based on heat pipe technology were developed and experimentally evaluated under a multitude of thermal conditions observed during aircraft operations. A heat exchanger and intermediary heat transfer elements comprise the cooling systems. The heat exchanger prototype consists of loop thermosyphons with two condensers and a common evaporator. The aircraft air conditioning system and the fuselage served as heat sinks for the heat exchanger condensers. Thermosyphons and a heat pipe served as intermediary heat transfer elements between a heat source (avionics) and the heat exchanger evaporator. Cylindrical and conical shaped condensers were tested as fitting geometries. The influence of filling ratio, inclination angle, input power and aspect ratio on the thermal performance of the intermediary thermosyphons were investigated. Distilled water was used as the working fluid.

The cooling prototypes were tested in laboratory conditions and on-board in an aircraft. The thermal performance of the fuselage condenser was tested with temperatures ranging from -56 to 50 ^{o}C in actual aerospace convective coefficients characteristics of a commercial aircraft operation. Experiments were performed on-ground and in-flight, including conventional flight maneuvers such as roller coaster and G-load. True aircraft air speeds of up to 878 km/h were registered in cruise conditions, corresponding to a flight Mach number of 0.78. Altitudes of up to 12 km above sea level were reached. Ordinary aircraft cabin electronics were simulated by means of cartridge resistances with input power of up to 900 W.

The effects of geyser boiling phenomenon on the heat exchanger system (loop-thermosyphons) in quasi steady-state and transient regimes were investigated. Evaporator structural vibrations induced by geyser boiling occurrence were measured. The effects of filling ratio, input heat flux and heat sinks thermal conditions on geyser boiling have been determined.

The main achievements of this study are:

- The cooling systems proposed in this study provide passive thermal control of on-board heat sources in the aircraft cabin on the ground or in-flight. The heat removal capacity of the fuselage heat sink is

largely dominant in-flight (10 kW/m^2), reducing the heat load at the air conditioning. Under in-flight and on-ground conditions, a vapor temperature of approximately 45 ^{o}C with an input power of 0.85 kW and 60 ^{o}C with 0.6 kW, respectively, ensures the avionics operation within the tolerable levels.

- The heat exchanger system can work properly even when low temperatures of the aircraft cabin-external air can freeze the working fluid. In these circumstances heat is removed without promoting any increase in the evaporator temperature or structural failure.
- Effects of the aircraft maneuvers on the thermal behavior of the prototypes are unimportant, with the exception of the pitch angle on the loop-thermosyphons.
- Heat pipes and thermosyphons can serve as intermediary heat transfer elements between on-board avionics and loop-thermosyphon evaporator dissipating 120 W and 500 W, respectively, within the tolerable temperature range. Conical and cylindrical shaped plugs showed to be possible fitting elements as condenser geometries of the intermediary thermosyphons. Alternatively, a convective system may be used where heat conduction between avionics and intermediary thermosyphons is not allowed. However, power consumption by fans and additional weight are major drawbacks of this solution.
- Geyser boiling phenomenon can eventually yields intense vibration of the loop-thermosyphons evaporator. In quasi-steady regime, the ratio of thermal resistances of the HES condensers and the filling ratio control the acceleration intensity. In transient regime, however, the geyser intensity is suppressed for vapor pressures higher than 25 kPa.
- With the results reported in this thesis the technology readiness level (TRL), which measures the maturity level of the product development, has been raised from 2 (technology concept) to 7 (system prototype demonstrated in space environment) in a development scale ranging from 1 to 9; See Fig. 76.

7.2 SUGGESTIONS FOR FUTURE WORKS

Some suggestions for future works are listed below:

- The condensation process in parallel channels connected by inlet and outlet manifolds can be analyzed in order to optimize the geometry of the fuselage and air conditioning condensers.

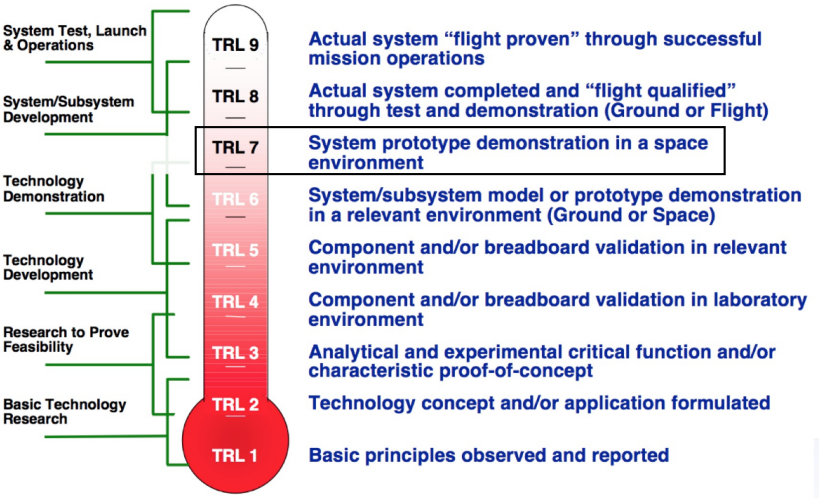

Source – Technology readiness assessment guide [85].

Figure 76 – Technology readiness level.

- A mathematical model could be developed to predict the mean operating temperature of the heat exchanger and intermediary elements based on boundary conditions and input power. Experimental results reported in this thesis can be used to validate the model.
- The influence of the contact thermal resistance on the mechanical coupling between the condensers of the intermediary elements and loop-thermosyphons evaporator could be better understood.
- The fictitious heat sources (cartridge resistances) could be replaced by real on-board electronic components.

REFERENCES

1 SARNO, C.; TANTOLIN, C.; PARBAUD, S. Cooling of seat electronics boxes with loop heat pipe. In: **IMAPS**. La Rochelle, France: [s.n.], 2009.

2 SAVINO, R.; ABE, Y.; FORTEZZA, R. Comparative study of heat pipes with different working fluids under normal gravity and microgravity conditions. **Acta Astronautica**, v. 63, n. 1–4, p. 24 – 34, 2008.

3 CAI, Q.; CHEN, C. Experimental investigation of an avionics cooling system for aerospace vehicle. **Journal of Spacecraft and Rockets**, v. 44, n. 2, p. 439 – 444, 2007.

4 DO-160G: Environmental conditions and test procedures for airborne equipment. Washington, USA: Radio Technical Commission for Aeronautics - RTCA, 2010.

5 CAI, Q.; CHEN, C.; ASFIA, J. F. Applications of advanced cooling technology in avionics system for aerospace vehicle. In: **43rd AIAA Aerospace Science Meeting and Exhibit**. Reno, Nevada: AIAA, 2005.

6 SARNO, C. Application of phase change systems in avionics. In: **Proc. 16th International Heat Pipe Conference**. Lyon, France: [s.n.], 2012.

7 LOHSE, E.; SCHMITZ, G. Inherently safe looped thermosyphon cooling system for aircraft applications using dielectric fluid h-galden. In: **International Refrigeration and Air Conditioning Conference at Purdue**. [S.l.: s.n.], 2010.

8 ZAGHDOUDI, M. C.; TANTOLIN, C.; SARNO, C. Experimental investigation on the use of flat mini heat pipes for avionics electronic modules cooling. **International Review of Mechanical Engineering**, v. 5, n. 4, p. 770 – 883, 2011.

9 TALAY, T. A. **Introduction to the aerodynamics of flight**. Washington, DC, 1975.

10 G. M. Grover. **Evaporation-condensation heat transfer device**. Jan 1966. US 3229759A.

11 R. S. Gaugler. **Heat transfer device**. June 1944. US 2350348.

12 REAY, D.; KEW, P. **Heat Pipes**. 5. ed. Oxford: Butterworth-Heinemann, 2007. 397 p. ISBN 978-0-7506-6754-8.

13 J. L. G Oliveira, K. V. Paiva, M. B. H Mantelli, R. Gandolfi and L. G. S Ribeiro. **Passive aircraft cooling systems and methods, United States Application Number or PCT International application number 14/322,133 filed on July 2**. 2014.

14 ZHANG, T. T.; TIAN, L.; LIN, C.-H.; WANG, S. Insulation of commercial aircraft with an air stream barrier along fuselage. **Building and Environment**, v. 57, p. 97 – 109, 2012.

15 ASHRAE Handbook: HVAC Applications. Atlanta: American Society of Heating, Refrigeration and Air-Conditioning Engineers, 2011.

16 RAITHBY, G. D.; HOLLANDS, K. G. T. Natural convection. In: ROHSENOW, W. M.; HARTNETT, J. P.; CHO, Y. I. (Ed.). **Handbook of Heat Transfer**. Second. New York, USA: McGraw-Hill, 1998. cap. 4, p. 4.1–4.99.

17 NELLIS, G. F.; KLEIN, S. A. **Heat Transfer**. New York, USA: Cambridge University Press, 2009.

18 HEAT pipes - performance of two-phase closed thermosyphons, ESDU Item 81038. London: Engineering Sciences Data Unit, 1981.

19 BECKER, S.; VERSHININ, S.; SARTRE, V.; LAURIEN, E.; BONJOUR, J.; MAYDANIK, Y. F. Steady state operation of a copper–water lhp with a flat-oval evaporator. **Applied Thermal Engineering**, v. 31, n. 5, p. 686 – 695, 2011.

20 ASHRAE Handbook: Fundamentals. Atlanta: American Society of Heating, Refrigeration and Air-Conditioning Engineers, 2001.

21 HOLMAN, J. P. **Experimental Methods for Engineers**. [S.l.]: McGraw-Hill Series in Mechanical Engineering, 1994.

22 COLEMAN, H. W.; STEELE, W. G. **Experimentation and Uncertainty Analysis for Engineers**. New York: Wiley-Interscience, 1989.

23 ROHSENOW, W. **Handbook of Heat Transfer**. [S.l.]: McGraw-Hill, 1998.

24 LIENHARD-IV, J. H.; LIENHARD-V, J. H. **A Heat Transfer Textbook**. Cambridge Massachusetts: [s.n.], 2008.

25 SHARIFI, N.; BERGMAN, T. L.; ALLEN, M. J.; FAGHRI, A. Melting and solidification enhancement using a combined heat pipe, foil approach. **International Journal of Heat and Mass Transfer**, v. 78, p. 930 – 941, 2014.

26 MORADGHOLI, M.; NOWEE, S. M.; ABRISHAMCHI, I. Application of heat pipe in an experimental investigation on a novel photovoltaic/thermal (pv/t) system. **Solar Energy**, v. 107, p. 82 – 88, 2014.

27 MEISEL, P.; JOBST, M.; LIPPMANN, W.; HURTADO, A. Design and manufacture of ceramic heat pipes for high temperature applications. **Applied Thermal Engineering**, v. 75, p. 692 – 699, 2015.

28 HU, B. wen; WANG, Q.; LIU, Z.-H. Fundamental research on the gravity assisted heat pipe thermal storage unit (gahp-tsu) with porous phase change materials (pcms) for medium temperature applications. **Energy Conversion and Management**, v. 89, p. 376 – 386, 2015.

29 YAU, Y. H.; NG, W. K. A comparison study on energy savings and fungus growth control using heat recovery devices in a modern tropical operating theatre. **Energy Conversion and Management**, v. 52, n. 4, p. 1850 – 1860, 2011.

30 TIARI, S.; QIU, S.; MAHDAVI, M. Numerical study of finned heat pipe-assisted thermal energy storage system with high temperature phase change material. **Energy Conversion and Management**, v. 89, p. 833 – 842, 2015.

31 ZHANG, L.; LEE, W. L. Evaluating the use heat pipe for dedicated ventilation of office buildings in hong kong. **Energy Conversion and Management**, v. 52, n. 4, p. 1983 – 1989, 2011.

32 SIDDIQUI, M. A. Heat transfer and fluid flow studies in the collector tubes of a closed-loop natural circulation solar water heater. **Energy Conversion and Management**, v. 38, n. 8, p. 799 – 812, 1997.

33 ZUO, Z. J.; GUNNERSON, F. S. Numerical modeling of the steady-state two-phase closed thermosyphon. **International Journal of Heat and Mass Transfer**, v. 37, n. 17, p. 2715 – 2722, 1994.

34 JIANG, F.; CHEN, W. jing; LIU, Z.; SHI, J. tao; LI, X. lun. Heat transfer enhancement in a three-phase closed thermosyphon. **Applied Thermal Engineering**, v. 65, n. 1–2, p. 495 – 501, 2014.

35 SHABGARD, H.; XIAO, B.; FAGHRI, A.; GUPTA, R.; WEISSMAN, W. Thermal characteristics of a closed thermosyphon under various filling conditions. **International Journal of Heat and Mass Transfer**, v. 70, p. 91 – 102, 2014.

36 CHEHADE, A.; LOUAHLIA-GUALOUS, H.; MASSON, S. L.; LéPINASSE, E. Experimental investigations and modeling of a loop thermosyphon for cooling with zero electrical consumption. **Applied Thermal Engineering**, v. 87, p. 559 – 573, 2015.

37 BOJIć, M.; LUKIć, N. Controlling evaporative three finger thermosyphon. **Energy Conversion and Management**, v. 43, n. 5, p. 709 – 720, 2002.

38 LU, X.; WEI, J.-J. Experimental study on a novel loop heat pipe with both flat evaporator and boiling pool. **International Journal of Heat and Mass Transfer**, v. 79, p. 54 – 63, 2014.

39 MITOMI, M.; NAGANO, H. Long-distance loop heat pipe for effective utilization of energy. **International Journal of Heat and Mass Transfer**, v. 77, p. 777 – 784, 2014.

40 NISHIKAWARA, M.; NAGANO, H. Parametric experiments on a miniature loop heat pipe with PTFE wicks. **International Journal of Thermal Sciences**, v. 85, p. 29 – 39, 2014.

41 SARNO, C.; TANTOLIN, C.; HODOT, R.; MAYDANIK, Y.; VERSHININ, S. Loop thermosyphon thermal management of the avionics of an in-flight entertainment system. **Applied Thermal Engineering**, v. 51, n. 1–2, p. 764 – 769, 2013.

42 CENGEL, Y. A.; BOLES, M. A. **Thermodynamics:An Engineering Approach**. [S.l.]: McGraw-Hill, 2006.

43 CHENG, K. C.; SEKI, N. **Freezing and Melting heat Transfer in Engineering**. Washington: Hemisphere Publishing, 1991.

44 CHO, S. H.; SUNDERLAND, J. E. Heat conduction problems with freezing or melting. **Journal of Heat Transfer**, v. 91, p. 421–428, 1969.

45 NIRO, A.; BERETTA, G. P. Boiling regimes in a closed two-phase thermosyphon. **International Journal of Heat and Mass Transfer**, v. 33, n. 10, p. 2099 – 2110, 1990.

46 CHEN, J.; YANG, S.; LIAO, S.; CAO, X. Experimental investigation of effective parameters on geyser periodicity in a vertical heated system. **Experimental Thermal and Fluid Science**, v. 68, p. 163 – 176, 2015.

47 FAGHRI, A. **Heat Pipe Science and Technology**. Washington, DC, USA: Taylor & Francis, 1995.

48 JAFARI, D.; FRANCO, A.; FILIPPESCHI, S.; MARCO, P. D. Two-phase closed thermosyphons: A review of studies and solar applications. **Renewable and Sustainable Energy Reviews**, v. 53, p. 575 – 593, 2016.

49 BEZRODNYI, M. K.; BELOIVAN, A. I. Investigation of the maximum heat transfer capacity of closed two-phase thermosyphons. **Inzhenerno-Fiziv-heskii Zhurnal**, v. 30, p. 590–597, 1975.

50 BOURE, J. A.; BERGLES, A. E.; TONG, L. S. Review of two-phase flow instability. **Nuclear Engineering and Design**, v. 25, n. 2, p. 165 – 192, 1973.

51 GRIFFITH, P. Geysering in liquid-filled lines. In: ASME. **ASME-AICHE Heat Transfer Conference and Exhibit**. Houston, Texas: ASME, 1962.

52 CASAROSA, C.; LATROFA, E.; SHELGINSKI, A. The geyser effect in a two-phase thermosyphon. **International Journal of Heat and Mass Transfer**, v. 26, n. 6, p. 933 – 941, 1983.

53 IMURA, H.; SASAGUCHI, K.; KOZAI, H.; NUMATA, S. Critical heat flux in a closed two-phase thermosyphon. **International Journal of Heat and Mass Transfer**, v. 26, n. 8, p. 1181 – 1188, 1983.

54 LARKIN, B. S. An experimental study of the two-phase thermosyphons tube. **Trans. Can. Soc. Mech. Engng.**, v. 14, 1971.

55 IMURA, H. Optimum fill quantity of liquid in two-phase closed thermosyphons. **Tech. Report Kumamoto Univ.**, v. 29, p. 9 – 18, 1980.

56 HARADA, K.; INOUE, S.; FUJITA, J.; SUEMATSU, H.; WAKIYAMA, Y. Heat transfer characteristics of large heat pipes. **Hitachi Zozen tech. Rev.**, v. 41, p. 167 – 174, 1980.

57 MANTELLI, M. B. H.; CARVALHO, R. D.; COLLE, S.; MORAES, D. D. Study of closed two-phase thermosyphons for bakery oven applications. In: ASME. **33rd National Heat Transfer Conference**. Albuquerque, New Mexico: ASME, 1999.

58 LIN, T. F.; LIN, W. T.; TSAY, Y. L.; WU, J. C.; SHYU, R. J. Experimental investigation of geyser boiling in an annular two-phase closed thermosyphon. **International Journal of Heat and Mass Transfer**, v. 38, n. 2, p. 295 – 307, 1995.

59 KUNCORO, H.; RAO, Y. F.; FUKUDA, K. An experimental study on the mechanism of geysering in a closed two-phase thermosyphon. **International Journal of Multiphase Flow**, v. 21, n. 6, p. 1243 – 1252, 1995.

60 EMAMI, M. R. S.; NOIE, S. H.; KHOSHNOODI, M.; MOSAVIAN, M. T. H.; KIANIFAR, A. Investigation of geyser boiling phenomenon in a two-phase closed thermosyphon. **Heat Transfer Engineering**, v. 30, n. 5, p. 408–415, 2009.

61 KHAZAEE, I.; HOSSEINI, R.; NOIE, S. H. Experimental investigation of effective parameters and correlation of geyser boiling in a two-phase closed thermosyphon. **Applied Thermal Engineering**, v. 30, n. 5, p. 406 – 412, 2010.

62 JOUHARA, H.; FADHL, B.; WROBEL, L. C. Three-dimensional CFD simulation of geyser boiling in a two-phase closed thermosyphon. **International Journal of Hydrogen Energy**, v. 41, n. 37, p. 16463 – 16476, 2016.

63 OLIVEIRA, J. L. G.; TECCHIO, C.; PAIVA, K. V.; MANTELLI, M. B. H.; GANDOLFI, R.; RIBEIRO, L. G. S. Passive aircraft cooling systems for variable thermal conditions. **Applied Thermal Engineering**, v. 79, p. 88 – 97, 2015.

64 OLIVEIRA, J. L. G.; TECCHIO, C.; PAIVA, K. V.; MANTELLI, M. B. H.; GANDOLFI, R.; RIBEIRO, L. G. S. In-flight testing of loop thermosyphons for aircraft cooling. **Applied Thermal Engineering**, v. 98, p. 144 – 156, 2016.

65 MANTELLI, M. B. H. **Thermosyphon Technology for Industrial Applications. Heat Pipes and Solid Sorption Transformations - Fundamentals and Practical Applications**. Boca Raton, Florida, USA: CRC Press, 2013.

66 EL-GENK, M. S.; SABER, H. H. Flooding limit in closed, two-phase flow thermosyphons. **International Journal of Heat and Mass Transfer**, v. 40, n. 9, p. 2147 – 2164, 1997.

67 CHANG, S.; LO, D.; CHIANG, K.; LIN, C. Sub-atmospheric boiling heat transfer and thermal performance of two-phase loop thermosyphon. **Experimental Thermal and Fluid Science**, v. 39, p. 134 – 147, 2012.

68 NEGISHI, K.; SAWADA, T. Heat transfer performance of an inclined two-phase closed thermosyphon. **International Journal of Heat and Mass Transfer**, v. 26, p. 1207–1213, 1983.

69 WANG, J. C. Y.; MA, Y. Condensation heat transfer inside vertical and inclined thermosyphons. **Journal of Heat Transfer**, v. 113, p. 777 – 780, 1991.

70 PAYAKARUK, T.; TERDTOON, P.; RITTHIDECH, S. Correlations to predict heat transfer characteristics of an inclined closed two-phase thermosyphon at normal operating conditions. **Applied Thermal Engineering**, v. 20, n. 9, p. 781 – 790, 2000.

71 ZUO, Z. J.; GUNNERSON, F. S. Heat transfer analysis of an inclined two-phase closed thermosyphon. **Journal of Heat Transfer**, v. 117, p. 1073–1075, 1995.

72 COHEN, H.; BAYLEY, F. J. Heat transfer problems of liquid-cooled gas-turbine blades. **Proc. Instn. Mech. Engrs.**, v. 169, p. 1063 – 1080, 1955.

73 STREL'TSOV, A. I. Theoretical and experimental investigation of optimum filling for heat pipes. **Heat Transfer-Soviet Research**, v. 7(1), p. 23–27, 1975.

74 ANDROS, F. E.; FLORSCHUETZ, L. M. The two-phase closed thermosyphon: An experimental study with flow visualization. In: **Proc. Symp. Workshop**. Fort Lauderdale, Florida: [s.n.], 1976. p. 547–550.

75 SHIRAISHI, M.; YONEYA, M.; YABE, A. Visual study of operating limit in the two-phase closed thermosyphon. In: **Proc. 5th International Heat Pipe Conference.** Tsukuba, Japan: [s.n.], 1984. p. 11–17.

76 PARK, Y. J.; KANG, H. K.; KIM, C. J. Heat transfer characteristics of a two-phase closed thermosyphon to the fill charge ratio. **International Journal of Heat and Mass Transfer**, v. 45, n. 23, p. 4655 – 4661, 2002.

77 NOIE, S. H.; EMAMI, M. R. S.; KHOSHNOODI, M. Effect of inclination angle and filling ratio on thermal performance of a two-phase closed thermosyphon under normal operating conditions. **Heat Transfer Engineering**, v. 28, n. 4, p. 365 – 371, 2007.

78 AGOSTINI, F.; HABERT, M.; MOLITOR, F.; FLUECKIGER, R.; KAUFMANN, L.; BERGAMINI, A.; ROSSI, M.; BESANA, S. Double-loop thermosyphon for electric components cooling. **IEEE Transactions on Components, Packaging and Manufacturing Technology**, v. 4, p. 223–231, 2014.

79 ALVARENGA, T. R. **Interface para a transferência de calor entre trocador de calor passivo e termossifão em circuito para aplicações em aeronaves**. Dissertação (Mestrado) — Universidade Federal de Santa Catarina, Florianópolis, 2016.

80 MARCUS, B. D. Technical report, **Theory and design of variable conductance heat pipes**. 1972.

81 FAGHRI, A.; ZHANG, Y.; HOWELL, J. **Advanced heat and mass transfer**. Columbia, MO, USA: Global Digital Press, 2010.

82 MATALLAH, H.; NEWTON, W.; JAMES, D.; CAMERON, I.; SIENZ, J.; ROMOCKI, S.; LAVERY, N. P. The development of a sub-atmospheric two-phase thermosyphon natural gas preheater using a lumped capacitance model and comparison with experimental results. **Applied Thermal Engineering**, v. 104, p. 767 – 778, 2016.

83 LI, P.; LI, Y.-M.; LEONG, J. C. Lumped-system analysis of a cavity with triangular porous layers. **Applied Mathematical Modelling**, v. 39, n. 18, p. 5507 – 5520, 2015.

84 XU, B.; LI, P.-W.; CHAN, C. L. Extending the validity of lumped capacitance method for large biot number in thermal storage application. **Solar Energy**, v. 86, n. 6, p. 1709 – 1724, 2012.

85 DOE-G-413.3-4A: Technology Readiness Assessment Guide. Washington, D.C, USA: U.S. Department of Energy, 2011.

86 PAIVA, K. V. **Comportamento térmico em gravidade e microgravidade de mini tubos de calor do tipo fios-placas**. Dissertação (Mestrado) — Universidade Federal de Santa Catarina, Florianópolis, 2007.

Appendix A – EXPERIMENTAL MEASUREMENTS

A.1 AIR VELOCITY IN RECTANGULAR DUCTS

Following the recommendation given by ASHRAE [20], the Log-Tchebycheff rule (equal area method) (ISO Standard 3966) was used to determine the air mass flow rate at the air-conditioning traverse duct, $\dot{m}_{AC}$. The average of individual point velocities can provide satisfactorily results when these points are determined following this rule. Fig. 77 illustrates the points where the velocity measurements must be taken in a rectangular duct with side dimensions between 762 and 914.4 mm. Log-tchebytcheff rule accounts the influence of wall friction and the fall-off of velocity near wall ducts, minimizing the positive error promoted by the failure account for losses at the duct wall.

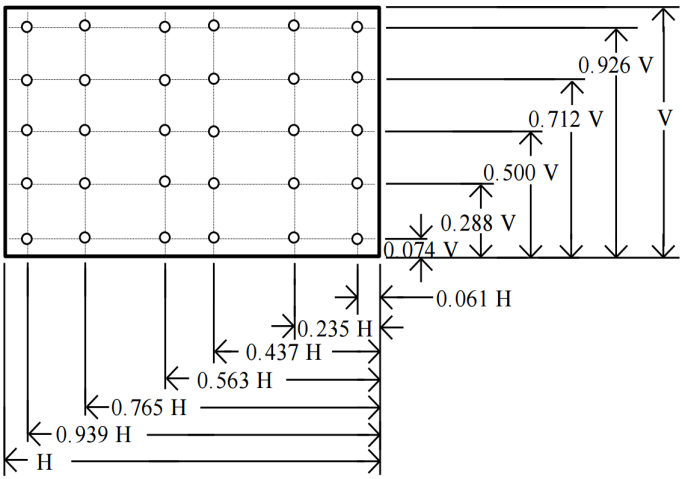

Source – ASHRAE [20].

Figure 77 – Location of measuring points for traversing rectangular ducts with dimensions between 762 and 914.4 mm.

The duct is divided into rectangular areas by using a minimum of 25 points. The velocity should be measured in each one of these points, which are adjusted according to the duct dimensions. For duct sides less than 762 mm 5 traversal points must be taken along that side. For duct sides between 762 and 914.4 mm, 6 points are recommended; see Fig. 77. If the duct side is greater than 914.4 mm, 7 point are necessary in that

side. Table 11 summarizes the location of the measuring points according to the number of traverse lines required in each side.

Table 11 – Location of measuring points in a traverse rectangular duct.

Number of points per side	Positions relative to ineer wall
5	0.074; 0.288; 0.5; 0.712; 0.926
6	0.061; 0.235; 0.437; 0.563; 0.765; 0.939
7	0.053; 0.203; 0.366; 0.5; 0.634; 0.797; 0.947

Source – ASHRAE [20].

The average velocity at the air-conditioning duct is then given by:

$$\bar{v}_{AC} = \frac{1}{n}\sum_{i=1}^{n} v_i \ ; \tag{A.1}$$

where n is the total number of points surveyed and v_i stands for the air velocity at point i. When velocities at individual points, v_i, fluctuate the reading should be averaged on time. The mass flow rate is then computed by

$$\dot{m}_{AC} = \rho \bar{v}_{AC} A_t; \tag{A.2}$$

where A_t and ρ stand for transversal area and air density, respectively.

A.2 VOLUMETRIC MASS FLOW RATE

The mass flow rate of the coolant fluid circulating at the calorimeter (fuselage heat sink), $\dot{m}_{tb}$, was measured by timing the amount of collected fluid. Although mass flow rate equipment such as rotameters and turbine flowmeters could be employed, timing given mass is the simplest and most precise method to measure volumetric or mass flow rate. The precision of the timing given mass method ranges from 0.1 to 0.5% whereas in rotameters and turbine flowmeters the precision can be as high as 5% [20]. Moreover, there are no restrictions of the measuring range. However, mass flow rates of corrosive or toxic fluids by this method should be avoided for safety reasons.

A.3 TEMPERATURE OF SOLID SURFACES

To measure temperature of solid surfaces K-type thermocouples were employed. In order to measure the temperature properly, the

following procedure suggested by Paiva [86] was adopted to fix the thermocouples.

- 1. The surface in which the thermocouple was installed was previously cleaned with acetone to ensure good adhesive properties.
- 2. Kapton tape was used the cover the thermocouple surface. This tape isolates the thermocouple electrically, preventing any electrical interference from the neighborhood in the temperature measurement; see Fig. 78.
- 3. An aluminum tape is used to promote contact between the thermocouple and the solid surface; see Fig. 78.

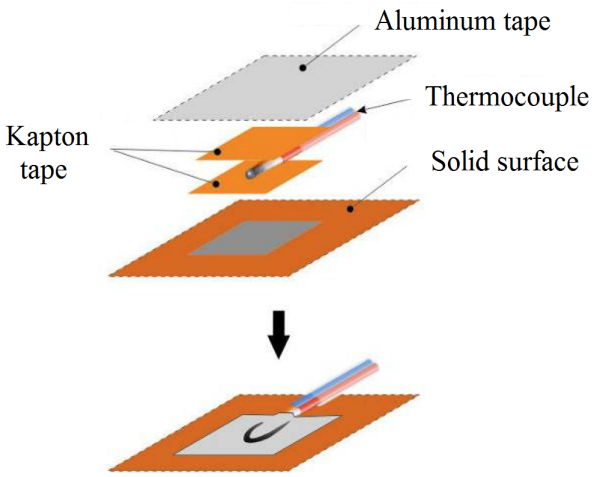

Source – Paiva [86].

Figure 78 – Schematics of the thermocouple fixing at the solid surface.

Appendix B – EXPERIMENTAL UNCERTAINTIES

The experimental study conducted in this work was subject to several measurement uncertainties due to systematic and random errors. Using the procedure proposed by Holman [21] it is possible to account the error propagation as follows.

B.1 INPUT POWER UNCERTAINTY

The input power, q_{in}, released in the cartridge resistances can be computed by:

$$q_{in} = Vi \ ; \tag{B.1}$$

where V and i stand for voltage and current, respectively. The standard uncertainty of the input power, $u(q_{in})$, is:

$$u(q_{in}) = \left\{ \left[\frac{\partial q_{in}}{\partial V} u(V) \right]^2 + \left[\frac{\partial q_{in}}{\partial i} u(i) \right]^2 \right\}^{1/2} \ ; \tag{B.2}$$

$$u(q_{in}) = \left\{ \left[iu(V) \right]^2 + \left[Vu(i) \right]^2 \right\}^{1/2} \ ; \tag{B.3}$$

where $u(V)$ and $u(i)$ stand for voltage and current standard uncertainties, in that oder. The expanded uncertainty, U, for q_{in} is then given by:

$$U(q_{in}) = t \cdot u(q_{in}) \tag{B.4}$$

where t represents the coverage factor. The number of degrees of freedom for V and i is considered as infinity, which implies $t \approx 2.0$ for a confidence interval of 95%. The expanded uncertainty $U(q_{in})$ is estimated to be about 3% of the measured value.

B.2 MASS FLOW RATE UNCERTAINTY

The mass flow rate, $\dot{m}$, circulating at the calorimeter of the fuselage condenser was measured by timing the amount of collected fluid as described in section A.2. Since the properties of the coolant fluid and the pressure drop along the pipe are nearly constant during the measuring process it is reasonable to assume that the mass rate show minor changes. Therefore, the mass rate can be treated as an invariable parameter. In

order to decrease the confidence interval n samples were measured. The mass flow rate can be expressed by

$$\dot{m} = \overline{\dot{m}} \pm U(\dot{m}) = \overline{\dot{m}} \pm t \cdot \frac{S_{\dot{m}}}{\sqrt{n}} \; ; \tag{B.5}$$

where $\overline{\dot{m}}$, t and $S_{\dot{m}}$ stand for the mean value of n samples, coverage factor and standard deviation, respectively. The standard deviation is expressed by:

$$S_x = \sqrt{\frac{1}{n-1}\sum_{i=1}^{n}(\dot{m}_i - \overline{\dot{m}})^2} \; ; \tag{B.6}$$

where $\dot{m}_i$ is the i-th measurement. The number of degrees of freedom is given by $\nu = n - 1$. Table 12 shows the uncertainty analysis for cases C1 presented in Chapter 4. A confidence interval of 95% was used.

Table 12 – Mass rate uncertainty for case C1. Water was used as coolant fluid with the thermal bath temperature set to 40 ^{o}C.

Time [s]	Mass [g]	$\dot{m}_i$, [g/s]	$\overline{\dot{m}}$ [g/s]	$S_{\dot{m}}$ [g/s]	ν	t	$U(\dot{m})$ [g/s]
5	206	41.20	40.53	0.68	5	2.571	0.71
5	202	40.40					
5	205	41.00					
5	201	40.20					
5	205	41.00					
5	197	39.40					

The uncertainty analysis for others thermal bath temperatures and coolant fluids followed a similar procedure as depicted in table 12.

B.3 HEAT TRANSFER RATE UNCERTAINTY

The heat transfer rate to the thermal bath and to the air conditioning system were computed by:

$$q = \dot{m}c_p(T_{out} - T_{in}) = \dot{m}c_p\Delta T \; ; \tag{B.7}$$

where $\dot{m}$, c_p and ΔT represent the mass rate, specific heat at constant pressure and temperature difference between the outlet and inlet sections of the calorimeter (Fus condenser) or the air conditioning duct (AC

condenser). Considering that c_p is a well known value ($u(c_p) = 0$), the standard uncertainty for q is given by:

$$u(q) = \left[\left(\frac{\partial q}{\partial \dot{m}} u(\dot{m}) \right)^2 + \left(\frac{\partial q}{\partial \Delta T} u(\Delta T) \right)^2 \right]^{1/2} ; \tag{B.8}$$

where $u(\cdot)$ represents the standard uncertainty. The effective number of degrees of freedom for q, $\nu_{ef,q}$, is computed by:

$$\frac{\left[\frac{u(q)}{q} \right]^4}{\nu_{ef,q}} = \frac{\left[\frac{u(\dot{m})}{m} \right]^4}{\nu_{\dot{m}}} + \frac{\left[\frac{u(\Delta T)}{\Delta T} \right]^4}{\nu_{\Delta T}} ; \tag{B.9}$$

where ν represents the number of degrees of freedom. Here, $\nu_{\Delta T}$ can be considered as infinity. The expanded uncertainty for the heat transfer rate, $U(q)$, can be written as:

$$U(q) = t \cdot u(q) \tag{B.10}$$

where t is determined by $\nu_{ef,q}$ for a confidence interval of 95%. The heat transfer rate measurement is then given by:

$$q = \bar{q} \pm U(q) ; \tag{B.11}$$

where $\bar{q}$ stand for the average heat transfer rate.

The uncertainty analysis for the heat transfer rates given by $q = hA\Delta T$, the heat transfer coefficients, $h = q/(A\Delta T)$ and for the overall thermal resistance, $R = (\overline{T}_{evap} - \overline{T}_{cond})/q_{in}$, follow a similar procedure as described above.